THESIS FOR THE DEGREE OF DOCTOR OF PHILOSOPHY

Opportunities for Weight Reduction in Composite Marine Structures

Luis Felipe Sánchez-Heres

Department of Shipping and Marine Technology
CHALMERS UNIVERSITY OF TECHNOLOGY
Gothenburg, Sweden
2015

Opportunities for Weight Reduction in Composite Marine Structures

LUIS FELIPE SÁNCHEZ-HERES

ISBN: 978-91-7597-173-5

Doktorsavhandlingar vid Chalmers tekniska högskola
Ny serie nr 3854
ISSN 0346-718X

Department of Shipping and Marine Technology
Division of Marine Technology
Chalmers University of Technology
SE-412 96, Gothenburg
Sweden
Telephone: + 46 (0)31-772 1000

Printed by Chalmers Reproservice
Gothenburg, Sweden 2015

Opportunities for Weight Reduction in Composite Marine Structures

LUIS FELIPE SÁNCHEZ-HERES
Department of Shipping and Marine Technology
Division of Marine Technology

Abstract

Composite marine structures are desirable for a variety of reasons. Compared to traditional steel structures, they enable the construction of vessels with lower fuel consumption, higher top speed, better stability, lower maintenance, higher cargo capacity, or combinations thereof. All these characteristics are highly desirable, as they influence the energy efficiency and profitability of the vessel.

One of the barriers for a more widespread adoption of composite marine structures is their acquisition cost. This PhD thesis deals with this barrier by exploring opportunities for further weight reduction. Reducing the weight of a composite structure reduces its acquisition cost and increases many of its financial benefits, making it more economically attractive.

Opportunities for weight reduction were identified in three areas: operational limits, material characterization, and structural design. For each of these areas, an approach for weight reduction was investigated.

For operational limits, the possibility of motivating values higher than the ones stated by design rules through reliability analyses was investigated. The results show that strength reliability analyses of fibre-reinforced plastic structures in tension are frail and uncertain, because uncertain details of the mechanical and probabilistic models, as well as definitions of laminate failure, highly influence the reliability estimates. Therefore, higher operational limits cannot be motivated for the studied cases. The highly sensitive and uncertain details should be the subject of future research.

For material characterization, the possibility of motivating more accurate mechanical properties for composites through advanced measuring techniques was explored. The results show that digital image correlation systems, as well as strain measuring devices with a large strain gauge, can improve the accuracy of material characterization methods. Higher material characterization accuracy may improve material utilization, leading to structural weight reduction.

For structural design, a method was developed to assess the weight reduction potential of searching the design space for lighter designs and modifying design constraints (motivating higher operational limits or more accurate mechanical properties). The results indicate that searching the design space is the most promising approach of these three.

Keywords: composites, lightweight design, material characterization, non-crimp fabrics, reliability, ultimate limit state.

Preface

This thesis presents work carried out during the years 2009-2015 at the Department of Shipping and Marine Technology at Chalmers University of Technology in Gothenburg, Sweden. The work has been partially funded by Chalmers Areas of Advance Materials Science, the Swedish Maritime Competence Centre, Lighthouse (www.lighthouse.nu), and the European Union project Breakthrough in European Ship and Shipbuilding Technologies (BESST; www.besst.it), for which a part of this work is a direct contribution.

I am forever grateful to *The Dynamic Duo*, Jonas Ringsberg and Erland Johnson. A pair of supervisors, not unlike superheroes, who joyfully share their wisdom and knowledge. You guys rock.

I would like to express my gratitude to David Samuelsson and Torsten Sjögren at SP Technical Research Institute of Sweden, as well as to Måns Håkansson and Sven-Erik Hellbratt at SAAB Kockums AB, for all their time, help, support, and valuable contributions with the experimental investigations presented in this thesis.

Special thanks to the merry crew of the Department of Shipping and Marine Technology. I first came to this department nearly eight years ago as a student. Since then, every year has been a delight thanks to you.

To my family and friends, thank you for all the support and kind words.

Extra special thanks to my fiancée, Sara, who is always there to listen and put me back on my two feet.

I would like to dedicate this thesis to my parents, María Eugenia and Héctor, who taught me to love science and have guts. Without both, this work would not exist.

Gothenburg, April 2015.

Luis Felipe Sánchez-Heres

Contents

List of appended papers

Paper I Sanchez, L., Ringsberg, J.W., Johnson, E. (2011). Optimization of composite maritime structures – effects of uncertainties on design criteria limits. In: *Advances in Marine Structure – Proceedings of the Third International Conference on Marine Structures (MARSTRUCT2011) in Hamburg, Germany, March 28-30, 2011, pp. 707-714*. Editors: C. Guedes Soares and W. Fricke. ISBN/ISSN: 978-0-415-67771-4.

The author of this thesis contributed to the ideas presented, planned the paper with the co-authors, performed the numerical simulations, and wrote most of the manuscript.

Paper II Sánchez-Heres, L.F., Ringsberg, J.W., Johnson, E. (2013). Study on the possibility of increasing the maximum allowable stresses in fibre-reinforced plastics. *Journal of Composite Materials*, **47**(16): 1931-1941.

The author of this thesis contributed to the ideas presented, planned the paper with the co-authors, performed the numerical simulations, and wrote the manuscript.

Paper III Sánchez-Heres, L.F., Ringsberg, J.W., Johnson, E. (2014). Influence of mechanical and probabilistic models on the reliability estimates of fibre-reinforced cross-ply laminates. *Structural Safety* **51**(1): 35-46.

The author of this thesis contributed to the ideas presented, planned the paper with the co-authors, performed the numerical simulations, and wrote the manuscript.

Paper IV Sánchez-Heres, L.F., Ringsberg, J.W., Johnson, E. Characterization of non-crimp fabric laminates – Loss of accuracy due to strain measuring techniques. *Submitted for publication to the ASTM Journal of Testing and Evaluation* (February 2015).

The author of this thesis contributed to the ideas presented, planned the paper with the co-authors, developed the algorithms, participated in the mechanical testing, performed the statistical analyses, and wrote most of the manuscript.

List of other published papers by the author

Näslund, C., Uyanik, O., Ringsberg, J.W., Sánchez-Heres, L.F. (2012). A parametric study of joint design in a HSLC composite vessel. In: *Proceedings of the Second International Conference on Light Weight Marine Structures (LIWEM2012) in Gothenburg, Sweden, March 27-29, 2012.* Published on CD-ROM, 11 pp.

Sánchez-Heres, L.F., Ringsberg, J.W., Johnson, E. (2012). Effects of matrix cracking on the estimation of operational limits of FRP laminates. In: *Proceedings of the Fifteenth European Conference on Composite Materials (ECCM15) in Venice, Italy, June 24-28, 2012.* Published on CD-ROM, 8 pp. ISBN/ISSN: 978-88-88785-33-2.

Sánchez-Heres, L.F., Ringsberg, J.W., Johnson, E. (2014). Modelling approaches for reliability estimations of fibre-reinforced plastic laminates. In: *Proceedings of the ASME Thirty-third International Conference on Ocean, Offshore and Arctic Engineering (OMAE2014) in San Francisco, California, USA, June 8-13, 2014.* Published on CD-ROM: OMAE2014-23145, 10 pp. ISBN: 978-0-7918-4542-4.

Central concepts and abbreviations

Below concepts and abbreviations are described as they are defined and used in this thesis.

AE system: Acoustic Emission system (see Section 3.4.1.1 for a description).

Design value: The value of a material property to be used in the design of a structure. Some design values are operational limits, but not all. (See Section 3.3.3 for a more details.)

DIC system: Digital Image Correlation system (see Section 3.4.1.2 for a description).

DNV's CC: Det Norske Veritas Offshore Standard DNV-OS-C105: Composite Components [1]

DNV's HSLC: Det Norske Veritas Rules for High Speed, Light Craft and Naval Surface Craft [2].

Maximum/minimum allowable stress/strain: A kind of operational limit or design value (see definition of design value).

NCF: Non-Crimp Fabric composite. A type of fibre-reinforced plastic.

Operational limit: The threshold condition after which a safety level is not met. More specifically, for material strength, the limit load above which a probability of failure of a structure is unacceptable.

Reliability estimate: A quantity of interest calculated through a reliability analysis.

Structural design: The act of designing a structure. Not to be confused with *structure design*.

Structure design: A particular design of a structure. In Chapter 3, for a catamaran, there are several structure designs, where each one is different but has the same function.

“Success is 1% inspiration, 98% perspiration, and 2% attention to detail.”

~ Phil Dunphy

Overweight

Above a desirable weight.

1 Introduction

Energy efficiency is nowadays a part of the business zeitgeist. Higher oil prices and environmental regulations have made it an important quality for many products and services; marine transportation being among them. There are several ways of improving the energy efficiency of marine transportation. Effective supply chain management, logistics, and navigation can reduce the energy consumption by optimizing the routes and sailing speed of a fleet. Furthermore, the energy efficiency of the vessels themselves can also be improved. Aerodynamic and hydrodynamic analyses can render designs with decreased drag, while better engines, machinery, and propulsion systems can cutback the thermal and mechanical energy losses. An additional approach for improving the energy efficiency of a vehicle is to reduce its weight.

Lighter vehicles consume less energy or are able to transport more cargo with the same amount of energy. Considering the plethora of upcoming regulations and economical challenges, both traits are highly desirable in a vessel. Lower fuel consumption not only reduces its operational costs, it also improves its IMO Energy Efficiency Index rating (EEDI) [3], and potentially its resale value [4]. Additionally, lower fuel consumption translates into lower CO2 emissions, a characteristic that will matter financially once market based measures for reducing CO2 emissions are implemented. While the fuel consumption of a vessel can be lowered through other approaches besides lightweight construction, increasing the cargo capacity of a vessel without increasing its displacement is an improvement that can only be made through lightweight construction. Larger cargo capacity is desirable because it can increase the revenue of a ship. Slow-steaming has proven to be an effective measure to reduce the emissions from shipping [5]. If slow-steaming becomes mandatory, more ships may be needed to fulfil the transportation demand. In such a case, vessels of a certain displacement with a larger cargo capacity will be more profitable [6,7]. Overall, lightweight construction makes vessels more profitable and resilient to upcoming environmental regulations and economical challenges.

Lightweight construction can be achieved through a variety of approaches, of which material selection is a prominent one [6]. Aluminium, high tensile steel and composites are materials suitable for lightweight construction. Composites are the subject of this work. In some ways, composites outperform high strength steel and aluminium as construction materials for marine structures. They are lighter, have a tuneable range of stiffness and strength, do not corrode, are buoyant, and have a longer fatigue life. A composite structure can easily be lighter than its equivalent in steel, and as light or lighter than its equivalent in aluminium. In engineering, the word “composites” is an umbrella term. It describes a variety of materials formed by the combination of two or more constituent materials with distinctive properties that complement each other. The most commonly used composites in marine engineering are Fibre-Reinforced Plastics (FRPs) and sandwich composites with FRP skins. Despite all their advantages, composites do have their drawbacks, chief among them are their flammability and cost.

Composites burn, release black smoke, and start loosing their structural stability at temperatures lower than steel or aluminium. The international convention for the Safety Of Life At Sea (SOLAS) used to demand non-combustible materials for the construction of load-bearing ship structures. Since 1940, composites have been used in boats, yachts, high-speed light craft, naval ships and submarines because these watercraft do not have to comply with SOLAS; whereas commercial ships do have to comply. SOLAS prevented the adoption of composites in commercial vessels until 2012, when it was amended with the Regulation 17 in Chapter II-2. This regulation allows for composite structures as long as their safety with respect to fire can be demonstrated. The Lightweight construction applications at sea (LÄSS) project [6] partially dealt with demonstrating that composite structures can meet the SOLAS safety requirements with fire control measures. In January 2015, the first composite structure in a SOLAS vessel, a composite hatch cover, was approved [8]. This approval may become a precedent that facilitates the widespread use of composites in commercial ships.

In general, the acquisition cost of a composite structure is higher than the one of a similar structure made out of aluminium or steel [6]. This higher acquisition cost can make composite structures economically unattractive even though they may have substantial advantages over metallic structures [6,9,10]. Most buyers are willing to pay a premium for a composite structure as long as it is a good investment. What constitutes a “good investment” depends on the buyer. A company may be interested in reducing operational costs, and therefore, be willing to pay a premium for a composite vessel if the savings in fuel consumption and maintenance pay for the premium in a reasonable amount of time, say five years. While another company may have a more long-term perspective. It may be willing to pay for the premium to brand itself as “green” and easily comply with future regulations on emissions and efficiency. Clearly, the point where the acquisition cost of a composite structure becomes economically unattractive depends on the business case. The high acquisition cost of a composite structure must be motivated through lifecycle cost analyses. It is up to the customer to decide on acceptable payback time. Lifecycle cost analyses are a necessary argument in favour of composite structures. International projects such as Breakthrough in European Ship and Shipbuilding Technologies (BESST) [11] as well as LÄSS have had lifecycle analyses in their agendas. Regardless of the type of structure, fuel prices, material cost, or any other detail on a lifecycle cost analysis, one

aspect is true for all composite structures: the smaller its premium cost is, the easier it is to sell it. Because of this aspect, there is always a need to reduce the acquisition cost of a composite structure. One of the largest parts of its acquisition cost is the material itself [6], so it is of great importance to guarantee that the material is efficiently used in the structure.

In the maritime industry, design rules are issued by classification societies, as these organizations are entrusted with the task of guaranteeing the safety of new ship designs. Due to the diversity of possible ship designs and the variation of engineering competence and engineering resources worldwide, the design rules are simple to use and understand. This simplicity, unfortunately, can come with a lack of accuracy, and consequently large safety factors that can lead to very conservative designs.

The conservatism is the result of a mixture of factors. First, the design time is very limited compared to other industries. For example, the lead time for a ship is rarely more than five years [12]. Vessels are usually task specific, and therefore, only a limited amount of sister ships (if any) are constructed. Since the design will not be used hundreds or thousands of times, like in the car or aircraft industries, there is a significant economical limitation on how many man-hours can be spent in the design [12]. Limited time and limited resources force the designers to rely on fast and trustworthy tools and methods, usually the ones stated in design rules.

To summarize, marine composite structures are commonly designed with simple and fast tools and methods, as well as large safety factors due to time and cost constraints. The design methodology can render too conservative designs that can be too expensive to be considered economically attractive. Marine composite structures could therefore benefit from more accurate design methodologies that would lead to the usage of less material through its better utilization. Essentially, what we are after is improving material efficiency. We want composites to be used to their full potential. Reducing the weight of a composite marine structure without compromising their safety is an act of increasing material efficiency.

1.1 Objective and methodology of this PhD thesis

The objective of this thesis is to reduce the weight of composite marine structures, so as to make them more economically attractive. It presents three approaches for doing so: operational limits, material characterization, and structural design. Albeit the three of them are significantly different, they are all intertwined in the design of a structure. To illustrate their relation, consider the following equation stated in DNV's Rules for Classification of High Speed Light Craft and Naval Surface Craft (DNV's HSLC) [2] for the "laminate calculation method",

$$\varepsilon_i \leq \frac{\varepsilon_{uf}}{R} \tag{1.1}$$

where ε_i is the strain in a composite laminate at direction i, ε_{uf} is the ultimate fibre strain of said laminate, and R is a safety factor against fibre failure. The quotient of ε_{uf}/R is the maximum allowable strain which must not be exceeded by ε_i.

This inequality determines, from a laminate strength perspective, whether or not a structure design is acceptable. If the inequality is not met, a structure designer usually has three possibilities to remediate the situation: modify the structure to reduce ε_i, select another laminate with a higher ε_{uf}, motivate the use of a smaller R value compared to the one stated in the rules, or combinations thereof. The first two options may or may not result in an increase of structural weight and material cost. The third option does not increase the weight of the structure, but it does increase its design time, and therefore, its design cost. These three possibilities are the three approaches explored in this thesis.

The value of R handles all the uncertainties: the variability of both the load and the material resistance, as well the differences between their true and predicted values. Strength reliability analyses are used, in some cases, to calibrate safety factors such as R, and are instrumental for motivating lower values. Chapter 2, operational limits, summarizes the contents of three publications dealing with strength reliability analyses of composite materials. The objective of the work in Chapter 2 was to explore the possibility of motivating lower composite material safety factors through improved reliability analyses and mechanical models. Reducing the safety factors is only acceptable if they can be shown to be over-conservative (i.e. they provide a safety level higher than the desired one).

The value of ε_{uf} is a material property determined through experimental testing and measuring. Ideally, its value is representative of the material, and to improve it, the only option is to change the material itself. Unfortunately, in reality, laboratory test cases are not perfectly representative of the conditions a material is subjected to in a structure, and the experimental measurements from which material properties are determined are imperfect. Better test designs and measuring technologies can improve the properties of a material without changing the material itself. Chapter 3, material characterization, presents experimental work exploring the possibility of obtaining more accurate mechanical properties for composite materials through non-standard measuring technologies.

The value of ε_i is the result of a structural analysis. Potentially, it can be reduced by improving the accuracy of the structural analysis. For example, performing detailed finite element calculations instead of simplified analytical calculations known to render conservative results. Furthermore, it can also be reduced by modifying the design of the structure itself. For example, the maximum strain in a panel under an out-of-plane pressure can be reduced by increasing its thickness or reducing its unsupported length. In lightweight design, the challenge is to find among the myriad of possibilities, a structural design or modification that exhibits the lowest possible stresses and strains under the required loads and has the lowest structural weight and cost. Chapter 4, structural design, presents an investigation that compares the weight saving potential of searching the design space for the best possible design, against the weight saving potential of the two past approaches: improved operational limits and material characterization. The objective is to answer a simple question: is searching better than modifying the constraints for reducing the weight of a structure?

1.2 The composition of this PhD thesis

Before continuing, a brief clarification regarding the composition of this thesis is needed. PhD theses are usually either a monograph or a combination of a brief summary and appended publications. This PhD thesis follows the latter type, however, the summary has been extended. The contents are the following: Chapter 2 contains a brief summary of the appended papers I, II, and II. Chapter 3 contains a brief summary of the appended paper IV, but also extensive descriptions and lessons learned of the experimental tests, measurements, and data post-processing. Finally, Chapter 4 contains only unpublished results; its objective is complement the work in Chapters 2 and 3.

Limit

A point or level that should not be passed.

2 Operational Limits

One of the most important tasks of designing a structure is to guarantee that it has the right safety level. In structural engineering, safety level is understood as the combination of the consequences of structural failure and the probability that such failure would occur. Operational limits guarantee the desired safety level in structures, they mark the load threshold over which the safety level is not met, or in other words, for a given consequence of failure, the limit load above which the probability of failure of a structure is unacceptable.

The estimation of operational limits for vehicle structures is very important. The unexpected failure of a structure due to the over estimation of an operational limit could lead to: interruption of service, expensive repairs, increased maintenance, bad reputation, complete loss of the vehicle, damage to the environment, and most importantly, loss of lives. In contrast, a structure with under estimated operational limits would perhaps never fail, but it would be unnecessarily heavy and strong. The extra weight and strength increase the manufacturing and operational costs of the vehicle and decrease its efficiency. This issue is exacerbated in composite structures since, compared to steel, composite materials are relatively expensive, and the main reasons for using them is to increase the efficiency of the vehicle.

Safety concerns, and therefore, operational limits, determine the type and quantity of material that is needed in a structure. The accurate estimation of operational limits is a crucial task on the design of an efficient lightweight structure, as they determine if the material is used to its fullest.

This chapter contains an overview and summary of the work in the appended papers I, II and III. The main purpose of the chapter is to consolidate the conclusions of these three papers by emphasizing their common goal and approach. Section 2.1 presents a brief background on the determination of operational limits for marine structures. Sections 2.2 to 2.4 contain the overview of the approach, while Section 2.5 summarizes the appended papers I, II and II. Section 2.6 contains final remarks regarding the estimation of operational limits as an approach for weight reduction in marine composite structures.

2.1 Background

A structure may have a number of undesirable limit states. The limit state design methodology usually considers four: Ultimate or strength Limit State (ULS), Serviceability Limit State (SLS), Accidental Limit State (ALS), and Fatigue Limit State (FLS). Which of these governs the design of a structure, depends on the structure itself. A slamming load (ALS) may be the governing requirement for composite hull bottom, while vibration requirements (SLS) may dictate the spacing between stiffeners on a composite deck. The ULS may or may not be the limit state governing the dimensioning of a structure, but for composites, its prediction is uncertain. Large number of mechanical models differing on damage, degradation and failure criteria are described in design standards and research [1,13-16]. The uncertainty regarding its prediction was identified as a research opportunity which may lead to higher operational limits. The ULS operational limits are commonly determined by design rules and standards as follows.

Safety factors are meant to guarantee that the probability of observing any of the limit states is acceptable. Consider Equation 1.1 presented in Chapter 1. The quotient of ε_{uf}/R is the maximum allowable strain, which is the operational limit for the ULS of the laminate evaluated with the equation. If the operational limit is exceed, the fracture of the laminate is not certain; however, its probability of occurrence is considered to be unacceptable. Equivalent expressions for the ULS and the other limit states, or mixtures of them, can be found in other design rules and standards [17,18]. In all of these, safety factors define the operational limit.

In Equation 1.1, R handles all the uncertainties: the variability of both the load and the material resistance, as well the errors and biases of the load and resistance models. Table 2.1 presents the values for R stated in DNV's HSLC rules. According to these rules, for most of the structure, R should be 3.3. In a ship, the superstructure and the hull-bottom are subjected to loads with very different magnitudes and frequencies. Nevertheless, the values of R that should be used for each of these components is the same. Furthermore, the values of R do not vary according to the composite material used. Depending on the constituents and the manufacturing method, composite materials can exhibit different degrees of variability in their mechanical properties. None of these aspects regarding the variability of loads and material properties influence the value of R. Clearly then, 3.3 is a conservative value for R that guarantees safe structural designs through simple calculations at the expense of material efficiency. In other words, simple design rules result in unnecessarily heavy composite structures.

Table 2.1 Values for the safety factor R in Equation 1.1 according to DNV's HSLC.

Structural member	R
Bottom panel exposed to slamming	3.3
Remaining bottom and inner bottom	3.3
Side structures	3.3
Deck structures	3.3
Bulkhead structures	3.3
Superstructures	3.3
Deckhouses	3.3
All structures exposed to long-term static loads (duration >3months)	4.5

An alternative to using a single safety factor such as R, that lumps together all the sources of uncertainty, is using partial safety and model factors (aka. Load and Resistance Factor Design). This is the design method adopted in DNV's Offshore Standard DNV-OS-C501: Composite Components (DNV's CC) [1]. It allows for a more relevant determination of the operational limits that are appropriate for the design in question. Consider the following equation, stated in DNV's CC, as the general design criterion for the case of a single load,

$$\gamma_F \gamma_{Sd} S_k \leq \frac{R_k}{\gamma_M \gamma_{Rd}} \tag{2.1}$$

where,

- S_k–local stress or strain based on characteristic load effect
- R_k–characteristic resistance of the material
- γ_F–partial load-effect safety factor
- γ_{Sd}–partial load-model factor
- γ_M–partial resistance safety factor
- γ_{Rd}–partial resistance-model factor

The adjective "characteristic" in the description of S_k indicates that the load is considered to unlikely exceed the stated value. Analogously, for R_k, the adjective "characteristic" indicates that the material resistance is unlikely to fall short of the stated value. The partial safety factors γ_F and γ_M are meant to account for, respectively, load and resistance variability; whereas the partial model factors, γ_{Sd} and γ_{Rd}, are meant to account for simplifications, errors, and biases on the models used to calculate the loads on the material and its resistance, respectively.

In DNV's CC, the partial safety and model factors are tuneable with respect to the limit state (e.g. ULS vs. SLS), the desired safety level (i.e. the acceptable probability that the limit state in question will be observed), the variability and characteristics of the material properties and loads, and finally, with respect to the models used to predict the response of the structure and material (e.g. analytical calculations vs. finite element analyses). Clearly, Equation 2.1 is more flexible than Equation 1.1, as the partial factors can be tuned to the characteristics of the analysed case. This flexibility can allow for less conservative operational limits that still provide the desired safety level. A HSLC composite structure designed according Equation 2.1 will be lighter than an equivalent one designed according to Equation 1.1. Equations 1.1 and 2.1 show

how safety and model factors stated in design rules and standards define operational limits, and by doing so, affect structural weight.

2.2 Objective

The objective of the work presented in this chapter was to explore the possibility of motivating higher operational limits, since the higher an operational limit is, the lighter a structure can be.

2.3 Methodology

Section 2.1 described how operational limits are stated by design rules and standards [1,2,17,18] through safety and model factors. An alternative method to define an operational limit is through structural reliability analyses, which in some cases are used to calibrate safety factors in design rules [19]. Reliability analyses were used to explore the possibility of motivating safety and model factors lower than the ones stated in design rules.

The following sub-sections state the limitations of the work, briefly describe the methodology employed for estimating operational limits through reliability analyses, and finally, explain the important role of mechanical models in reliability analyses.

2.3.1 Limitations

- *Type of FRP*–There is a wide variety of FRP laminates available on the market. Their mechanical properties are not only dependent on the type of fibre and plastic matrix, but also on the architecture of the material itself. The failure event of a chopped strand mat FRP laminate (medium sized fibres randomly oriented in a plane) is significantly different from the one of a textile FRP. Studying the operational limits of all the different types of FRPs would be a monumental task; therefore, we limited our investigations to laminates made with unidirectional plies of pre-impregnated FRPs. This type of "prepreg" (contraction of pre-impregnated) consists of long unwoven "straight" carbon or glass fibres. This type of prepreg has the best in-plane mechanical properties out of all the existing types of FRPs, and therefore, it has been heavily studied. Unidirectional prepregs are commonly used in the aerospace industry and high performance one-of-kind vehicles. In marine structures, Non-Crimp Fabric (NCF) is one attractive type of FRP [20]. The operational limits of NCF laminates were not investigated for two reasons: first, experimental data for NCFs was not available at the beginning of this work, second, NCFs have a more complex meso-structure than unidirectional prepregs; it was considered reasonable to start the investigation with the simplest material.
- *Type of FRP construction and loading condition*–With the exception of pultruded components, laminates are the most simple construction made out of FRPs that can be found in a structure. Combinations of laminates with other materials can form sandwich panels, stiffeners, and joints. The work in this chapter deals only with FRP laminates under monotonically increasing uniaxial tension loads with low loading rates at room temperature. More complex FRP constructions and other loading conditions were not investigated for two reasons. First, as with the type of FRP, it was considered reasonable to start the

investigation with the simplest case. Second, tension, and combinations thereof, is the prime loading case that causes matrix cracking.

- *Limit state*–As stated in Section 2.1, according to limit state design, structures may have four limit states. The work in this chapter deals only with the ULS of laminates.

2.3.2 Estimation of operational limits

An operational limit is meant to provide a certain level of safety. With respect to limit state, safety can be interpreted as an acceptable probability of observing the limit state in question. Therefore, estimating operational limits of a limit state requires two things: determining an acceptable probability of observing it, and calculating the condition (e.g. load) at which this probability is exceeded.

For a structure, considering the consequences of reaching any of its limit states, one can motivate acceptable probabilities for the occurrence of the limit states through risk assessments. Classification societies and other organizations meant to ensure the safety of structures present the results of their own risk assessments as rules, standards or codes. In this sort of documents, acceptable probabilities of the occurrence of a particular limit state are stated as function of different factors. In DNV's CC, the target probability of failure (*failure* henceforward referring solely to the occurrence of the ULS) is determined through its "safety class". The safety class is in turn determined by the consequences of the failure, and the "failure type", the degree of pre-warning given by the structure. In contrast, the Joint Committee in Structural Safety states in its Probabilistic Code [21] that the target probability of failure of a structure is determined through the relative cost of the safety measure and the consequences of its failure. In summary, acceptable probabilities of failure can be determined from risk assessments, codes, rules, or standards.

A structure may respond to a loading condition by exhibiting damage, deformation, vibration, and fracture. Calculating the probability of any of these structural responses require two fundamental elements: a mechanical model and a set of models describing the variability of the input for the mechanical model. The upper part of Figure 2.1 presents a simple diagram of how these two fundamental elements can be used to estimate the probability of a structural response through a Monte Carlo simulation (a suitable method because it does not require the analytical manipulation of the mechanical model). Instances of each of the random models (dimensions, loads, and material properties) are the input to the mechanical model. Each set of instances generates an output (black dots in Figure 2.1). Overall, since the input to the structural model is random, so is its output. From the random output, consisting of large numbers of output instances, the empirical probability distributions related to the structural responses can be calculated. Exactly what the output is depends on the model. For the structural reliability analyses dealt with in this work, the main desired output is the load at which the structure presents the conditions that are considered as the ULS of the structure.

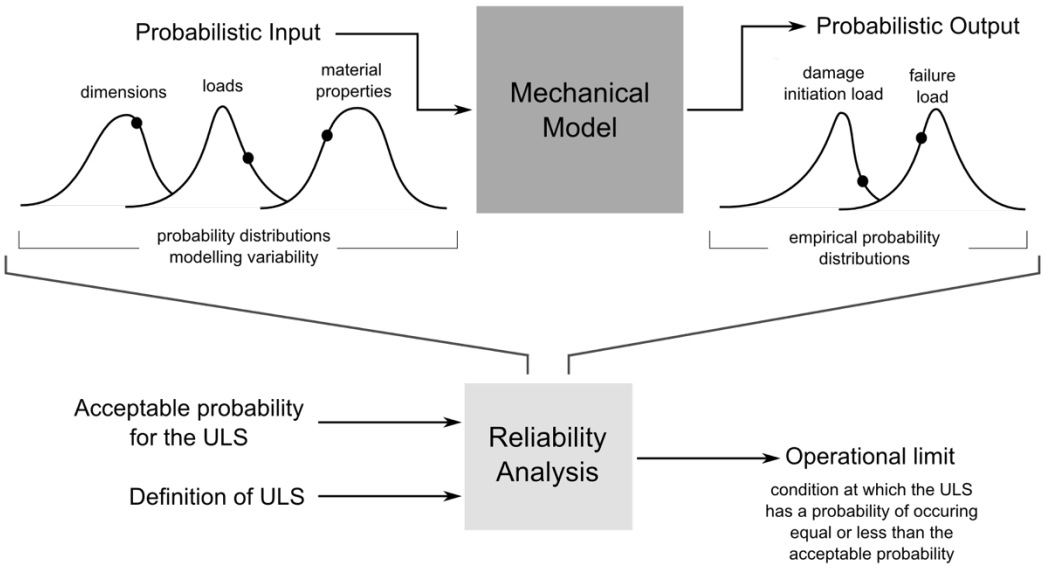

Figure 2.1 Necessary elements for the estimation of operational limits. Dots represent instances of the input and output variables.

From Figure 2.1, it should be clear that the mechanical model is central to the calculation of operational limits. All mechanical models are based on simplifications and assumptions. Some models treat materials as homogenous continuums with isotropic mechanical properties, neglecting anisotropy and variation in mechanical properties throughout the volume, while other models idealize the geometry of the structure. It is important to realize that all models have their limitations, and that their limitations affect the calculation of desired probabilities.

2.3.3 Mechanical models

When loaded in tension or shear, non-unidirectional FRP laminates present a linear elastic response up to a point. Afterwards, the response becomes non-linear. Arguably, the most prominent cause for non-linear laminate behaviour is the progressive degradation of its stiffness due to damage (other causes may be the viscoelastic behaviour of the resin or the stiffening of carbon fibres [22]). As explained in the previous section, the mechanical model of a structure is one of the fundamental elements necessary to calculate probabilities related to its responses. Ignoring the non-linearity caused by the progressive degradation of the laminate stiffness in a mechanical model, or accounting for it in different ways, affect the calculation of probabilities, and consequently, the estimation of operational limits. Using mechanical models that account for progressive degradation ideally results in more accurate estimates[1] of operational limits.

[1]"Accurate estimates" is an oxymoron, as the word "estimate" conveys inaccuracy. Nevertheless, this construction is technically appropriate. Improving the mechanical model improves the accuracy of the methodology for estimating the operational limits.

In the literature, two main damage modes have been associated with the progressive degradation of laminate stiffness: matrix cracking (aka. matrix fracture and inter fibre fracture, transverse cracking) [23-31], and delamination [32-36]. The two of them are progressive, and their development has been linked to not only the material of the plies (e.g. carbon/epoxy unidirectional prepreg), but also to the stacking sequence of the laminate and the thicknesses of the individual plies.

Matrix cracking and its modelling has also been the subject of a very large number of studies [13,31,37-40]. In the literature, two aspects of matrix cracking are treated in opposite ways. The first aspect is the prediction of matrix cracking. Some authors claim that strength-based criteria are capable of predicting its initiation [41,42], while others claim that strength-based criteria are inappropriate [24,31,43]. The latter group base their claims on experimental evidence showing that by reducing the thickness of a ply embedded in a laminate, the laminate stress at which the ply exhibits matrix cracking increases. This is contrary to what a strength-based criterion would predict. A reduction in ply thickness decreases its cross-section area, increasing the stress to which it is subjected to. Reducing the thickness should result in matrix cracking being observed at a lower laminate stress; not at a higher one. The second aspect is regarding the nature of the development of matrix cracks. Some authors treat matrix cracking as a sudden, fully developed event, while other authors treat is as a progressive event (either discrete or continuous) [13]. Experimental results show that in a laminate, matrix cracking is without a doubt a progressive event [23-31]. Treating matrix cracking as a sudden and fully developed event is a convenient simplification, as predicting its development and effects is not easy.

Delamination, being such a clear drawback of the lamination construction, has been the subject of a large number of studies regarding its modelling. Analytical and numerical techniques for modelling its initiation and development are widely available [35,37,38,44,45] with varying degrees of accuracy.

Matrix cracking, and delamination are modes of damage, but they can also be treated as modes of failure. This ambiguity complicates the definition of “laminate failure”. Failure is the state or action of not functioning. For the sake of this discussion, the function of a laminate is to safely carry a load for an extended period of time; therefore, the inability to do so constitutes laminate failure (i.e. the ULS of the laminate). Matrix cracking, fibre fracture, and delamination affect the integrity of the laminate. One could define laminate failure as the state on which any of these damage mechanisms initiate; however, this definition would be very conservative. As mentioned earlier, these damage mechanisms are progressive, and in fact, they may initiate at very low loads compared to the ones where laminates completely fracture [34]. First Ply Failure (FPF) with respect to matrix cracking and fibre fracture, or just fibre fracture, is a common definition of laminate failure [1,43,46,47]. Generally, in this definition, both fibre fracture and matrix cracking are sudden and fully developed events predicted in any of the plies of a laminate through failure criteria.

In DNV's CC, several "structural analyses" are mentioned. The difference between them is the manner in which the progressive degradation of laminate stiffness is accounted for (or disregarded) by mechanical models. The definition of laminate failure depends on the structure and its function. For example, matrix cracking may or may not be acceptable in a pressure vessel depending on whether it has an inner lining or not.

Figure 2.2 presents a sketch of how the different models predict the degradation of the longitudinal stiffness of a laminate when subjected to a uniaxial tensile load. For the linear elastic model and the linear elastic model with full stiffness degradation, the longitudinal laminate stiffness does not change as the load increases. However, they do not exhibit the same longitudinal stiffness. Each of these two models is an extreme. The linear elastic model is non-conservative because it disregards stiffness degradation due to matrix cracking. In contrast, the linear elastic model with full degradation is perhaps too conservative because it exaggerates the stiffness degradation due to matrix cracking. These extremes bound the two models incorporating progressive degradation. The discrete degradation model predicts a step-like degradation with the occurrence of matrix cracking in each of the plies in the laminate. The abrupt loss of laminate stiffness is the result of considering matrix cracking as a sudden and fully developed event. The continuous degradation model predicts an abrupt loss of stiffness followed by for a more gradual reduction. An important aspect is that both of the models with progressive degradation differ not only in the rate of loss of stiffness, but also with respect to the load at which matrix cracking initiates and how it develops.

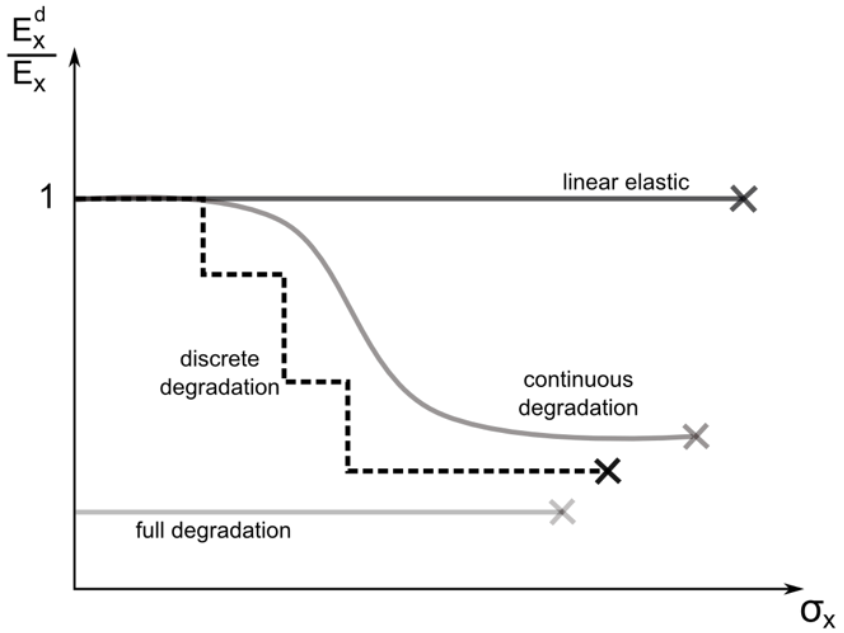

Figure 2.2 Loss of laminate stiffness according to the laminate response models (E_x^d: degraded longitudinal laminate stiffness, E_x: undegraded longitudinal laminate stiffness; "linear elastic" is omitted in most names for clarity). Failure is predicted with the maximum strain criterion; hence, the different failure stresses.

The mechanical models used in the appended papers I, II and III are different. A brief overview all of them follows.

Linear elastic

- The laminate has a linear elastic response up to laminate failure.
- The mechanical properties of the laminate are in pristine conditions until laminate failure. The effects of matrix cracking, delamination, progressive fibre fracture, and all other degradation mechanisms are completely disregarded.

Linear elastic with full degradation

- The laminate has a linear elastic response up to laminate failure.
- The mechanical properties of the laminate are treated as fully degraded by matrix cracking from the beginning. The plies are capable of carrying loads only in the fibre direction. In the model, this is achieved by setting the matrix-dominated thermal and mechanical properties of the plies to 1% of their pristine condition value. The effects of all degradation mechanisms, except matrix cracking, are disregarded.

Linear elastic with progressive *discrete* degradation

- The laminate has a linear elastic response up to matrix cracking in one of the plies.
- Matrix cracking is considered to be a sudden and fully developed event. It can only occur once in each ply.
- Matrix cracking in a ply is predicted with a stress-formulated criterion where a ply embedded in a laminate is considered to crack under the same stress conditions as a stand alone one.
- Matrix cracking in a ply degrades its matrix-dominated thermal and mechanical properties to an amount determined by reduction factors. The degradation is progressive because as the load increases and matrix cracking is predicted in the plies, their mechanical properties are reduced, resulting in a progressive and discrete degradation of the mechanical properties of the laminate.
- Reduction factors are calibrated against experimental laminate stress-strain curves.
- The degradation caused by delamination, progressive fibre fracture, and all other degradation mechanisms, except matrix cracking, is disregarded.
- *Note: This mechanical model is only used in appended paper I where it is referred to as "linear elastic with progressive degradation".*

Linear elastic with progressive *continuous* degradation

- The laminate has a linear elastic response up to matrix cracking in a set of plies.
- Matrix cracking is considered to be a continuous and accumulative event.
- Matrix cracking initiation and development is predicted with a fracture-energy-formulated criterion. The criterion is capable of accounting for the effects that ply thickness and adjacent plies have on the initiation and development of matric cracking.

- Matrix cracking degrades continuously the thermal and mechanical properties of the laminate.
- The degradation caused by delamination, progressive fibre fracture, and all other degradation mechanisms, except matrix cracking, is disregarded.

2.4 Summary of appended papers I, II and III

The papers here summarized were written in a span of several years. Not that the terminology is not consistent throughout the papers. The terminology used in each paper reflects what the authors considered to be the appropriate or best at the time of writing. The section "Central concepts and abbreviations" at the beginning of this thesis (page iii), clarifies the different terms used in the thesis and appended papers.

2.4.1 Paper I: Optimization of composite maritime structures – effects of uncertainties on design criteria and limits

The paper assesses the pros and cons of the linear elastic and the linear elastic with progressive discrete degradation models in deterministic and probabilistic analyses. The linear elastic model with progressive degradation was initially considered as a promising model for motivation of lower model and safety factors. The study case in both types of analyses, deterministic and probabilistic, was a quasi-isotropic carbon/epoxy laminate under biaxial tensile loading. The deterministic analysis compared the laminate response predicted with both models against experimental measurements and maximum allowable strains determined by design rules. The probabilistic analysis compared the probabilities of matrix cracking, predicted with the linear elastic with progressive discrete degradation model, against the maximum allowable strains.

Figure 2.3 presents the results of the deterministic analyses with both mechanical models. In the figure, it is clear that the linear elastic with progressive discrete degradation model matches the experimental measurements better than the linear elastic one. Nevertheless, this model has several flaws and problems. First, matrix cracking seems to be under predicted in all the plies. Second, this mismatch between prediction and experiments is close to the maximum allowable strains, exactly where the model should be accurate. In the probabilistic analysis, the linear elastic with progressive discrete degradation model predicts with almost certainty the occurrence of matrix cracking at strains below the maximum allowed ones.

The main conclusion of this paper was that the linear elastic with progressive discrete degradation model provided no benefits compared to the linear elastic model. The progressive discrete degradation model just ads complexity and uncertainty to the structural analysis, and cannot be used to motivate an increase of the maximum allowed loads. Furthermore, it was recognized that a better model for matrix cracking was necessary.

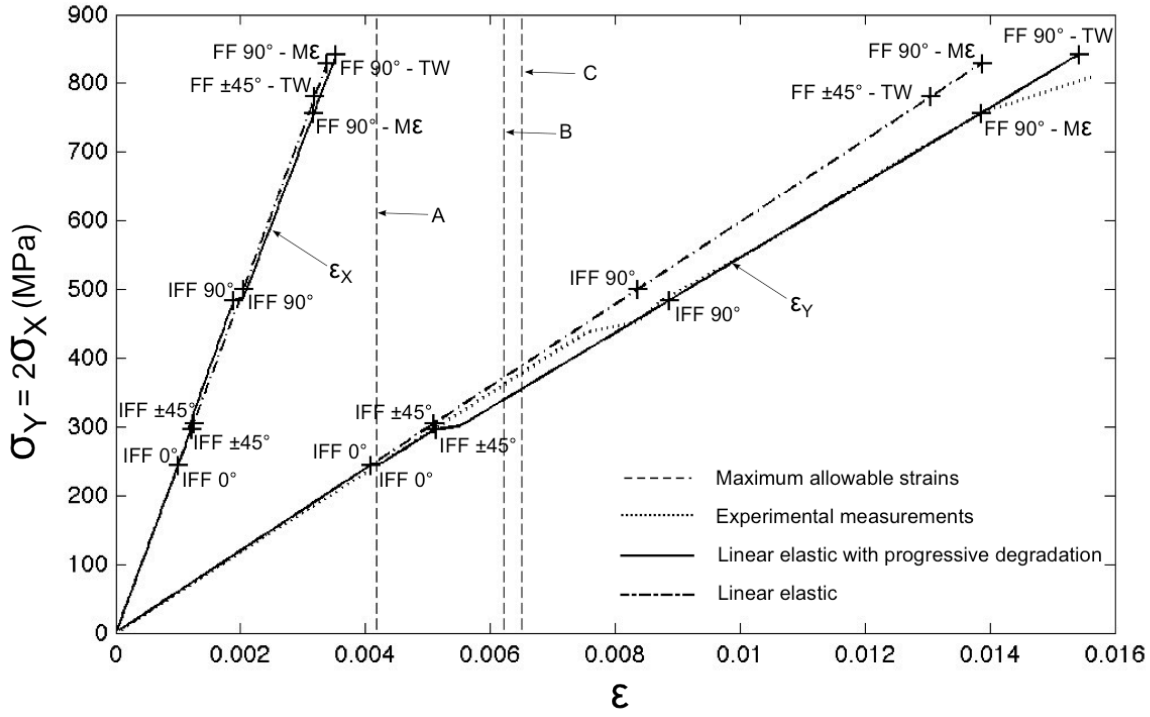

Figure 2.3 Stress-strain response of a quasi-isotropic carbon/epoxy laminate subjected to monotonic biaxial tensile loading. (IFF: Inter Fibre Fracture (matrix cracking), FF: Fibre Fracture, Mε: maximum strain failure criterion, TW: modified Tsai-Wu failure criterion, A: maximum allowed strains as stated in DNV 2010b, B and C: maximum allowed strains as stated in DNV 2010a; for more details, see Paper I).

2.4.2 Paper II: Study on the possibility of increasing the maximum allowable stresses in fibre-reinforced plastics

In this paper, the operational limits of a group of carbon/epoxy cross-ply laminates were estimated through reliability analyses using the linear elastic with progressive continuous degradation model, and via deterministic analyses using the linear elastic model with safety and model factors as stated by design rules. Both sets of operational limits were compared to determine if the operational limits estimated with the design rules methodology were too conservative, and therefore, if higher operational limits can be motivated. Additionally, the operational limits were compared against probabilistic predictions of matrix cracking initiation and development (see Figure 2.4), so as to qualitatively evaluate the suitability of such operational limits. A sensitivity analysis was performed to determine how does the type stochastic modelling of the material properties, used in the probabilistic analyses, affect the estimation of the operational limits.

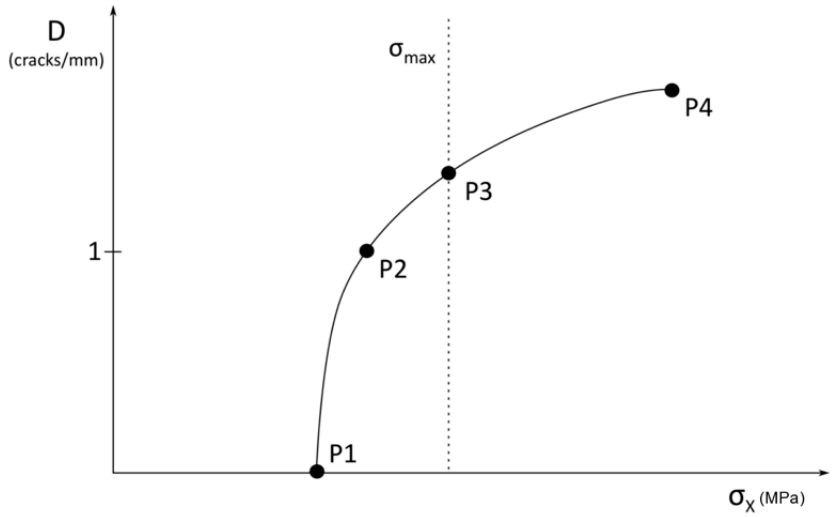

Figure 2.4 Measurements of interest in the average crack density vs. longitudinal stress curve of cross-ply laminate. (P1: stress at matrix cracking onset, P2: stress at matrix cracking density equal to 1 crack/mm, P3: crack density at the maximum allowed longitudinal laminate stress, P4: stress and crack density at the ULS.)

The investigation concluded that the operational limits estimated with the design rules methodology are unlikely to provide the desired safety level. This conclusion was based on two main observations. First, depending on the type of distribution chosen for the ultimate longitudinal tensile strength, the operational limits calculated by means of probabilistic analyses were higher or lower than the ones calculated through the design rules methodology as shown by the two types of boxplot in Figure 2.6 (for a description of the boxplots, see Figure 2.5). Since none of the distribution types can be considered strictly right or wrong, the operational limits estimated with the design rules methodology are in an uncertainty region. Second, the linear elastic with progressive continuous degradation analyses showed that the cross-ply laminates are very likely to present considerably high matrix crack densities at the operational limits. The effects of such high crack densities, beyond the reduction of the thermal and mechanical stiffness of the laminates, were not considered, and therefore, the estimated probabilities of failure at the operational limits are not conservative.

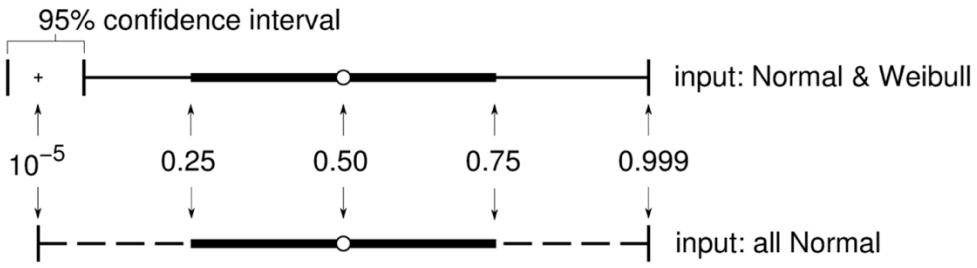

Figure 2.5 Boxplots are used to describe the shape of the distributions of the probabilistic model responses. The left and right whiskers indicate the quantiles where the state has a probability of occurrence equal or less than 10^{-5} and 0.999, respectively. The sides of the box indicate the 0.25 and 0.75 quantiles while the white circle marks the location of the median.

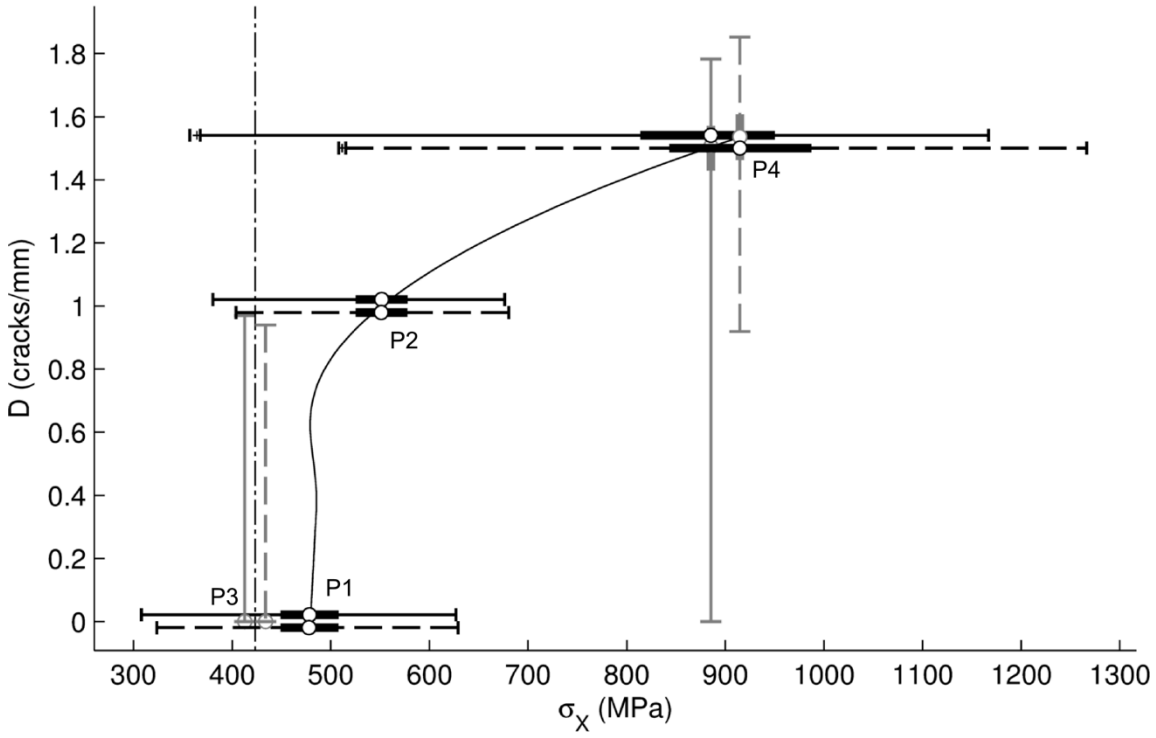

Figure 2.6 Comparison between the deterministic average crack density vs. laminate stress curve of a $[0/90]_S$ carbon/epoxy cross-ply laminate, and the probabilistic response of the measurements of interests indicated in Figure 2.4. (Dashed-dot line indicates the maximum allowable stress determined through DNV's CC.)

2.4.3 Paper III: Influence of mechanical and probabilistic models on the reliability estimates of fibre-reinforced cross-ply laminates

In this study, the operational limits of a number of carbon/epoxy and glass/epoxy cross-ply laminates were calculated with different mechanical and probabilistic models. The objective was to assess the influence of these models on the operational limit.

Figures 2.7 and 2.8 show how the modelling of laminate stiffness degradation and choice of probability distributions affect the estimation of maximum allowable stresses. The estimates in the figures vary mostly not due to the different types of laminate or desired safety level, but due to the mechanical and probabilistic models used in their calculation. Figure 2.7 corresponds to glass/epoxy cross-ply laminates with "first ply failure due to fibre fracture" as the definition of laminate failure. This definition allows for matrix cracking in the laminate, and therefore, for the degradation of the laminate stiffness. Figure 2.8 corresponds to carbon/epoxy cross-ply laminates with "first ply failure due to matrix cracking or fibre fracture". This definition does not allow for the development of matrix cracking. In this figure, it is clear that the most critical aspect of the estimation of the maximum allowable stresses is the mechanical model. The main difference between the two mechanical models is the definition of matrix cracking as a failure. In the linear elastic model with the Tsai-Wu criterion model (TW in Figure 2.8), matrix cracking is a sudden fully developed event which can be predicted with this strength based criterion. In the linear elastic model with progressive continuous degradation model (progD-MS in Figure 2.8), matrix cracking as a failure is a certain crack density considered as unacceptable. This distinction results in widely different reliability estimates.

The study has three major conclusions. First, for laminates with a definition of failure that allows for matrix cracking, mechanical models that account for the progressive loss of stiffness may be useful for motivating higher operational limits than the ones obtained with a full degradation model. Second, for laminates with a definition of failure that does not allow for matrix cracking, the exact definition of "failure due to matrix cracking" is a key on motivating higher operational limits. Third, the choice of probability distributions for the mechanical properties is not trivial.

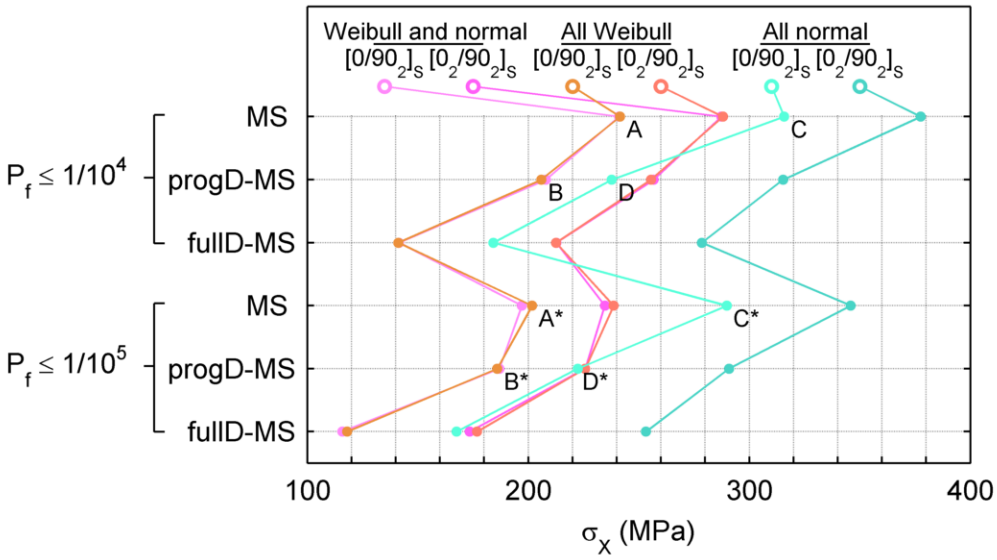

Figure 2.7 Comparison of the maximum allowable stress estimates of two glass/epoxy cross-ply laminates with "first ply failure due to fibre fracture" as the definition of laminate failure. The maximum allowable stresses were calculated for two safety levels ($P_f \leq 1/10^4$ and $P_f \leq 1/10^5$) with three different sets of probability distributions ("All Weibull", "Weibull and normal", and "all normal"), and three different mechanical models (linear elastic: MS, linear elastic with progressive continuous degradation: progD-MS, and linear elastic with full degradation: fullD-MS).

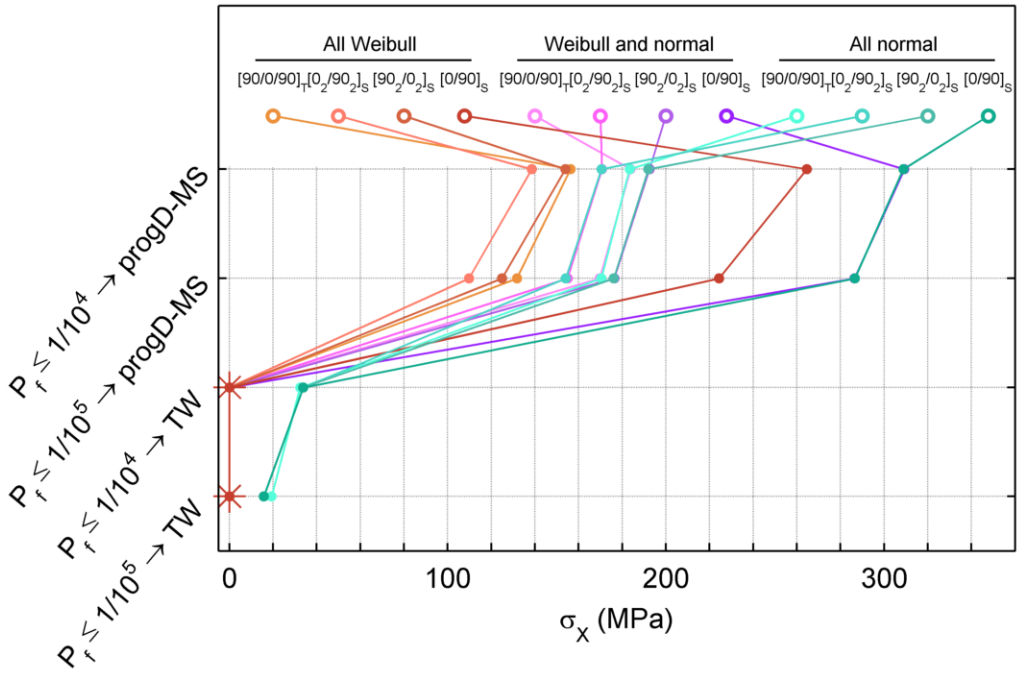

Figure 2.8 Comparison of maximum allowable stress estimations of four carbon/epoxy cross-ply laminates with the "first ply failure due to matrix cracking or fibre fracture" as the definition of laminate failure. The maximum allowable stresses were calculated for two safety levels ($P_f \leq 1/10^4$ and $P_f \leq 1/10^5$) with three different sets of probability distributions ("All Weibull", "Weibull and normal", and "all normal"), and two different mechanical models (linear elastic Tsai-Wu: TW, and linear elastic with progressive continuous degradation: progD-MS).

2.5 Concluding remarks

The work presented in this chapter aimed at exploring the possibility of motivating higher operational limits for marine composite structures through reliability analyses. All the investigations focused on the probabilistic response of the material, since compared to the loads, material response is a much more common element in different structures. Furthermore, in all the investigations, matrix cracking and loss of laminate stiffness was a central theme, because these two interconnected events on the response of a composite laminate are generally dealt with crude simplifications. Modelling the progressive development of matrix cracking and loss of stiffness held promise of gains in material optimization.

Arguably, the most significant contribution of this work is that it demonstrates how frail and uncertain are strength reliability analyses of FRP laminates in tension. Changes in material and layup, factors which one can be certain of, have a relatively small effect on the estimated operational limits compared with changes in the mechanical and probabilistic models, and definition of laminate failure. Of these three high influence factors, probabilistic modelling is the most prominent one. The appended papers II and III show that the choice of probability distributions is not trivial. A very large number of investigations have dealt with the question of assigning probability distributions to the mechanical properties of FRPs. Nevertheless, despite decades of research, there is no consensus on which probability distributions should be

used. Considering that in a structure very low probabilities of failure are sought, and how sensitive are strength reliability analyses of FRP structures to probability distributions, engineers should be conservative and use the Weibull distribution for strength properties. Furthermore, a sensitivity analysis should be a requirement for the acceptance of the results of any kind of reliability analysis.

Can higher operational limits for composite marine structures be motivated through reliability analyses? Maybe. The investigations presented in this chapter are not exhaustive. Despite that for the analysed cases higher operational limits could not be motivated, there is the possibility that for other cases the conclusion might be the opposite. The second most significant contribution of this work is the identification of the uncertainties that highly influence strength reliability analyses of FRPs. If these uncertainties are resolved, significant increases in material utilization could be achieved.

Characterization

The process of determining the nature or features of something.

3 Characterization of Mechanical Properties

Material characterization is the procedure of determining the probabilistic characteristics of the properties of a material. Essentially, the procedure consists of experimentally measuring the properties of a representative sample of material specimens, and subsequently, determining their probabilistic characteristics through statistical inference. The probabilistic characteristics of a material property are central to deterministic and probabilistic structural design. In a deterministic structural design, they are used to determine the design values used to dimension the structure.

Material properties are fundamental information in all structural analyses. Whether the analyses are deterministic or probabilistic, disregard degradation or consider it, predict structural failure or only deformation, material properties are always a necessary input. A mechanical model is only as good as its input. If the input does not represent reality, neither will the predicted response.

In some cases, it may be difficult to determine the properties of a material (as well as the characteristics of a load, and the exact geometry of a structure with all its imperfections). For these cases, approximate values must be used. If the mechanical model is not sensitive to the approximate inputs, one can be confident that the predicted response will match reality to an extent sufficient to make it useful, despite the uncertainty of some of the model inputs. Unfortunately, the sensitivity of mechanical models is both a blessing and a curse. If the inputs to which the model is sensitive are the uncertain ones (e.g. the ultimate strength of the material), small changes in their values will lead to large changes in the predicted structural response. The sensitivity of a mechanical model to material properties make their accurate determination of great importance, as small changes may lead to great gains or losses in material utilization. Reducing the scatter of a material property can strongly

influence its design value in a deterministic analysis (or its probabilistic modelling in a reliability analysis), potentially allowing for lighter and cheaper structure designs.

This chapter begins with a short background of the experimental work carried out in this PhD project (Section 3.1) and its objective (Section 3.2). Section 3.3 contains an introduction to Non-Crimp Fabric (NCF) composites and their characterization. The purpose of this section is to facilitate the understanding of the work presented in this chapter for readers unfamiliar with NCFs and characterization methods. Next the experiments and testing methodologies are thoroughly described (Section 3.4), and the results analysed (Section 3.5). Both the description and analysis of the experiments include mistakes and failures, to hopefully serve as a valuable reference for experimental researchers. Finally, concluding remarks are presented in Section 3.6.

3.1 Background

FRP structures can be weight and cost optimized by tailoring the mechanical properties of the laminates to the loads they are meant to carry. In its simplest form, tailoring consists of selecting the type of fibres and resin, as well as ply stacking sequence, number, orientation, and thicknesses (further tailoring could include manufacturing process). Transverse and longitudinal stiffeners are a good example of tailoring. The flanges of these components are meant to carry mainly uniaxial tensile and compressive loads, so most of the fibres in the laminate of the flange are oriented in the load direction. Tailoring the laminates requires that in the preliminary design of an FRP structure, a wide range of laminates under a number of loading conditions can be evaluated; therefore, the prediction of laminate design values is an important step on the preliminary design of an FRP structure. It is impractical to perform mechanical tests with the sole purpose of determining design values for *candidate* laminates. While access to large databases of laminate test measurements relieves the dependence on predictions, databases are unlikely to substitute predictions entirely, as the possible combinations are nearly infinite.

Predictions of laminate mechanical properties are calculated through the mechanical properties of individual plies, mechanical models and failure criteria. The mechanical properties of a ply are determined through standardized testing, and along with the layup of a laminate, are used as input values for the mechanical models and failure criteria. The fundamental assumption is that a ply can be considered as a “building block” whose properties are neither dependent nor affected by the laminate architecture (i.e. a “standing alone” ply behaves in the same way as an identical one embedded in a laminate) [43,46]. This approach enables the prediction of the mechanical properties for a large number of laminates from a relatively small amount of mechanical tests.

Unfortunately, the predictions are not always useful. While the elastic properties of an undamaged laminate can be predicted fairly accurately, damage, degradation and failure remain a challenge [14-16,48]. This statement is true for prepregs and textile composites. For example, the first worldwide failure exercise evaluated a large number of failure theories, and the results were sobering. None of the evaluated failure criteria could predict the final failure of multidirectional laminate within ±10% in more than 40% of the cases [14]. In the second world wide failure exercise, the evaluated failure

criteria did not perform much better. The best failure predictions were only within ±10% of the experimental value in 30% of the test cases [15]. Even though great efforts have been made in the modelling of damage and degradation [13], there is still no widely accepted model for prepregs [16]. The situation for NCF composites is significantly more complex [48]. The resin pockets and fibres distortions caused by the stitches complicate the analyses. The most recent models for predicting degradation and failure of NCF composites rely on detailed finite element simulations of its meso-structure. Unfortunately, this type of analyses are not a silver bullet. While the results are promising, their predictions do not generally match the experimental observations [48,49], and furthermore, their calculation time and complexity makes them unsuitable for the design of unique components (i.e. components that will be built a number of times that do not justify large costs associated with their design).

Because of the poor performance of laminate degradation and failure models, predictions based on ply properties are used, in most cases, only for preliminary structural design. The qualification and approval of an FRP structure design requires a certain degree of certainty that these predictions cannot provide. In DNV's HSLC, the approval of a structure requires that the laminate design values are determined through mechanical testing, while DNV's CC does allow for laminate design values based on ply properties, as long as conservative values are used.

The mechanical properties of FRP plies and laminates are not easy to characterize. The heterogeneity, anisotropy, and layered construction of the material lead to a number of practical and theoretical challenges that are not encountered when characterizing metals (and arguably any other homogenous and isotropic materials). Nevertheless, the standard techniques and devices used to characterize the in-plane properties of FRP laminates are the same ones used to characterize metals: load rig, grips or fixtures, bonded strain gauges, and physical extensometers. For decades, these devices have been used for characterizing FRPs. Any improvement in the characterization of FRPs will consequently improve the predictions of laminate mechanical properties based on ply properties (generally used for preliminary design) and the experimentally determined laminate properties (generally used for final dimensioning and approval).

3.2 Objective

Chalmers University of Technology and SP Technical Research Institute of Sweden (SP) have a good cooperation in research and education. Knowing that mechanical models of FRP laminates are sensitive to stiffness and strength values (appended papers II and III), and that matrix cracking initiation and development play an important role in the utilization of FRPs (appended papers I, II, and III), both parties identified the following experimental research question of common interest:

Can higher material utilization of FRPs be achieved through non-standard measuring techniques?

The term “non-standard measuring techniques” is clearly subjective. In this text, it refers to techniques not explicitly described in characterization standards for FRPs [50,51]. Considering the findings of the work presented in Chapter 2, higher material utilization would be the result of any of the following three scenarios:

1. Non-standard measuring techniques lead to higher mean values for the laminate stiffness, ultimate stress, and/or ultimate strain.
2. Non-standard measuring techniques lead to lower scatter in mechanical properties.
3. Non-standard measuring techniques lead to less conservative allowances for matrix cracking initiation and development.

If it can be shown that the mechanical properties of a laminate are better than the ones determined through standard measuring techniques (i.e. the laminate is actually stiffer, stronger, less prone to degradation, or more tolerant to it), then higher loads would be admissible on the laminate, meaning higher material utilization. If it can be shown that the scatter in mechanical properties is lower, smaller resistance safety factors may be used in deterministic structural analyses, or probability distributions with lower spread may be used in reliability analyses. Both options lead to higher operational limits.

3.3 Introduction to non-crimp fabrics and their characterization

3.3.1 Non-crimp fabric laminates

The economical and practical advantages of NCFs have made them an attractive structural material for a large number of industries: aerospace manufacturing companies are substituting prepregs with NCFs [52,53]; wind turbine blades, recreational boats, and naval composite vessels, are commonly manufactured with NCFs; and even a mass produced composite car incorporates NCFs [54].

NCFs are a type of FRP manufactured by impregnating a textile preform sheet, known as a non-crimp fabric, with a resin. The term “NCF” can be considered to encompass a wide range of textile preforms with small fibre crimp. In this work, NCF refers exclusively to “multi-axial multiply warp knitted fabrics”. In the literature, NCF composites are also called “stitched composites”, while the NCF textile preform is also called “NCF mat”, “stitched preforms” and several other variations. Clearly, the terminology is not rigorous, so to avoid confusions, the NCF textile preform will be henceforward exclusively referred to as “NCF mat”, and all other mentions of “NCF” will refer to the composite laminate.

NCF mats consist of fibre tows stitched together into several layers, each of which may have their own orientation. Figure 3.1 presents a diagram of the construction of a bi-axial NCF mat. The stitched and layered construction has two main effects: it lowers the manufacturing cost compared to a laminate built with unidirectional prepregs, and results in similar or slightly worse in-plane stiffness and strength than unidirectional prepregs [55,56].

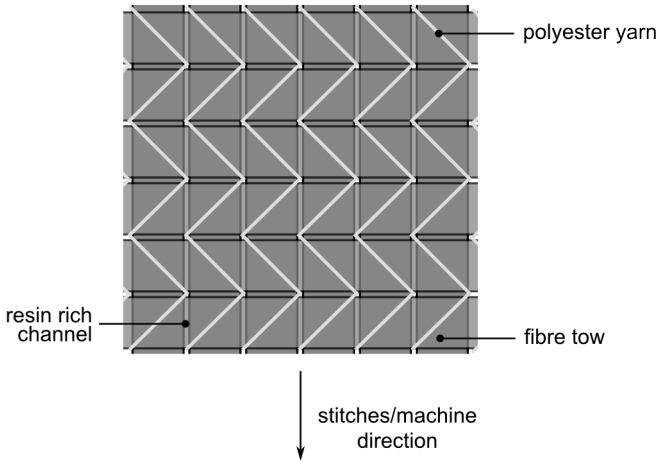

Figure 3.1 Diagram of a bi-axial NCF mat.

A unidirectional prepreg ply is a thin arrangement of fibres embedded in a thermoset resin and aligned in a single direction. As raw materials, prepregs are sold with the thermoset resin partially cured. The name prepreg is a contraction of the adjective "pre-impregnated", as in "resin pre-impregnated fibres". For unidirectional prepregs, having the fibres pre-impregnated eases their handling (dry loose fibres are very difficult to handle), and to a large extent, guarantees good and consistent mechanical properties. Since the fibres are not free to move, resin rich areas cannot be formed and the fibres cannot crimp or curl. The first inconvenience regarding the manufacturing of laminates out of unidirectional prepreg plies is that as raw materials they require refrigeration. Once initiated, the curing processes of the thermoset resin cannot be halted; it can only be slowed-down through cold temperatures. Since the curing process can only be slowed down, raw prepregs have a shelf life. The next inconvenience of unidirectional prepregs is that they do not drape very well. In composites manufacturing, the drapeability of a raw material (whether it is a unidirectional prepreg, a NCF mat, or a chopped-strand mat) is the ease to which it takes the form of the mould. Another inconvenience is that to obtain the best mechanical properties, prepregs must be cured in an autoclave (a high pressure oven), limiting the component to the size of the autoclave. The high acquisition cost of the unidirectional prepregs, the necessary refrigerated storage, the shelf life of the plies along with the slow manufacturing, makes unidirectional prepregs an option sensible only for very high end products (e.g. sport cars) or vehicles that greatly benefit from weight reduction and require very tight quality controls (e.g. airplanes and spaceships).

On the other side of the spectrum, FRPs manufactured through "spray-up" are perhaps the cheapest alternative, at the cost of significantly worse mechanical properties compared to laminates built with unidirectional prepregs. The spray-up manufacturing process consists of spraying chopped strands of glass fibre and uncured resin with an air gun on a open mould. After spraying, the surface is compressed manually with rollers to remove as much air as possible before the resin cures. The end result is an FRP with relatively low aesthetic and mechanical properties, caused by the relatively "short" length and random orientation of the fibres, the large variation in skin thickness and fibre content across the surface, and the extensive presence of air pockets. The low-end mechanical properties make spray-up FRPs suitable only for low

performance structural components with complex shapes (e.g. boat). The same arguments can be used for FRPs made out of chop-strand mat and manufactured through hand-layup.

Arguably, NCFs have a good balance between manufacturing price and mechanical performance [20]. Usually, NCFs are manufactured through vacuum infusion. Vacuum infusion consists of stacking up NCF mats on a mould and placing an infusion mesh and a bag on top of them. The infusion mesh facilitates the flow of resin throughout the component, improving the impregnation of the fibres. The bag is sealed at edges of the mould and used along a vacuum pump to remove as much air as possible from the NCF mats. Once a negative pressure is achieved in the mould, the vacuum is used to suck the uncured resin out of its container and into to mould, impregnating the fibres. Once the fibres are impregnated, the vacuum pump is stopped and the NCF is left to cure at atmospheric pressure and generally, room temperature. Compared to laminates built with unidirectional prepregs, the manufacturing tools for NCF laminates are significantly cheaper, and the manufacturing process is considerably less labour intensive. Additional advantages of vacuum infused FRPs are the low investment cost for manufacturing tools compared to prepregs (e.g. refrigerators and autoclave vs. vacuum pump and disposables), as well as the lower health risks compared to FRPs manufactured through hand-layup or spray-up (e.g. air emissions of styrene, direct contact of the workers with the resin).

The in-plane stiffness and strength of NCF laminates are different from the ones of laminates built with unidirectional prepregs for a number of reasons. In a NCF laminate, the fibres are neither perfectly aligned, evenly distributed, nor straight, as in a unidirectional prepreg. First, since the fibres are grouped into tows, a resin rich pocket sometimes referred to as a “channel” forms between the fibre tows [57]. Second, contrary to its name, non-crimp fabric mats do exhibit some crimp. Crimp is the difference in distance between the total length of a fibre and the length of the fibre in the fabric preform. So a crimped fabric is a distorted one. The slight distortion of the fibre tows forms resin pockets around the stiches [56,57]. Different stitching patterns are used depending on the number of reinforcing fibre layers, their area weight, and their orientation. The stitching pattern, tension and length, as well as the width of the stitching yarn determine the number and magnitude of fibre distortions, as well as the number a size of the resin pockets.

A large number or studies have compared the mechanical properties of NCFs and their non-stitched equivalents: laminates with exactly the same characteristics (e.g. fibre and resin types, curing process of the resin, etc.) with the exception of the presence of stitches. Regarding stiffness and tensile strength of unidirectional laminates, some studies indicate a reduction, some an increase, and some an equivalence [56]. Fibre misalignment and fibre volume fraction are considered to be the mechanisms governing the differences. Regarding compressive strength, nearly all studies suggest a reduction [56]. Shear strength of angle-ply laminates has been shown to depend on the stitching direction, possibly because the stitches prevent the free rotation of the fibre tows in the machine direction [58]. In all these investigations, fibre volume fraction, resin pockets, and fibre distortions are possible sources for the reduction in mechanical properties.

3.3.2 Characterization of fibre-reinforced plastics

Overall the methods for characterizing the elastic and strength properties of FRP laminates require four basic elements: a material specimen, grips or fixture, a testing machine, and a strain measuring device. The grips or fixture transfers the load applied by the testing machine to the material specimen in a way that it results in a desired loading condition, while the strain measuring devices captures the response of the material specimen. The grips or fixture and the shape of the material specimen are tightly related to the property being measured. The elastic and strength in-plane properties of FRP laminates in tension and shear can be determined by measuring the deformation of specimens shaped like coupons under a tensile load [50,51]. A coupon is a rectangular laminate conformed of several plies oriented at predefined directions. Arguably, for these type of tests, common strain measuring devices are bonded strain gauges and physical extensometers [59]. In the literature, bonded strain gauges are usually referred to as "strain gauges". In this text, the adjective "bonded" is added for clarity, as in this text, the strain measurements and the gauge sizes of bonded strain gauges and extensometers are widely discussed. The term "extensometers" covers a wide range of devices, some of which require physical contact between the device and the material specimen (e.g. clip-on and bi-axial extensometers) and some which do not (e.g. video extensometers) [60]. In this text, "physical extensometers" refers to the devices that require physical contact.

The characterization of FRPs is by no means straightforward. Test standards recognize that the characterization of FRP requires craftsmanship [50]. The anisotropic mechanical properties and heterogeneous micro- and meso-structure of FRPs are factors that make characterization difficult. The sources of variability in the measurement results of mechanical properties can be divided into two groups: test specimen and test setup.

The manufacturing of the coupons consists of several steps that may influence their performance. The coupons must be thick enough to be gripped and comply with testing standards [50]. This requires more than one unidirectional prepreg ply or NCF mat, and therefore, single plies or NCF mats cannot be characterized. Thus, thickness may be a factor influencing the measured mechanical properties of unidirectional prepreg plies or NCF mats. The stacking of plies or NCF mats bring another source of variation. The plies and NCF mats forming a laminate need to have their fibres oriented in a certain direction. Depending on the layup, small changes in orientation could lead to reductions of the effective load bearing fibres in the coupon (see Figure 3.2) [61]. Cutting the coupons is yet another possible source of variability. Common cutting methods are diamond saws and water jets [50,59]. The roughness of the coupon edges is a factor that can affect the performance of the coupon [59]. It is therefore necessary to smoothen the edges of the coupons after the cutting process (especially for diamond-cut coupons).

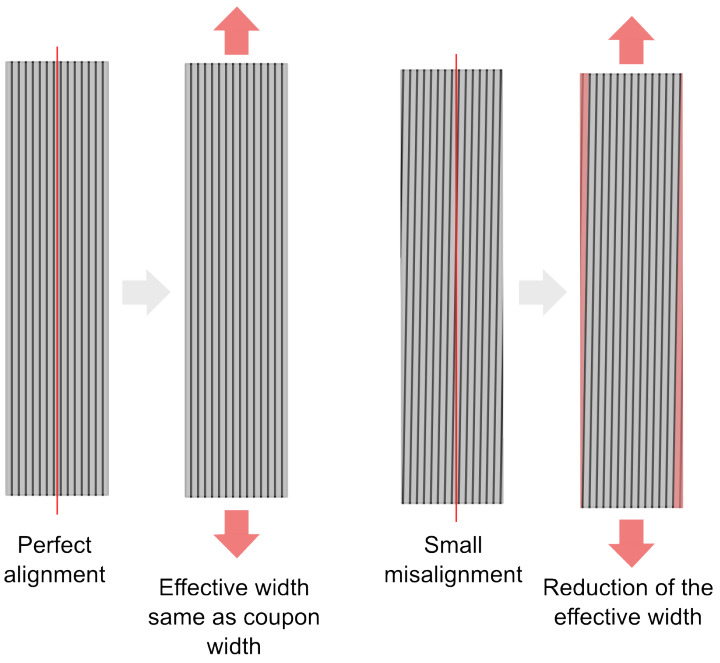

Figure 3.2 Reduction of the effective load bearing fibres due to fibre misalignment.

The test setup is another important source of variability. The adequate method for gripping coupons has been extensively researched without reaching consensus. Tabs are recommended for certain types of tests, but the their design varies extensively in the literature [59,61]. Test standards leave the use of tabs to the criterion of the tester [50]. The type of grips used by the load rig can also affect the results of the test. Pressure grips hold the coupon with the same pressure throughout the test, while wedge action grips increase the pressure of the grip as the testing load increases. FRPs are not particularly strong in the through thickness direction, and can therefore be damaged easily by the grips. Damage at the grips will without a doubt affect negatively the performance of the specimen.

Characterization of NCFs uses the same standardized tests, tools and techniques used for unidirectional prepregs. No modifications of the testing procedure or the analysis of the results are mentioned in testing standards [50,51] or in design rules and standards [1,2]. This denial or disregard for the differences between laminates built with unidirectional prepregs and textile laminates in characterization methods will be shown to be questionable in Section 3.6.

3.3.3 Design values

According to the design rules [2,18,62] the average value of a sample of experimentally measured material properties is the design value for the laminate mechanical property in question. As stated in Chapter 1, the design values are the material property values used along safety factors to determine the operational limits. The sample average for a material property is a reasonable definition since the average of a sample of instances of a variable is a measure of its central tendency. One could claim that this definition of design value is non-conservative, as lower values than the average may be observed. However, the resistance safety factors to be used with the design value account for this. For strength properties, another possible definition for a design value is as a quantile of a probability distributions deemed to represent its variability [1,46]. The probability

distribution is deemed as representative through statistical analyses performed on the sample of experimentally measured strength values.

3.4 Experiments and techniques

Two non-standard measuring techniques were explored: Digital Image Correlation (DIC) and Acoustic Emission (AE). To determine whether they could lead to higher material utilization, these non-standard measuring techniques were used in the characterization of a series of NCF laminates. This section is organized as follows. First, the non-standard measuring techniques are introduced, Second, the characterization tests are presented and motivated. Third, experimental setups and post-processing methods are described.

3.4.1 Introduction to non-standard measuring techniques for characterization

3.4.1.1 Acoustic emission system

An Acoustic Emission (AE) is a transient elastic wave that radiates from a specific location within a material as the result of a sudden release of strain energy due to a micro-structural change. Occasionally, AEs are intense enough and within the right frequency range to be audible by the human ear without the assistance of a device. This is the case of cracking wood, chips, spaghetti, glass, and even bending steel (at least in the movies). In all other occasions, AEs are inaudible. Either their frequency is out of the audible range of the human ear, their intensity is too low, or both.

An AE *system* is essentially an audio recorder tailored for high frequency, low intensity AE. The basic components of an AE system are: coupling medium, sensor (microphone), pre-amplifier and filter, and processing unit. The coupling medium facilitates the transmission of AE from the material to the sensor, which then transforms the elastic wave into an electrical signal. The signal is filtered to eliminate background noise that is irrelevant to the detection of microstructural changes in the material. The amplification is necessary so that the processing unit can register the signal. Some AE systems can record the filtered signal as it is (the complete waveform); however, this is seldom done. AE systems have a very high sampling rate to capture high frequency AE, and therefore, the sizes of the files containing the complete waveforms can be very large (in the order of gigabytes). Large files are difficult to analyse, so in most cases, the waveform is summarized according to a set of characteristics defining an AE *event*.

In FRPs, AEs can be related to the formation of cracks. Ideally, an AE system enables the detection of damage initiation and development, the differentiation between possible damage phenomena (e.g. fibre fracture, matrix cracking, and delamination), and the location of the damage within the material. Theoretically, the detection of damage initiation and development is possible by relating them to AE events with certain characteristics [63]. The challenge is to determine which AE event characteristics relate to the different damage events. The details of the AE system used in our studies are presented in Section 3.4.3.4.

3.4.1.2 Digital image correlation system

Digital Image Correlation (DIC) is an optical method for measuring the 2D or 3D position and displacement of points on a surface. Each surface point is identified through a facet–a rectangular area of a pre-defined size (typically 15x15 pixels) containing a particular distribution of grey-scale pixels. As the surface deforms, so does the facets. The DIC system manages to individually recognize the facets because the distribution of grey-scale pixels within a facet is the same in the deformed and undeformed state. Besides calculating the position and displacement of points on a surface, DIC systems are capable of estimating the strain in a facet by calculating a deformation tensor from the displacement of the facets adjacent to the studied one.

Compared to bonded strain gauges and physical extensometers, a DIC system is an advanced measuring technique because it allows for the study of the deformation of a whole surface at a local level. The measurements obtained from a DIC system are more than equivalent to hundreds or thousands of bonded strain gauges or physical extensometers. At a given instance, a physical extensometer or a bonded strain gauge renders only one measurement: strain in the gauge direction. In contrast, a DIC system renders for all the facets it recognizes: their current location in a 2D or 3D global coordinate system, their displacement with respect to the previous or initial measurement, the strains in the global coordinate system, the magnitude and direction of the major and minor strains, and more. Clearly, the amount of information obtained from a DIC system is extensive. The challenge is to make it useful. The details of the DIC system used in our studies are presented in Section 3.4.3.3.

3.4.2 Series of mechanical tests

The mechanical tests here presented aimed at obtaining the mechanical properties of an ideal NCF ply and a quasi-isotropic NCF laminate. The adjective “ideal” is used to emphasize that a ply does not exist as such in NCFs. A ply is a thin arrangement of fibres in a single direction [47], and a single NCF mat is much more complex than a single ply.

The following sections contain descriptions of the NCF laminates tested: type, test standard, construction, as well as the motivation behind their testing. In this chapter, a set of NCF laminate specimens is referred to as a “Series” followed immediately by an identification number. The purpose of this referencing system is to facilitate the distinction between general terms (e.g. quasi-isotropic laminates) and the particular laminates here described. It also makes the text more concise. Despite their differences, all the NCF laminates presented have the following common features:

- **Manufacturing method:** vacuum infusion.
- **Manufacturer of the laminates:** SAAB Kockums.
- **Fibre volume fraction:** approximately 0.5.
- **Resin:** Reichhold DION 9102-501 vinylester.
- **Fibre:** Toray 700S carbon fibre.
- **Cutting method:** waterjet.

3.4.2.1 Series 1: $[0]_T$ Unidirectional laminate

- **Purpose:** Determine the in-plane tensile stiffness and strength of a NCF carbon/vinylester ideal ply in the fibre direction.
- **Testing standard:** ASTM D3039 standard.
- **Testing setup:** General setup (see Section 3.4.4.1).
- **Layup:** Symmetrically stack of two *L(X) 440-C10* NCF mats. Each *L(X) 440-C10* NCF mat has two layers of carbon fibres at 0° and two layers of E-glass fibres at ±45° respectively for stabilizing the textile. The NCF mats were stacked so the stabilizing glass-fibres were on the *outside* of the laminate.
- **Orientation:** The 0° direction of both NCF mats were aligned with the longitudinal direction of the coupon.
- **Coupon width:** 15 mm (chosen so that the breaking load did not exceed the capacity of the testing machine).
- **Coupon thickness:** Approximately 1 mm.
- **Coupon length:** 280 mm.

3.4.2.2 Series 2 $[90]_T$ Unidirectional laminate

- **Purpose:** Determine the in-plane tensile stiffness and strength of a NCF carbon/vinylester ideal ply in the direction perpendicular to the fibre direction.
- **Testing standard:** ASTM D3039 standard.
- **Testing setup:** General test setup (see Section 3.4.4.1).
- **Layup:** Symmetrically stack of two *L(X) 440-C10* NCF mats. Each *L(X) 440-C10* NCF mat has two layers of carbon fibres at 0° and two layers of E-glass fibres at ±45° respectively for stabilizing the textile. The NCF mats were stacked so the stabilizing glass-fibres were on the *inside* of the laminate.
- **Orientation:** The 90° direction of both NCF mats were aligned with the coupon's longitudinal direction.
- **Coupon width:** 25 mm.
- **Coupon thickness:** Approximately 1 mm.
- **Coupon length:** 140 mm.

3.4.2.3 Series 3: $[90/0]_S$ Cross-ply laminate

- **Purpose:** Determine the in-plane tensile strength of a NCF carbon/vinylester ideal ply in the fibre direction.
- **Testing standard:** Did not follow a standard; it followed [61]. According to the referenced sources, backing-out the ultimate stress and strain from a cross-ply laminate results in higher and more representative values than the ones obtained from a stand-alone ply (as in ASTM D3039).
- **Testing setup:** General test setup (see Section 3.4.4.1).
- **Layup:** Symmetrical stack of two *LT 450-C10-C* NCF mats. Each *LT 450-C10-C* NCF mat has two layers of carbon fibres, one at 0° and one at 90°, both with the same area weight.
- **Orientation:** The 0° direction of both NCF mats were aligned with the coupon's longitudinal direction.
- **Coupon width:** 25 mm.
- **Coupon thickness:** Approximately 1 mm.
- **Coupon length:** 280 mm.

3.4.2.4 Series 4: $[90/0]_{4S}$ Cross-ply laminate

- **Purpose:** Determine the in-plane compression strength of a NCF carbon/vinylester ideal ply.
- **Testing standard:** ASTM D6641 standard.
- **Testing setup:** Not described in this document.
- **Layup:** Symmetrical stack of eight *LT 450-C10-C* NCF mats. Each *LT 450-C10-C* NCF mat has two layers of carbon fibres, one at 0° and one at 90°, both with the same area weight.
- **Orientation:** The 0° direction of both NCF mats were aligned with the coupon's longitudinal direction.
- **Coupon width:** 15 mm.
- **Coupon thickness:** Approximately 3.7 mm.
- **Coupon length:** 250 mm.

3.4.2.5 Series 5: $[-45/+45]_{2S}$ Angle-ply laminate

- **Purpose:** Determine the in-plane shear modulus and ultimate shear strain and stress of the NCF carbon/vinylester ideal ply.
- **Testing standard:** ASTM D3518 standard.
- **Testing setup:** General test setup (see Section 3.4.4.1).
- **Layup:** Stack of two *DB 420-C05* NCF mats. Each *DB 420-C05* NCF mat consists of two layers of carbon fibres, one at +45° and one at -45°, and a 90° layer of E-glass fibre as a stabilizer.
- **Orientation:** The 0° of the first NCF mat was aligned with the longitudinal direction of the coupon, while the 0° of the second NCF mat was aligned with the transverse direction. Neglecting the E-glass layer, the result is a symmetrical NCF laminate. However, if the E-glass layer is considered, the result is an asymmetrical laminate. Another characteristic of this layup is that the stitches of one NCF mat run in the longitudinal direction, while the stitches of the other NCF runs in the transverse direction. This asymmetry was accidental. The stitches should have been in the same direction.
- **Coupon width:** 25 mm.
- **Coupon thickness:** Approximately 1.8 mm.
- **Coupon length:** 280 mm.

3.4.2.6 Series 6: $[90/-45/0/+45]_{2S}$ Quasi-isotropic laminate

- **Purpose:** Determine the in-plane stiffness and strength of this quasi-isotropic carbon/vinylester NCF laminate in the longitudinal direction.
- **Testing standard:** ASTM D3039 standard.
- **Testing setup:** General test setup (see Section 3.4.4.1).
- **Layup:** Symmetrically stack of four *DBLT 800-C05* NCF mats. Each *DBLT 800-C05* NCF mat consists of four layers of carbon fibres with the orientations 0°, +45°, 90°, -45°.
- **Orientation:** The 0° of all the NCF mats was aligned with the longitudinal direction of the coupon.
- **Coupon width:** 25 mm.
- **Coupon thickness:** Approximately 3.7 mm.
- **Coupon length:** 280 mm.

3.4.2.7 Series 6 (2nd Round): $[90/-45/0/+45]_{2S}$ Quasi-isotropic laminate

This laminate in this series is identical to the one in the original Series 6. The test setup was modified to allow for a larger field of view for the DIC system and measurements with a video extensometer.

- **Purpose:** Compare DIC system and video extensometer measurements.
- **Testing setup:** Special test setup for 2nd round of Series 6 (see Section 3.4.4.3).

3.4.3 Equipment

3.4.3.1 Testing machines

With the exception of Series 1, all the coupon series were tested in an Instron 1341 servohydraulic testing machine with a 100 kN load cell. Series 1 had to be tested in an Instron 1273 servohydraulic testing machine with a 250 kN load cell in order to be able to break them. The testing machine with the 250 kN load cell was not used for all the coupons in order to have better load reading accuracy.

3.4.3.2 Fixtures and grips

The Instron 1273 and 1341 testing machines use hydraulic grips to seize the test specimens. An important feature of this type of grips is that as the grips close, a small longitudinal tensile load is applied to the test specimen. This characteristic plays an important role in the post processing of the measurements and on the fracture of the Series 2 coupons.

Series 1 required the manufacturing of special fixtures since the Instron 1273 testing machine did not have grips capable of seizing 1 mm thick specimens. The special fixtures were manufactured out of aluminium (see Figure 3.3). Through trials, it was determined that neither tabs nor emery cloth were necessary to prevent slippage or fracture of the grips.

Series 2 was tested in two rounds. In the first one, the coupons were gripped with standard flat serrated grips (see Figure 3.4). The DIC system measurements showed that the longitudinal tensile load applied by the grips upon closure damaged the coupons. For the second round, the Series 2 coupons were “gripped” by dipping them in steel profile filled with glue (see Figure 3.7). This procedure ensured that nearly no longitudinal load was applied to the Series 2 coupons.

Series 3, 5 and 6 were directly gripped with standard flat serrated grips (see Figure 3.4). Through trials, it was determined that neither tabs nor emery cloth were necessary to prevent slippage or fracture at the grips, or fracture inducing surface damage. Series 4 were gripped with the CLC fixture required by the ASTM standard [64].

Figure 3.3 Custom made aluminium grips for Series 1.

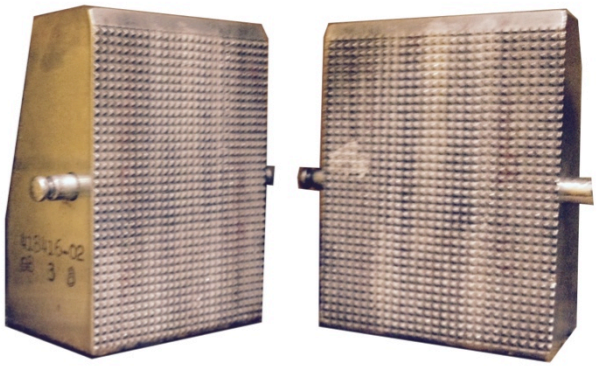

Figure 3.4 Serrated grips. Used for Series 2, 3, 5 and 6.

3.4.3.3 DIC system

The DIC system used in all the tests was Gesellschaft für Optische Messtechnik (GOM) ARAMIS v5.3.0 system. The system was setup to capture the 3D deformation of the test specimens surface at a frequency of 1 Hz. Each capture is called a "stage". The calculation of facet-strains is based on a zero-stage where the surface is considered as undeformed. The zero-stage on all series is the first stage captured by the DIC system.

3.4.3.4 Acoustic Emission system

The AE system used was a six channel Micro-II Digital AE system by Physical Acoustics Corporation with R15alpha sensors. Only two channels were used during the testing: one sensor at the top, and one at the bottom of the coupon (see Section 3.4.4.1).

3.4.3.5 Video extensometer

The video extensometer used in the 2nd round of Series 6 was a Messphysik Video extensometer ME46. The video extensometer is capable of tracking markings on the surface of the coupon or the location of pins if the coupon is illuminated from the back.

The DIC system requires the illumination of the surface, so pins were used for the measurements. For more details of the setup, see Section 3.4.4.3.

3.4.4 Testing setups

Figure 3.5 presents a diagram of all the equipment providing measurements and the information flow. Not all the equipment was used in all the tests. The applied load is the only information shared by all devices, as their individual recording time could not be synchronized.

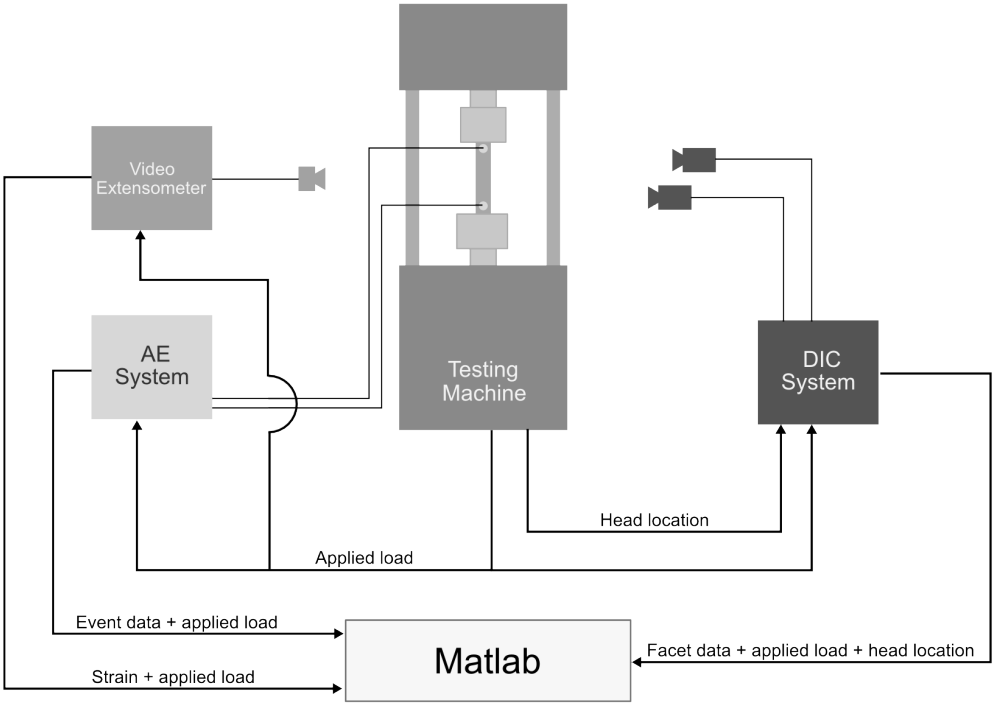

Figure 3.5 Diagram of the testing equipment that provides measurements and the flow of information.

3.4.4.1 General test setup

Figure 3.6 presents a diagram of this setup. It was used for the testing of all series except Series 4. In the diagram, “hydraulic grips” refer to either the custom made aluminium grips for Series 1, or the serrated grips for Series 2, 3, 5, and 6. Two AE sensors were placed at the top and bottom of the specimen, and the area between them was captured with the DIC system. The loading rate was 2 mm/min as dictated by the ASTM standards [50,51].

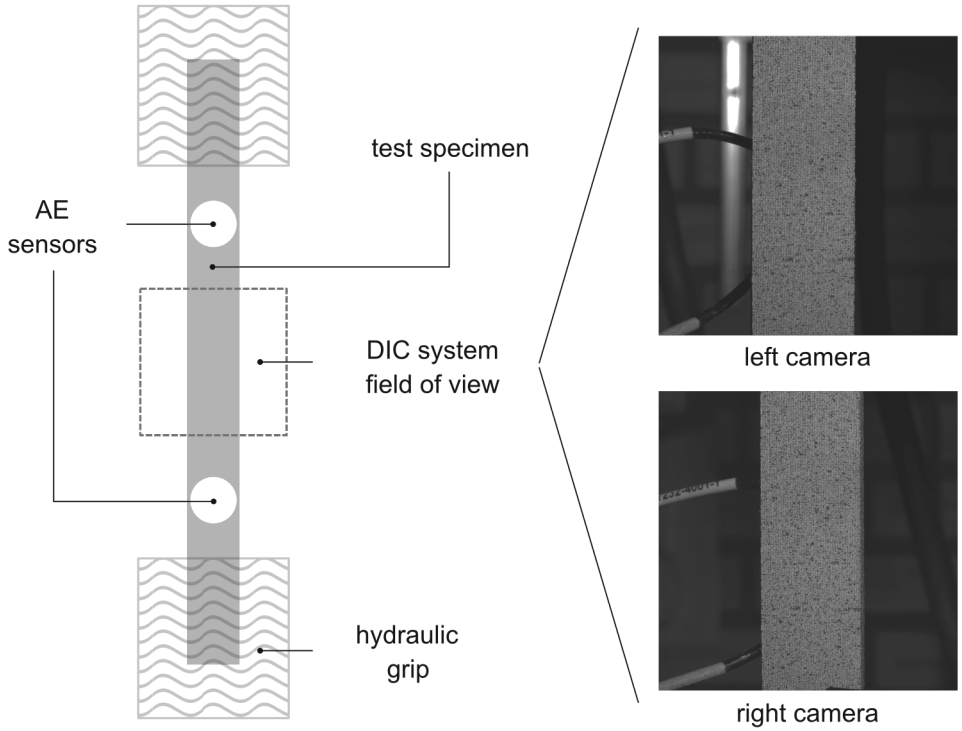

Figure 3.6 Diagram of the general test setup.

3.4.4.2 Special test setup for Series 2

Figure 3.7 presents a diagram of this setup. It was only used for the testing of Series 2 (see Section 3.5.2). The main difference between this setup and the general test setup is the method for gripping the specimens. To avoid damaging the specimens upon the closure of the grips, the specimens were glued to tabs already gripped (see Figure 3.7). Additional differences compared to the general test setup are the omission of the AE system, and that the field of view of the DIC system covers nearly the full free-length of the specimen. The AE system was omitted for two reasons. First, the AE sensors create blind zones were the surface and its potential cracking cannot be observed. This drawback was considered unacceptable after the first round of testing of Series 2. Second, since the AE sensors are relatively heavy, they could damage the specimen. The DIC system does not capture the full free-length of the coupon because part of the hydraulic gripping mechanism blocked the view of the DIC system cameras (shown in "left camera" and "right camera" images in Figure 3.7).

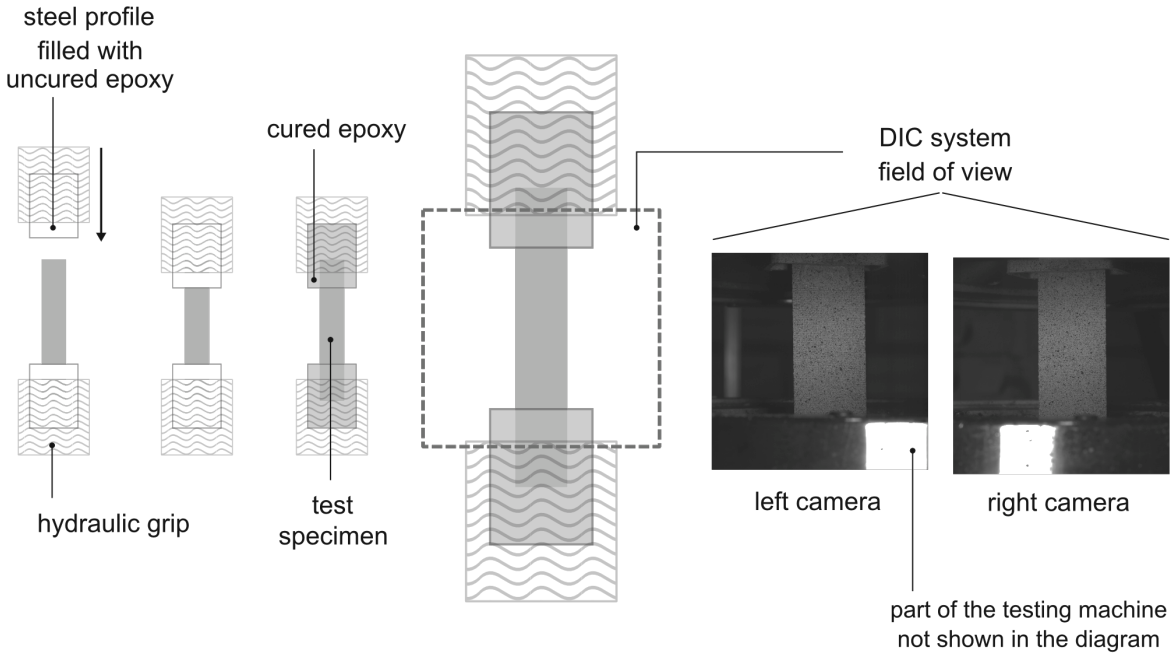

Figure 3.7 Diagram of the special test setup for Series 2.

3.4.4.3 Special test setup for 2nd round Series 6

Figure 3.8 presents a diagram of this setup. It was only used for the second round of testing of Series 6 to compare the laminate strain measurements of the video extensometer and the DIC system. Compared to the general test setup, this one does not include the AE system, the field of view of the DIC system encompasses nearly the full free-length of the coupon, and pins were added for additional strain measurement with the video extensometer. The AE system was omitted to be able to measure nearly the full free-length of the coupon with the DIC system. As with the other special test setup, the full free-length of the coupon cannot be captured because the hydraulic mechanism blocks the view of the DIC system cameras. Figure 3.9 presents a picture of this setup, and in it, one can appreciate the location of the DIC system and the video extensometer. The light on the left illuminates the surface for the DIC system cameras, while the one between the cameras is the backlight of the video extensometer.

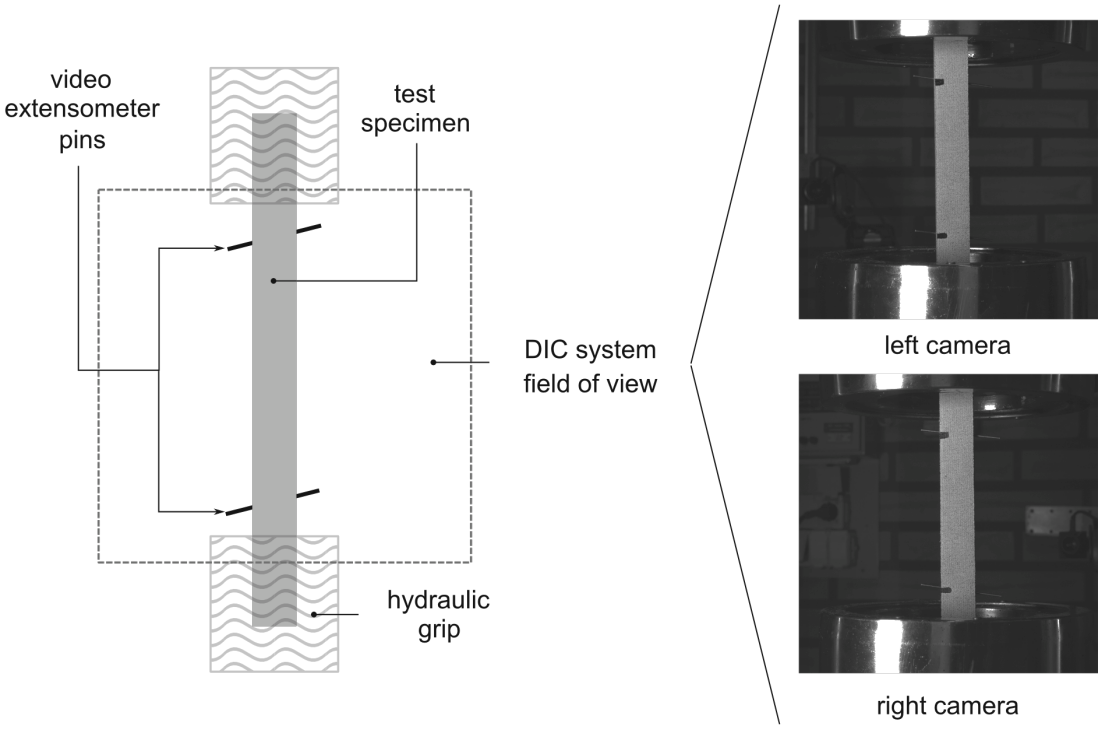

Figure 3.8 Diagram of the special test setup for the 2nd round of Series 6.

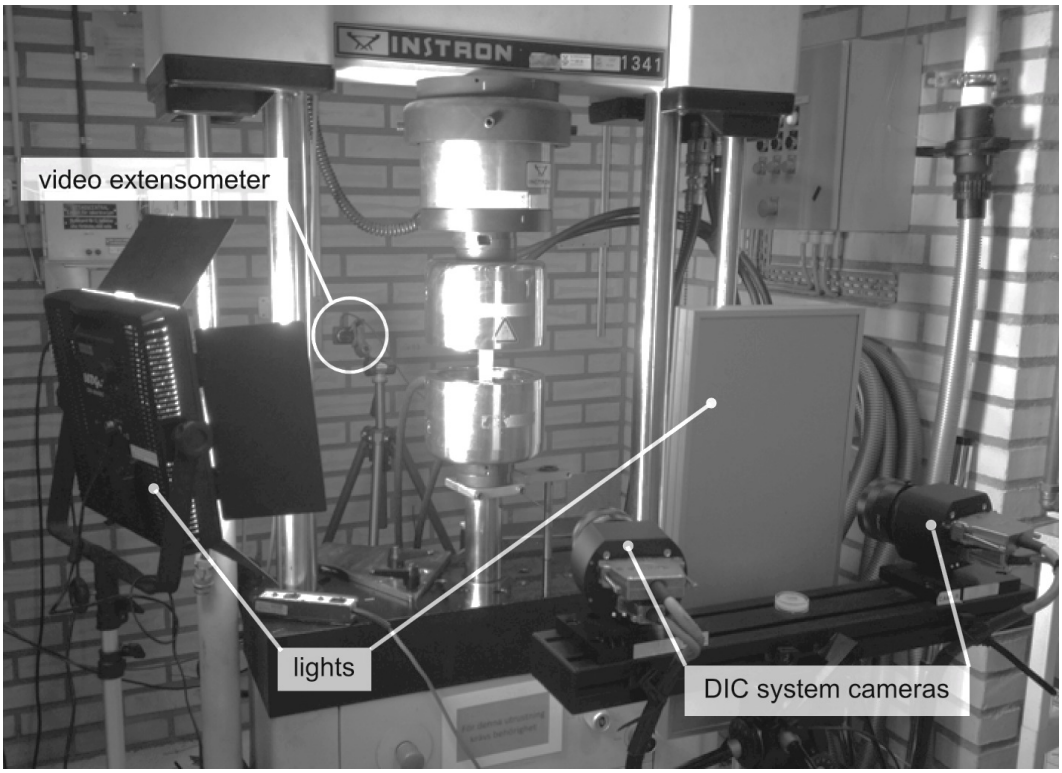

Figure 3.9 Picture of the special test setup for the 2nd round of Series 6.

3.4.5 Testing procedure

The procedure for testing each specimen was the following:

1. Select a coupon.
2. Look for imperfections (e.g. damage at the edges, large changes of thickness, wrinkles).
3. Give the coupon a reference number.
4. Measure the thickness and width.
5. Spray a speckled pattern on the smooth side of the coupon.
6. Glue pins for the video extensometer (only done on the second testing round of Series 6).
7. Mount the coupon in the testing machine.
8. Align the coupon.
9. Check the quality of the speckled pattern with the DIC system.
10. Fully close the grips at the pre-approved pressure (empirically determined by trial and error: high enough to hold the specimen, and low enough to not damage it).
11. Start recording with the DIC system (not used in Series 4).
12. Start recording with the bonded strain gauges (only used in Series 4).
13. Start recording with the AE system (not used in the second testing round of Series 2 and 6).
14. Start recording with the video extensometer (only used in the second testing round of Series 6).
15. Start loading the coupon.
16. Wait for complete fracture (the coupon is unable to carry a load in the longitudinal direction).
17. Stop loading the coupon.
18. Stop recording with the DIC system (only if applicable).
19. Stop recording with the AE system (only if applicable).
20. Stop recording with the video extensometer (only if applicable).
21. Stop recording with the bonded strain gauges (only if applicable).

3.4.6 Post-processing of the data

3.4.6.1 Trimming

As mentioned in the previous Section (3.4.5), recording with the DIC system started before the testing machine, and stopped after the coupon had fully fractured and the testing machine had been stopped. This meant that the DIC system recorded stages (see Section 3.4.3.3) before the coupon was loaded and after the coupon fractured. Only the stages that correspond to the time where the coupon was being loaded are of interest for material characterization, so they had to be identified and kept, while the other stages had to be removed, as keeping them complicated the handling of the data.

Figure 3.10 presents the applied load vs. stage curve of coupon no. 4 of Series 1 recorded by the DIC system. The blue-dotted curve indicates all the captured stages, while the black circles represent the ones kept for further analyses. The x-axis indicates the stage number rather than the time, as talking about stages rather than time facilitates the description of the trimming and other post-processing procedures. In the figure, one can appreciate that in the first stages, the applied load is nearly constant

and not zero. Both irregularities have the following explanations. First, the applied load is not zero because, as mentioned in Section 3.4.3.2, the grips exert a small displacement on the coupon as they close, loading it. Second, the initial load due to the grip-closure is not perfectly constant because the measurement accuracy of the load cell is close to the magnitude of the initial load. The stages to be kept were the ones between a stage identified as the "first stage" and another one identified as the "last stage". Initially, algorithms for selecting the both stages were developed, but after reviewing the selections, it was determined that a manual selection was the best option. The first stage is roughly the one before a stage that has an applied load value larger than the one of the initial load. The last stage is the one before a stage with an applied load value close to zero.

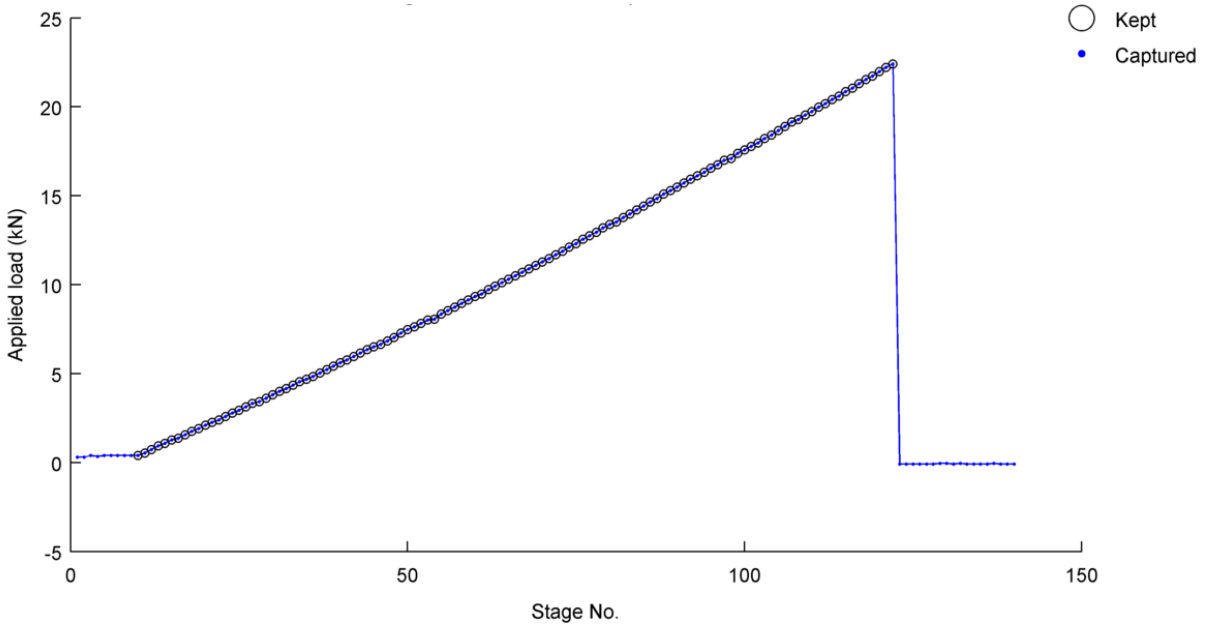

Figure 3.10 First example of trimming the DIC system measurements (coupon no. 3 Series 3).

Figure 3.11 presents a slightly more complex situation than Figure 3.10 regarding the selection of the last stage. The curve in Figure 3.11 is somewhat typical for the coupons in Series 1. As they are loaded, the coupons in this series exhibit partial fractures, resulting in multiple large drops in applied load. In the case of Series 1, the images taken by the DIC system were instrumental on selecting the last stage. As will be shown, the coupons of Series 1 fracture completely in a violent manner, disappearing from the field of view of the DIC system cameras.

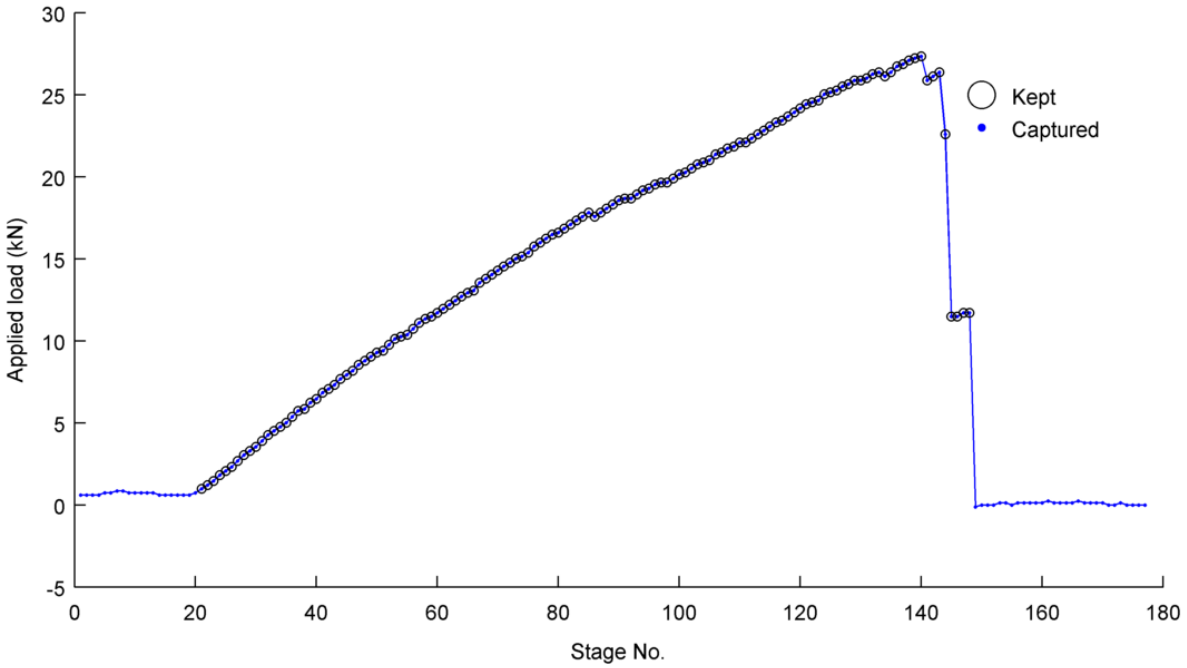

Figure 3.11 Second example of trimming the DIC system measurements (coupon no. 7 Series 1).

3.4.6.2 Time synchronization

As mentioned in Sections 3.4.4 and 3.4.5, all the devices were started at different times and the applied load output signal of the testing rig was the only common signal between them. Their measurements were synchronized in Matlab through a function that compared the time vs. applied load curves of the devices, calculated the time lag by varying it until the curves matched (time lag with the minimum root mean square error), and subsequently, modified the time of capture of the measurements.

3.4.6.3 Local coordinate system

Figure 3.12 depicts two coordinate systems and the loading direction of the testing machine. The coordinate system with the 123-axes corresponds to the coupon, while the one with the xyz-axes corresponds to the DIC system. Henceforward, each system will be referred to as the local and global coordinate systems respectively. The origin of the local coordinate system is on the middle of the coupon surface facing the DIC system cameras, and the 1- and 2-axes are parallel to the length and width of the coupon. In an ideal alignment, the xy-plane and 12-plane are parallel, as well as the loading direction, the y-axis and the 2-axis. In reality, this perfect alignment is unfeasible. In the tests, a disagreement of a fraction of a degree between the 2-axis and the loading direction was deemed as acceptable (pictured right in Figure 3.12), as well as between the yz-plane and the loading direction. Both considerations do not warrant parallelism between the xy- and 12-planes, nor between the yz- and 23-planes. Figure 3.13 shows an example of the differences between the local and global coordinate systems.

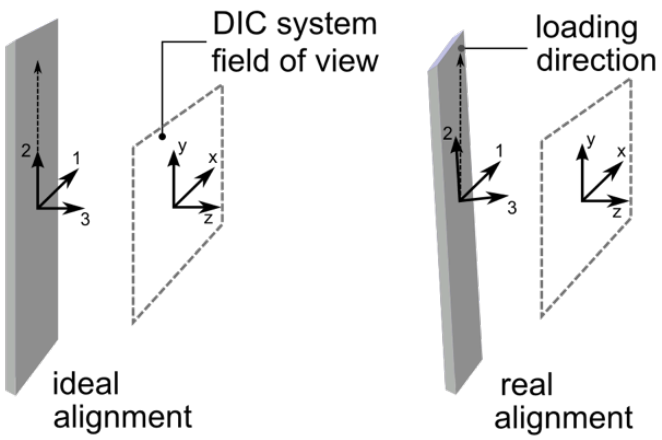

Figure 3.12 Alignment between the coordinate systems of the coupons (local: 123) and the DIC system (global: xyz).

The local coordinates of the coupon surface facets were calculated in Matlab as follows. A plane that best fits the global location of all the facets at the first stage (least square of the normal distance to the plane) is found through the Matlab function *affine_fit* [65]. A vector in the y-direction is projected onto the plane, defining the direction of the 2-axis in the global coordinate system. Then, the direction of the 1-axis is determined through the normal of the plane (direction of the 3-axis) and the direction of the 2-axis. The origin of the local coordinate system is set to the middle of the coupon on one of the edges of the captured surface. The local coordinate system is used to determine if the coupons bent during loading, as well as for trying to identify the initiation and development of matrix cracking. Both applications are discussed further in the next section and 3.6.2.2.

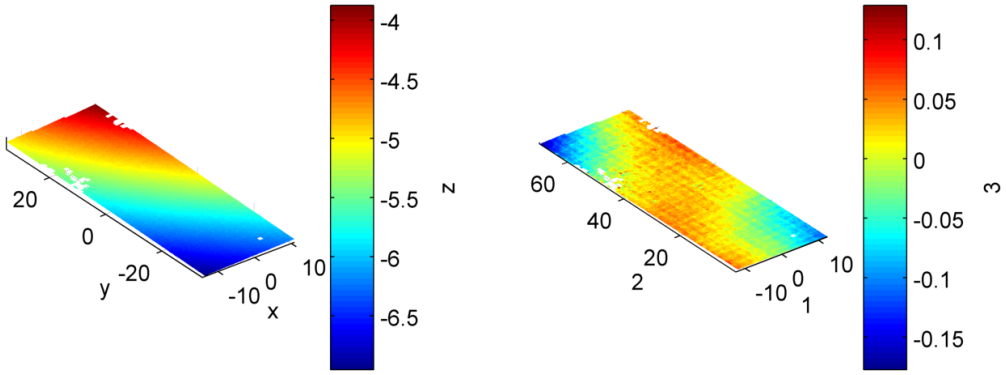

Figure 3.13 Location of the coupon surface facets in the global coordinate system (left) and local coordinate system (right) at the first stage. (Coordinates in mm; coupon no. 14 Series 3.)

3.4.6.4 Specimen flatness

The local coordinate system was used in all the series to visually determine if the specimens remained flat during testing. The procedure consists of plotting the location of the facets in the 3-axis of the local coordinate at different loading conditions. Figure 3.14 is an example of one of such plots.

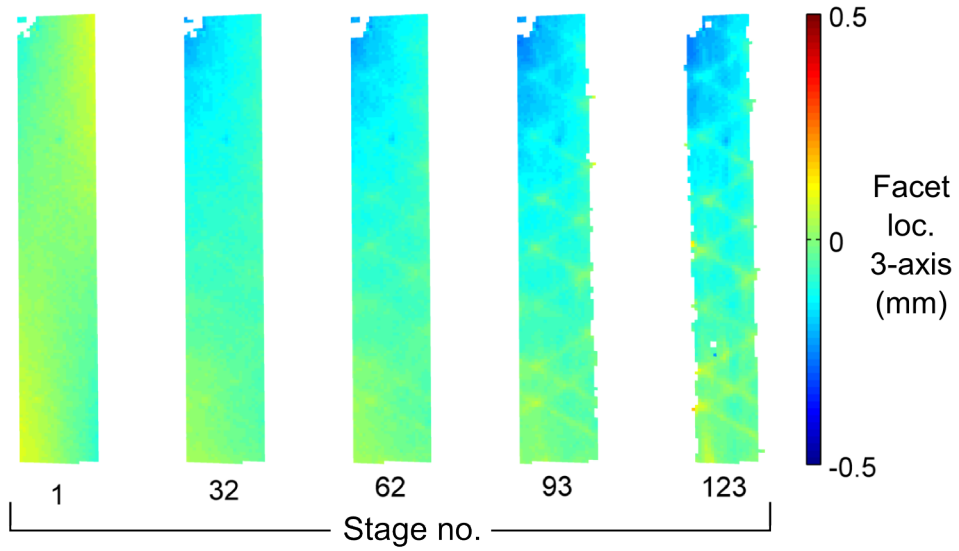

Figure 3.14 Facet locations in the 3-axis of the local coordinate system at five different stages (coupon no. 8 Series 1; total number of stages: 123).

3.4.7 Strain measuring techniques

3.4.7.1 Facet strains

The strains of each facet (ε_x, ε_y, ε_{major}, and ε_{minor}) are calculated by the DIC system through the change in location of the adjacent facets with respect to their location at stage zero. While the facet *locations* are available in the global and local coordinate system (see Section 3.4.6.3), the facet *strains* are not. The facet strains were not transformed in Matlab to the local coordinate system, so in all figures, facet strains are in the global coordinate system.

3.4.7.2 Virtual extensometer technique

The virtual extensometer is the basic element of most of the strain calculations in this investigation. A virtual extensometer consists of the identification of two viable facets aligned in the longitudinal or transverse direction, and on the recording of the Euclidian distance between them as the load increases. Figure 3.14 presents an example of longitudinal and transverse virtual extensometers. The contour plots in the figure show the location of each extensometer on the first and last stage captured with the DIC system. The first recorded distance (corresponding to the first stage) is the initial length out of which the strain is calculated. A viable facet is one that exists in all of the kept stages from the DIC system. Facets may disappear for a number of reasons. Damage in the surface may result on the DIC system not being able to recognize the facet, or the damage may be so harsh that the facet is not longer there. Facets may also blink, appear and disappear, due to small changes in the lighting conditions and the capacity of the DIC system to recognise them. Figure 3.15 presents an example of the strain obtained from a pair of longitudinal and transverse virtual extensometers. The surface plots on the left side of the figure show where the virtual extensometers are located, while the curves on the right show the strains captured by both extensometers.

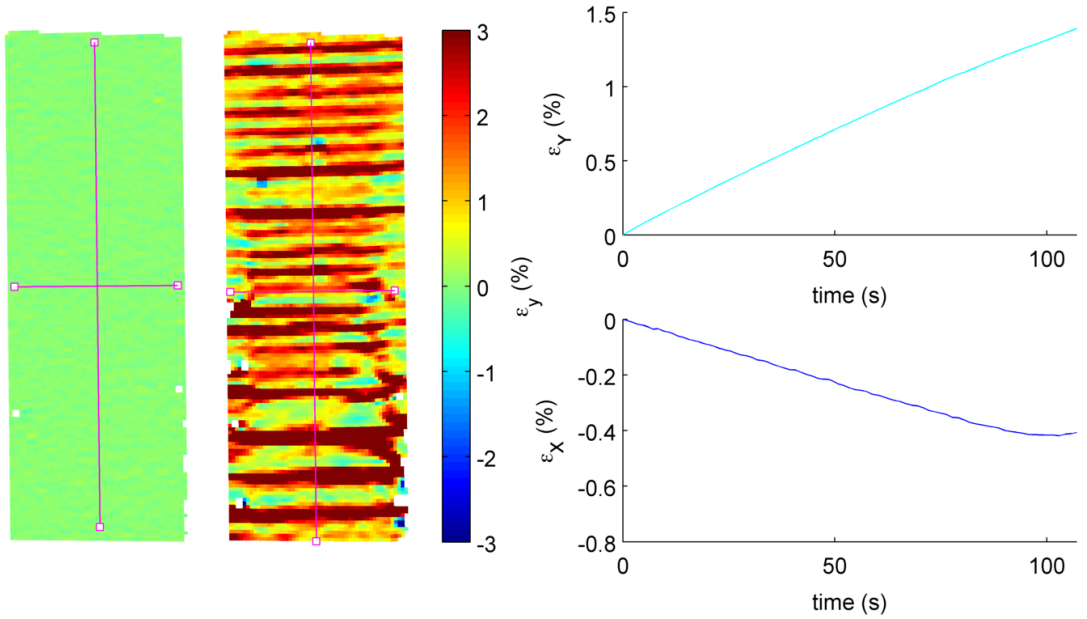

Figure 3.15 Location and measured strains of a longitudinal and a transverse virtual extensometer respectively (coupon no. 2 Series 6).

3.4.7.3 Virtual strain gauge technique

A virtual strain gauge is an arrangement of horizontal and vertical virtual extensometers set to mimic the measurement capacity of a bonded strain gauge or a clip-on extensometer. Figure 3.16 presents three examples of how the virtual extensometers are arranged to form virtual strain gauges of different sizes. The strain measurements of all the longitudinal and transverse virtual extensometers respectively are averaged to render single measurements of the longitudinal and transverse strain. This strain measuring technique is the one used in Paper IV.

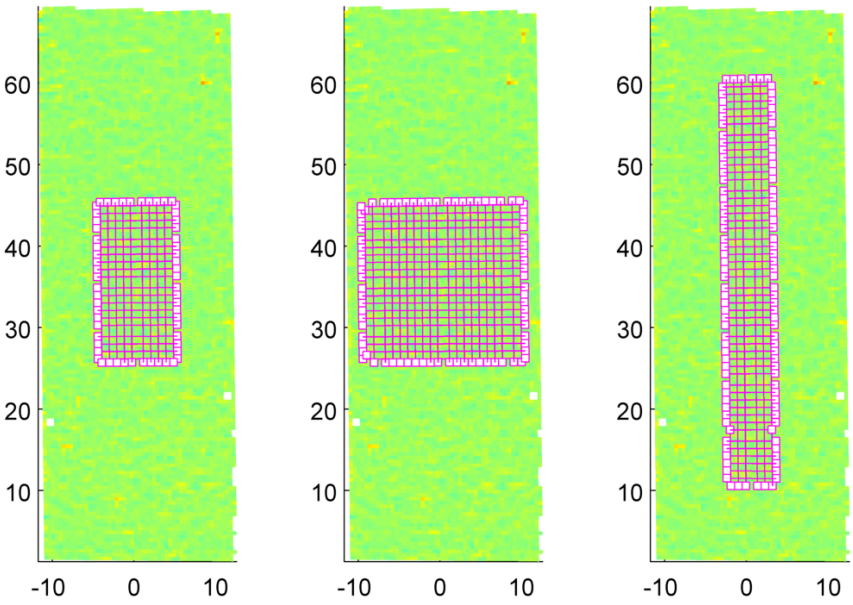

Figure 3.16 Examples of virtual strain gauges (20×10, 20×20, 6×50 mm).

3.4.7.4 Random virtual extensometers technique

The random virtual extensometers measurement is an arrangement of randomly located longitudinal and transverse virtual extensometers throughout the captured surface. Figures 3.17 and 3.18 present two examples of this technique being applied in different laminate types. On the left side of the figures one can appreciate the random location, while on the right side, one can appreciate how the strain measurements of each virtual extensometer differ. The black curves in the top-right and bottom-right plots are the average of the strain measurements of all the longitudinal vertical virtual extensometers respectively. This strain measuring technique is especially useful for the Series 1. The coupons in this series fracture partially as they are loaded, reducing the amount of facets recognized by the DIC system. The virtual strain gauge technique is not feasible for measuring the ultimate strain of the coupons in this series, as the virtual strain gauge does not fit on the reduced captured surface. Figure 3.18 shows how the random virtual extensometers technique manages to accommodate itself to the viable facets. The transverse strain measurements in Figure 3.18 exhibit significantly more scatter than the ones in Figure 3.17 because the transverse virtual extensometers are significantly smaller (6 vs. 20 mm). In Figure 3.18, the transverse virtual extensometers cannot be larger because otherwise they would no fit in the surface captured by the last stage.

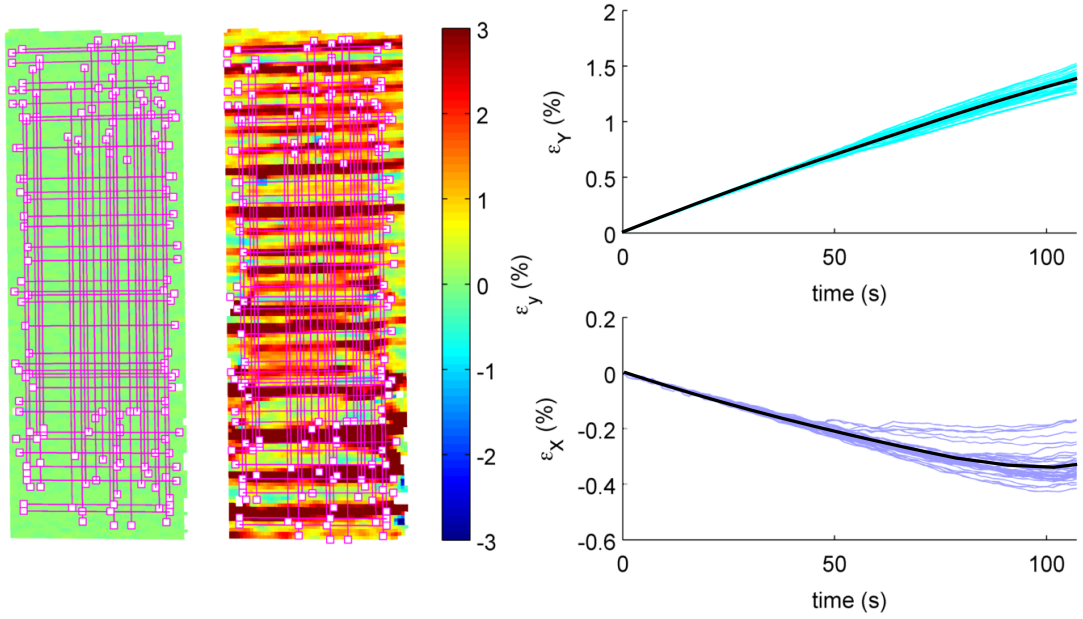

Figure 3.17 Locations and strains measured by randomly located longitudinal and a transverse virtual extensometers (cyan and blue/lila lines) respectively, and the average of their measurements (black lines). (Length of the longitudinal virtual extensometers: 50 mm, width of the transverse virtual extensometers: 20 mm, total number of virtual extensometers: 40; coupon no. 2 Series 6.)

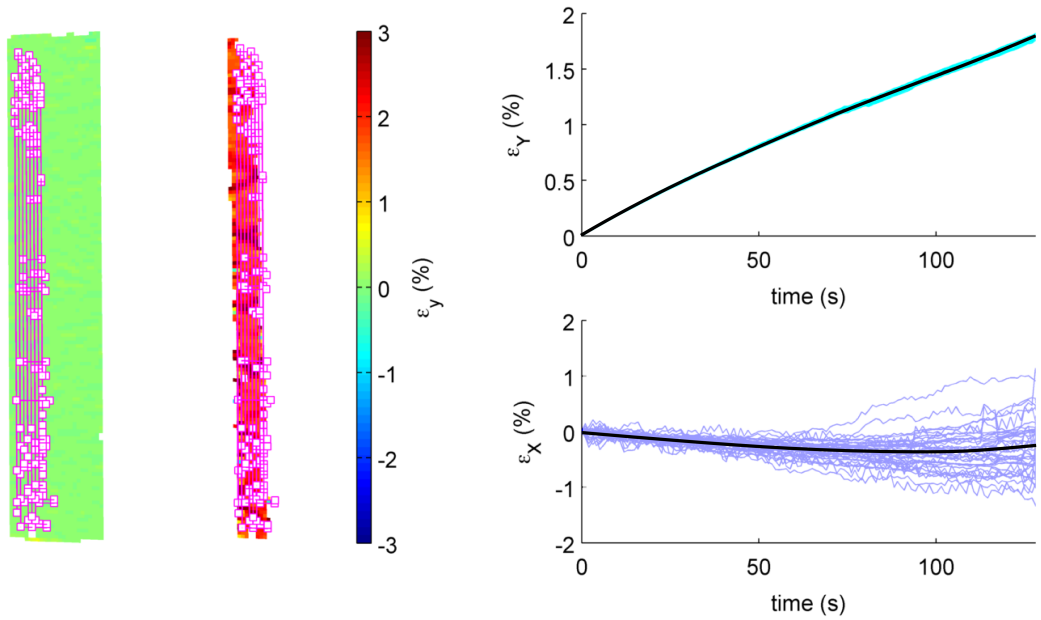

Figure 3.18 Location and strains measured by randomly located longitudinal and a transverse virtual extensometers (cyan and blue/lila lines) respectively, and the average of their measurements (black lines). (Length of the longitudinal virtual extensometers: 60 mm, width of the transverse virtual extensometers: 6 mm, total number of virtual extensometers: 40; coupon no. 7 Series 1.)

3.4.7.5 Facet strain average technique

The facet strain average technique is commonly used [66-69]. It consists of averaging all the facet strains calculated by the DIC system at a given stage. Figure 3.19 presents three comparisons between the longitudinal strains calculated with this technique and the ones calculated with the random virtual extensometers technique. The plot in the left shows a very good agreement between both techniques, while the plots on the centre and right shows discrepancies. The discrepancy between both techniques can be explained as the result of high facet strains due to surface damage or calculation errors. The average of a sample is not a robust statistic, meaning that a small number of individuals with very high values can skew its value. Close to the fracture of the coupon some facets have very high strains that skew the average to high value. Because of this effect, the random virtual extensometers technique was considered to be more accurate and stable than the facet average strain technique. It is worth mentioning that for most of the coupons in Series 1 and 6 the agreement between both techniques is fairly good.

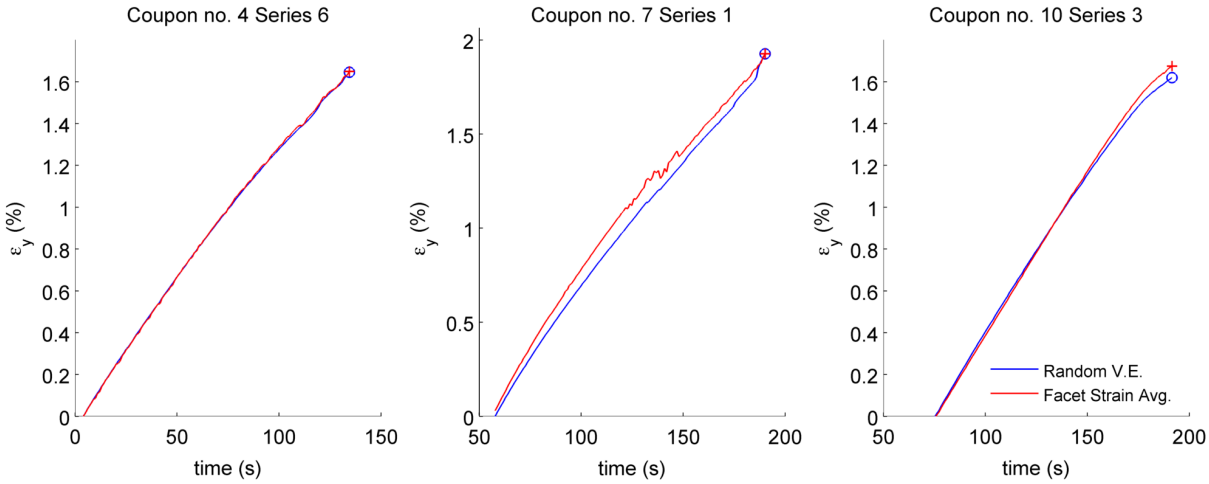

Figure 3.19 Comparison between the longitudinal strains calculated with the facet strain average technique and random virtual extensometers technique.

3.4.7.6 Strain measurement correction

As mentioned in Section 3.4.3.2, the hydraulic grips exert a small displacement on the coupon upon full closure. Since the DIC system starts recording after the full closure of the grips, the strain caused by the small displacement is not recorded. This initial strain can be calculated through the value of the applied load at the first stage and the longitudinal modulus of the coupon. Figure 3.20 shows how the longitudinal stress-strain curves are corrected. The correction is only significant for the coupons in Series 1.

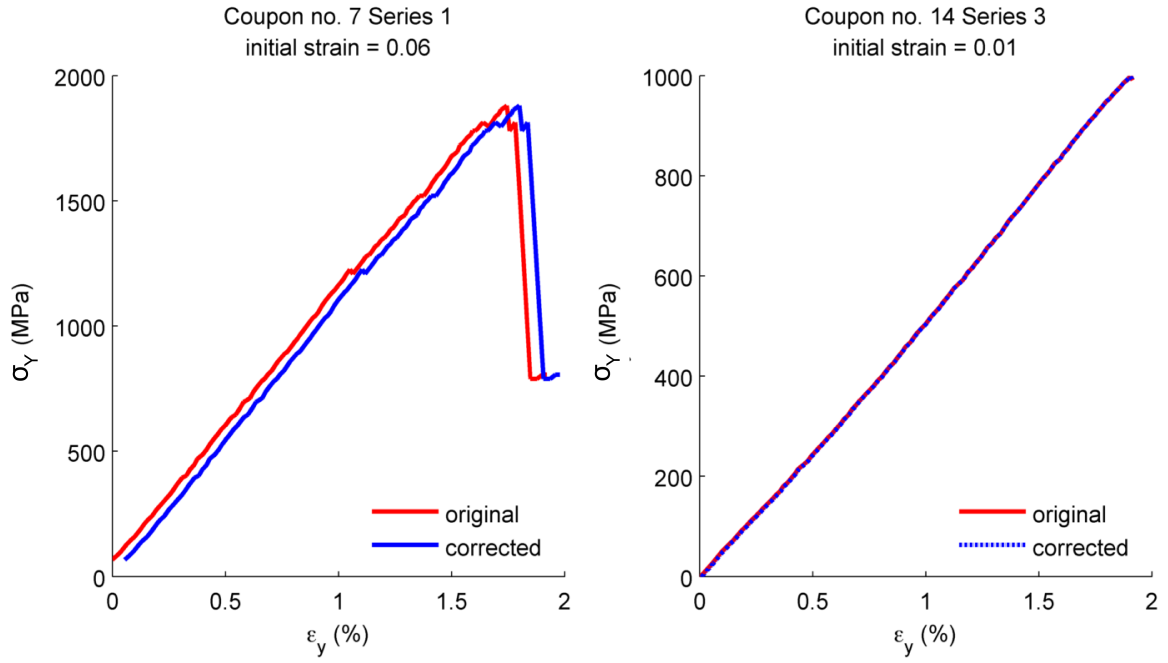

Figure 3.20 Comparison between the original and corrected longitudinal stress-strain curves. In the right figure, both curves are nearly exactly the same.

3.4.7.7 Ultimate stress, ultimate strain and corrected ultimate strain

The ultimate strain is not used by DNV. Instead, a corrected ultimate strain derived from the ultimate stress and the elastic modulus of the laminate is used. The purpose of the corrected ultimate strain is to have congruent material properties. To do so, the definition of the corrected ultimate strain must consider the shape of the stress-strain curve (see Figure 3.21).

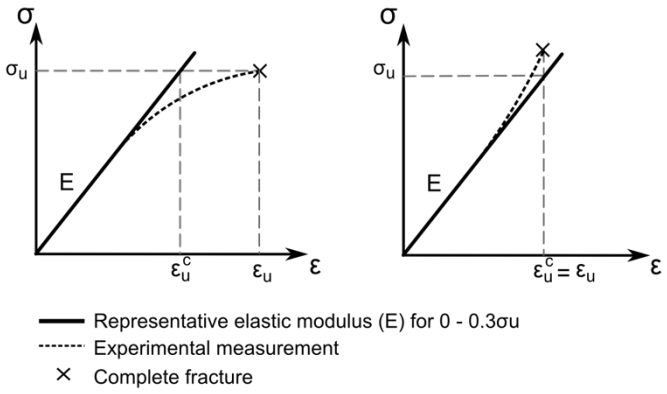

Figure 3.21 Definition of the ultimate stress, ultimate strain, and corrected ultimate strain according to the shape of the stress-strain curve (left: convex; right: concave).

3.5 Experimental results

3.5.1 Series 1: $[0]_T$ Unidirectional laminate

The most remarkable characteristic of the coupons in Series 1 is that as they are loaded, they fracture progressively from the edges to the centre of the coupon. Figures 3.22 and 3.23 present two examples of this behaviour. The progressive fracturing means that the cross-section area of the coupon is reduced during the test, in a manner somewhat analogous to the necking of steel under a tensile load. If the loss of cross-section area is not accounted for in the calculation of the longitudinal stress, the ultimate stress is an underestimation of the carrying capacity of the laminate.

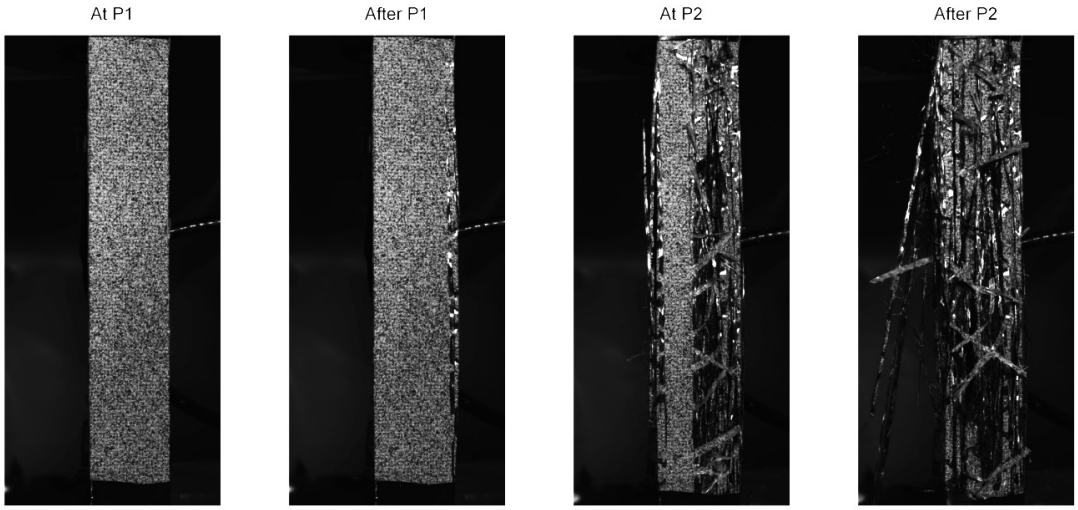

Figure 3.22 Example of the progressive fracture of the coupons in Series 1 (P1: before first fracture; P2: before complete fracture; coupon no. 7).

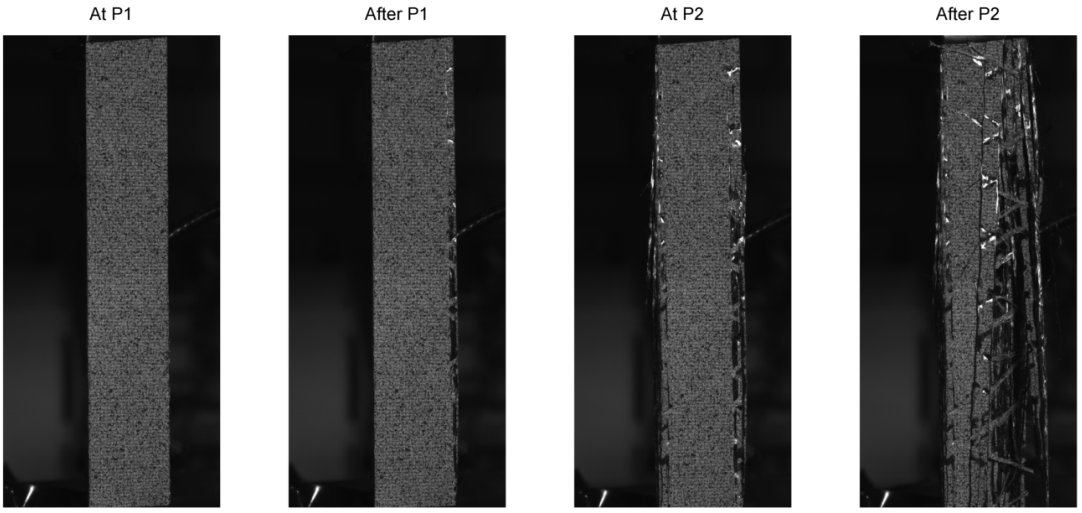

Figure 3.23 Example of the progressive fracture of the coupons in Series 1 (P1: before first fracture; P2: before complete fracture; coupon no. 8).

Figure 3.24 presents the analysis of the DIC system measurements of one of the coupons in Series 1. The loss of cross-section area was approximately calculated by averaging the width of the captured surface along its length in each stage. The curve is not perfect, as it occasionally increases. This is because some facets become recognizable by the DIC system at later stages. Using this curve, a stress-strain curve corrected with respect to the loss of cross-section area was also calculated. In Figure 3.24, one can observe that the corrected stress-strain curve diverges from the uncorrected one straight after the first loss of cross-section area.

Figure 3.24 shows three important characteristics of the coupons in Series 1. First, the stress-strain curve is slightly convex up to the first partial fracture. This behaviour is uncommon in unidirectional carbon fibre composites [49,70,71]. One possible explanation for it is that as the coupon is loaded the carbon fibres become less crimped, increasing the longitudinal modulus. This stiffening is lost in the normal stress-strain curve (blue curve in Figure 3.24) because of the partial fractures; however, it is evident in the corrected stress-strain curve (red curve in Figure 3.24). Second, the corrected stress-strain curve gives a significantly higher ultimate stress (24% higher in Figure 3.24). As stated previously, the loss of cross-section area curve is not perfect, so the increase in ultimate stress stated by the corrected curve may be an overestimation; however, it still seems clear that the characterization of this type of laminate without accounting for the loss of cross section area will result in an underestimation of the ultimate stress.

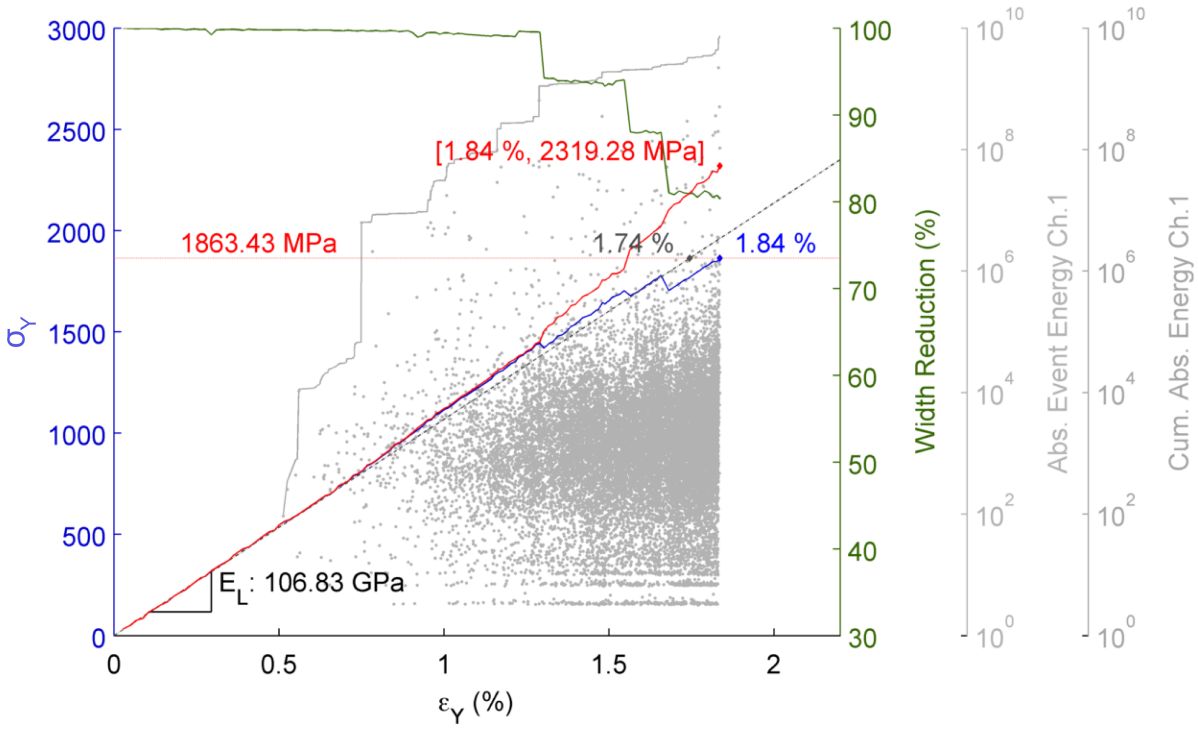

Figure 3.24 DIC system and AE system measurements of coupon no. 7 in Series 1. (Blue curve: longitudinal stress-strain curve calculated with the random virtual extensometers technique; Red curve: longitudinal stress-strain curve corrected for loss of cross-section area; Green curve: loss of cross-section area curve; Grey curve: cumulative absolute energy of the AE events recognized by the AE system; Dark grey dots: absolute energy of the individual AE events.)

The partial fracture of the coupons may be the result of a misalignment between the longitudinal direction of the coupon and the carbon fibre tows. Such a misalignment has been described [61] as a possible cause for the premature fracture of unidirectional prepregs laminates for ply characterization. Prepreg unidirectional laminates do not exhibit this progressive fracture. A possible explanation for this behaviour is that in a unidirectional NCF laminate the fibre tows are separated by resin pockets. This feature may arrest the fracture of the fibre tows to the ones at the edges. If the coupons have been made wider, the fracture of the fibre tows at the edges would constitute a smaller

percentage of the total cross-section area, and therefore, the drops in loads observed in the stress-strain curve would have been smaller. However, increasing the width of the coupon means that a higher load is required to break it, and therefore, that more pressure needs to be applied on the grips to hold the coupon. Depending on the size of the grip area this may or may not increase the risk of fracture at the grips.

The AE results presented in Figure 3.24 will be further discussed in Section 3.6.2.1.

3.5.2 Series 2: $[90]_T$ Unidirectional laminate

In the trial round of Series 2, the coupons were damaged by the initial loading applied by the grips upon closure. Therefore, the test setup was modified, but unfortunately, despite the efforts regarding the grips, the coupons in Series 2 could not be successfully tested. The fracture load of the coupons was so low that barely a couple of stages could be recorded with the DIC system before they started cracking. Furthermore, the loads at which the coupons started cracking were close in magnitude to measurement accuracy of the load cell, so the recorded load measurements are noisy. Figure 3.25 shows the applied load, while Figure 3.26 shows three longitudinal stress-strain curves calculated with the virtual extensometer technique. The stress-strain curves are clearly of poor quality. The curves zig-zag due to the low accuracy of the applied load measurement, and flatten because of the cracking of the coupon.

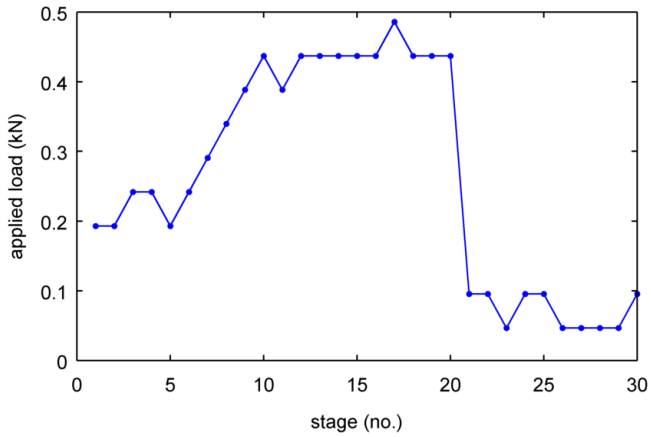

Figure 3.25 Applied load recorded by the DIC system for coupon no. 14a in Series 2.

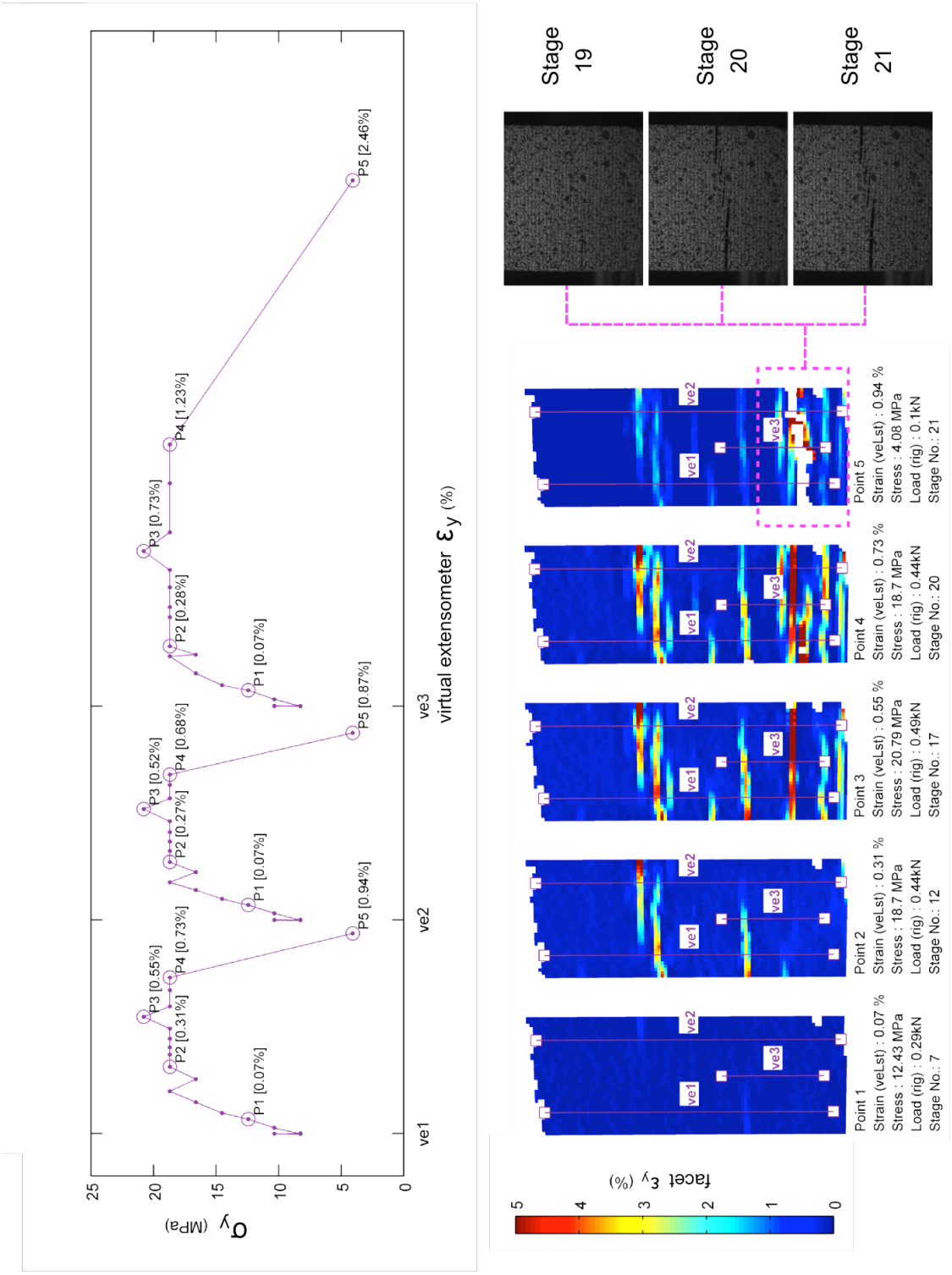

Figure 3.26 DIC system measurements of coupon no. 14a in Series 2.

3.5.3 Series 3: $[90/0]_S$ Cross-ply laminate

The coupons in Series 3 had clearly concave stress-strain curves up till their complete fracture. There was neither partial fractures at the edges nor any apparent loss of cross-section area. Figure 3.27 presents the stress-strain curve for one of the coupons of this series calculated with the random virtual extensometer technique. Figure 3.28 shows nearly horizontal stripes of highly strained facets. As the load increases, so does the gradient between the low and high strain facets. Interestingly, some of the facets get negative longitudinal strain values, indicating that they relaxed (possibly due to matrix cracking).

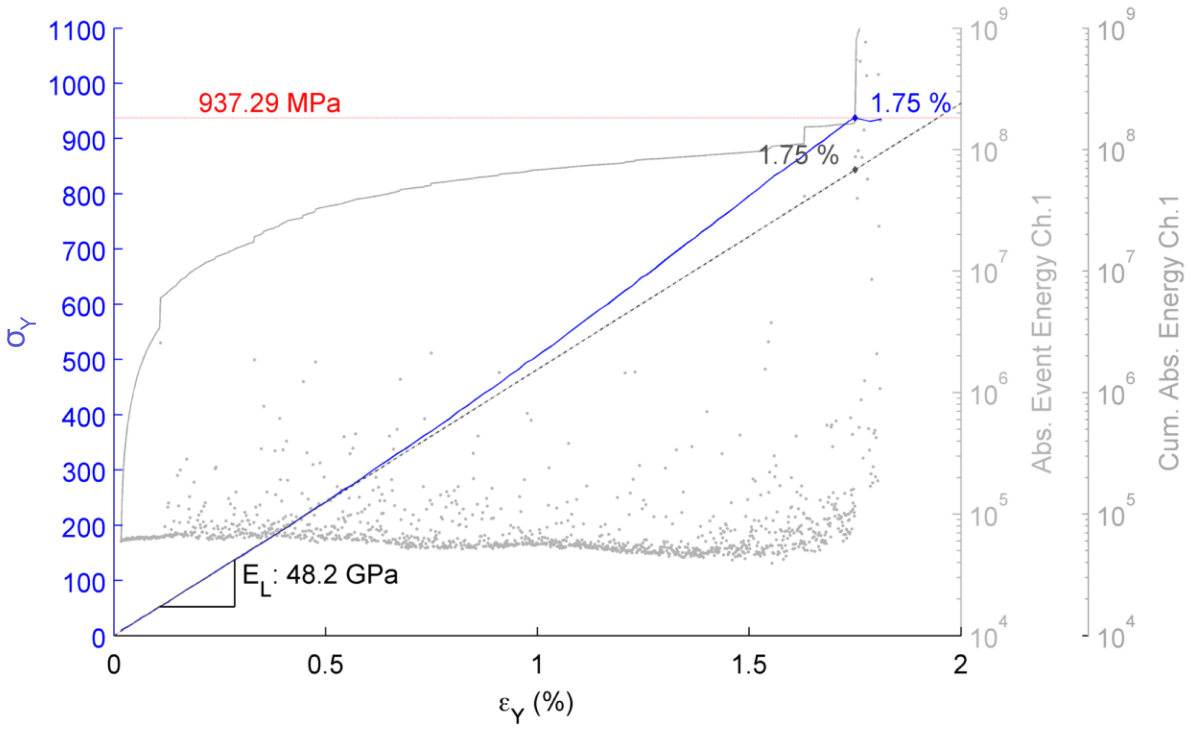

Figure 3.27 DIC system and AE system measurements of coupon no. 6 in Series 3. (Blue curve: longitudinal stress-strain curve calculated with the random virtual extensometers technique; Grey curve: cumulative absolute energy of the recognized events by the AE system; Dark grey dots: absolute energy of the individual events.)

Unfortunately, the coupons in this series were very difficult to test. One of the surfaces was very irregular, making it difficult to evenly distribute the pressure throughout the gripped area. The irregularity on the surface seemed to be the result of a wrinkled vacuum bag in the manufacturing of the laminate. Most of the coupons fractured at the grips, and of the ones that seemed to have fractured correctly, only four showed no slippage. The strength measurements obtained from these coupons cannot be used for characterization, as the variation in thickness exceeds the allowables set by the test standard [50].

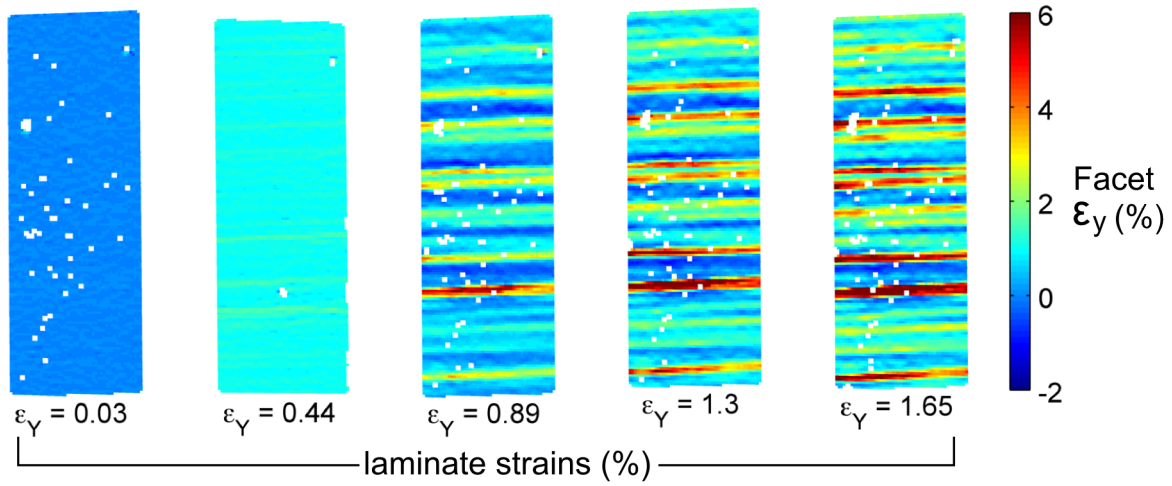

Figure 3.28 Facet strains of a coupon in Series 3 at five laminate strains. (Coupon no. 4 Series 6; laminate strain was calculated with the random virtual extensometer technique.)

3.5.4 Series 4: $[90/0]_{4S}$ Cross-ply laminate

As mentioned in Section 3.4.2.4, the coupons of Series 4 were tested in compression using a CLC fixture, and therefore, there was no room for the AE sensors or a direct view to specimen surface, meaning that measurements with the DIC system were not possible. The results from this series are excluded from this document, as they are not related to any non-standard measuring technique.

3.5.5 Series 5: $[-45/+45]_{2S}$ Angle-ply laminate

All the specimens in this series presented the typical shear stress-strain curve: a linear segment followed by a non-linear increase up to a plateau. Figure 3.29 presents the stress-strain curve for one of the specimens in this series. The curve is cut after a shear strain of 5%. By looking only at the stress-strain curves, the behaviour of the specimens in this series seems unremarkable; however, the DIC facet measurements and visual inspections of the tested specimens reveal an interesting detail. All the specimens in this series curved with respect to the same face as they were loaded (see Figures 3.30 and 3.31). As stated in Section 3.4.2.6, neglecting the E-glass fibres, the layup of this series was balanced and symmetric, but the stitches of the two NCF mats were perpendicular to each other. Presumably, the specimens curved because the stitches limited the scissoring of the fibres more on one side than on the other one. The scissoring of the fibres and its obstruction by the stiches is mentioned in [58] as a possible explanation for differences in shear properties with respect to the direction of the stitches. In [58], the angle-ply NCF laminates do not curve, possibly because the stitches of all the NCF mats constituting the laminates presented in the reference are aligned. The acoustic emission results are discussed in Section 3.6.2.1.

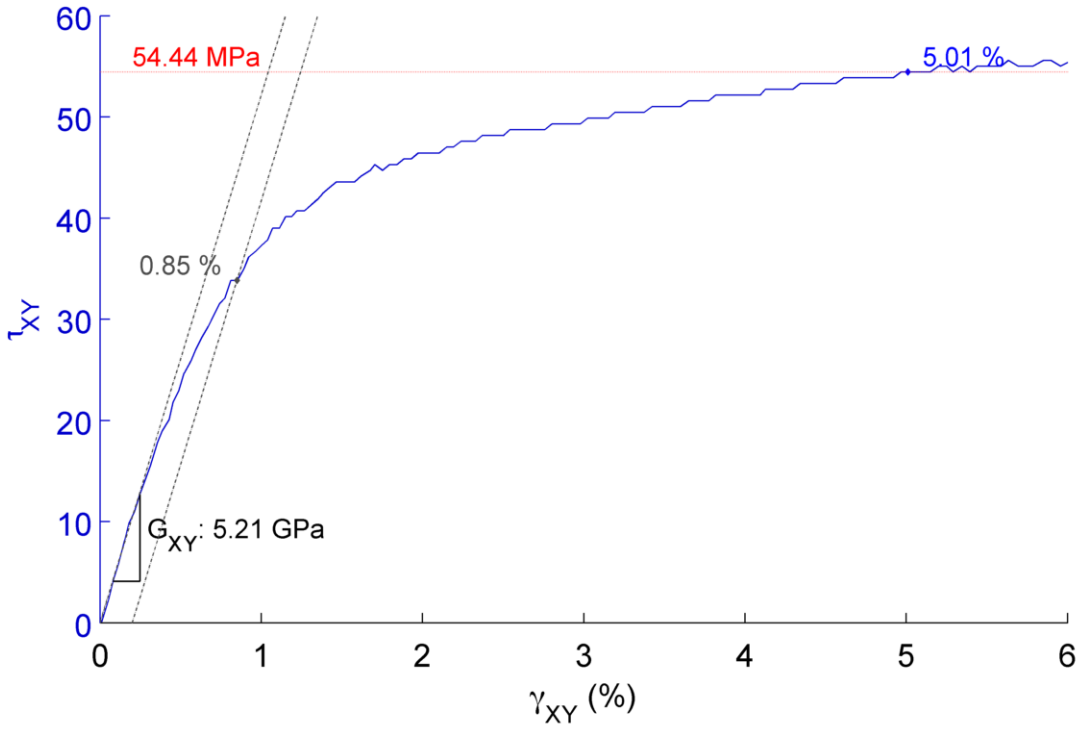

Figure 3.29 Typical shear stress-strain curve (coupon no. 3 Series 5).

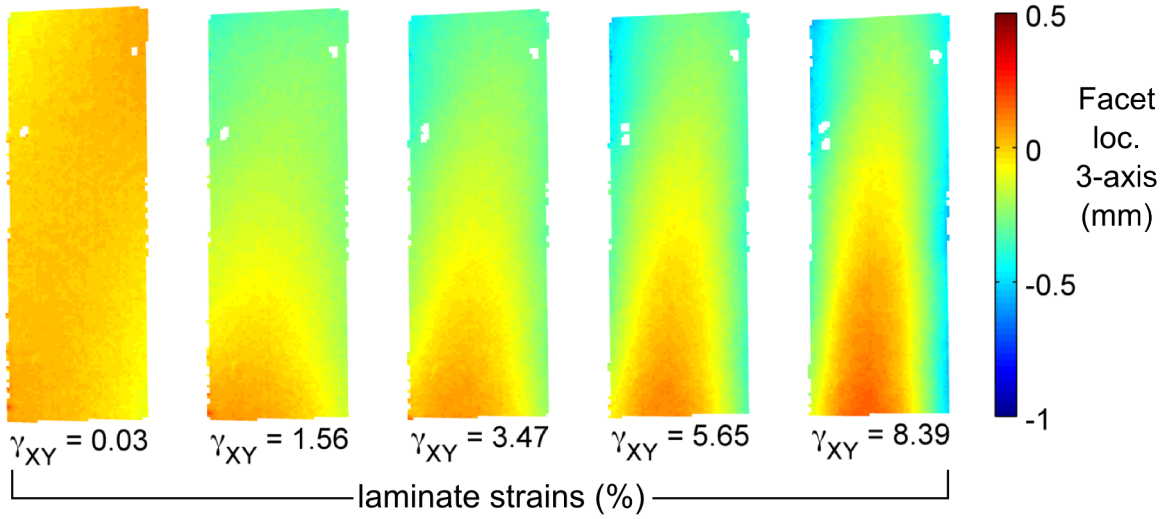

Figure 3.30 Facet locations in the 3-axis of the local coordinate system of a specimen in Series 5 (angle-ply laminates). Note that as the laminate shears it curves in the longitudinal and transverse directions. Laminate strain was calculated with the random virtual extensometer technique (coupon no. 6 Series 5).

Figure 3.31 Series 6 coupons curve with respect to the same side when tensile tested.

3.5.6 Series 6: $[90/-45/0/+45]_{2S}$ Quasi-isotropic laminate

Unlike the coupons in Series 1 and 3, the coupons in Series 6 had a convex stress-strain curve (see Figure 3.32). A possible explanation for this difference is that these coupons have considerable smaller fraction of carbon fibres in the longitudinal direction compared to the coupons of Series 1 and 3. As the coupons are loaded, the carbon fibres in the longitudinal direction possibly un-crimp as hypothesized in Series 1 and 3, leading to some stiffening, but at the same time matrix cracking and shear damage occur in the 90°, +45° and -45° layers, eclipsing the stiffening.

The coupons in this series share a feature with the ones of Series 3: they have the 90° layer on the outside. Figure 3.37 presents the longitudinal facet strains for one of the Series 6 coupons. This image is fairly similar to Figure 3.28 (corresponding to a coupon of Series 3), where also stripes of highly strained facets were observed. As stated for Series 3, the facets with very high strains in relation to the laminate strain may indicate matrix cracking.

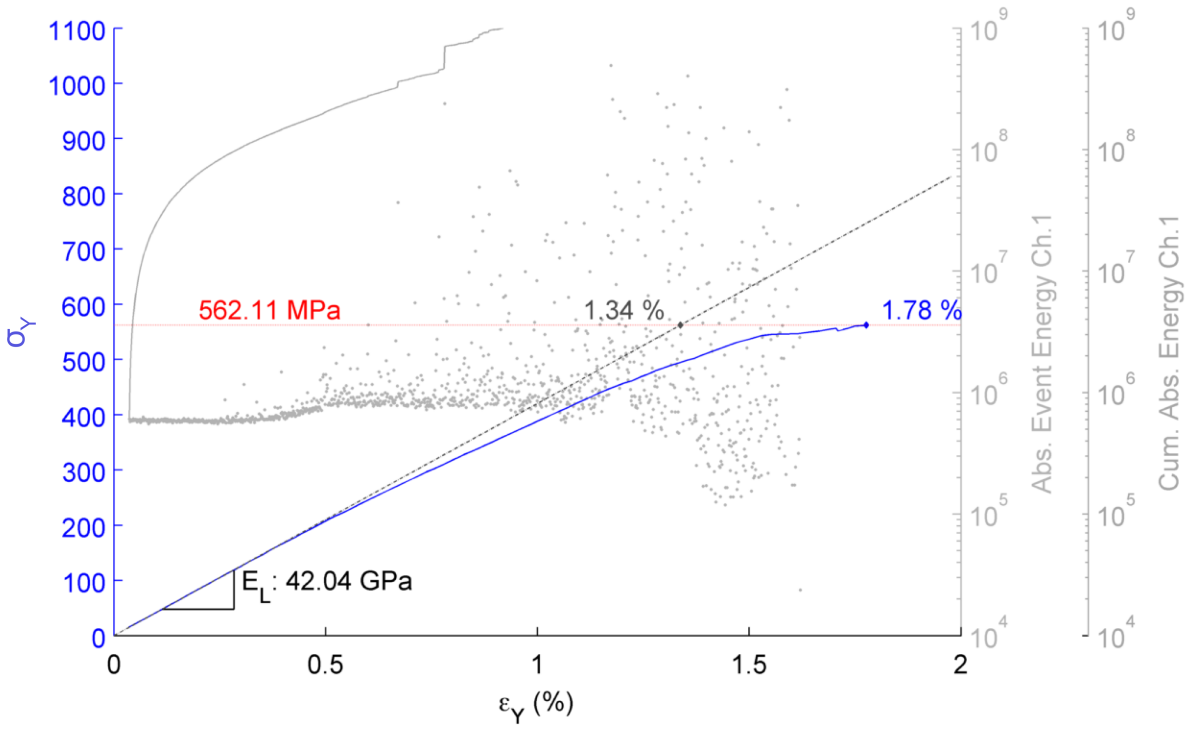

Figure 3.32 DIC system and AE system measurements of coupon no. 1 in Series 6. (Blue curve: longitudinal stress-strain curve calculated with the random virtual extensometers technique; Light grey curve: cumulative absolute energy of the recognized events by the AE system; Dark grey dots: absolute energy of the individual events.)

3.5.7 2nd round of Series 6

Figures 3.33 and 3.34 present comparisons between the laminate strains measured with the video extensometer and DIC system with the random virtual extensometers technique. The most important difference between the techniques are the strain measurements prior to the complete fracture of the coupons. On the left plot of Figure 3.33, one can appreciate that there is a jump in the strain measured by the video extensometer. This jump is the result of a local fracture on the surface of the coupon, causing the sudden movement of one of the pins (in some occasions the pin flew-off before the coupon fractured completely). This is one disadvantage of the video extensometer when it is configured to measure strains by tracking the locations of pins. The pins must be glued to the surface of the coupon, and damage on the surface may change their location. Overall, both figures show a fairly good match between both techniques except close to the coupon fracture.

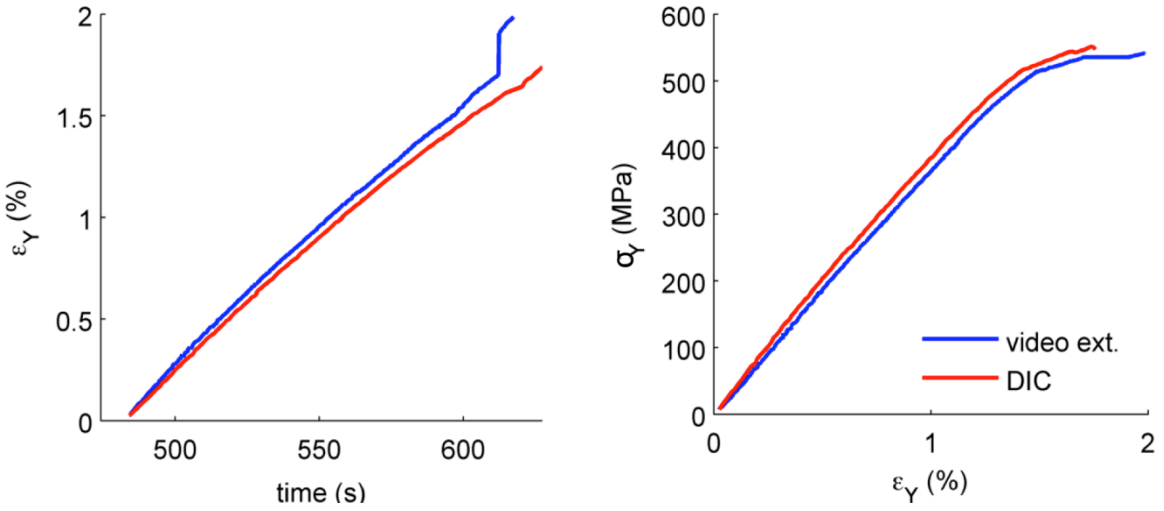

Figure 3.33 Comparison between the laminate strain measurements made with the video extensometer and the DIC system (random virtual extensometer technique; coupon no. 11 Series 6).

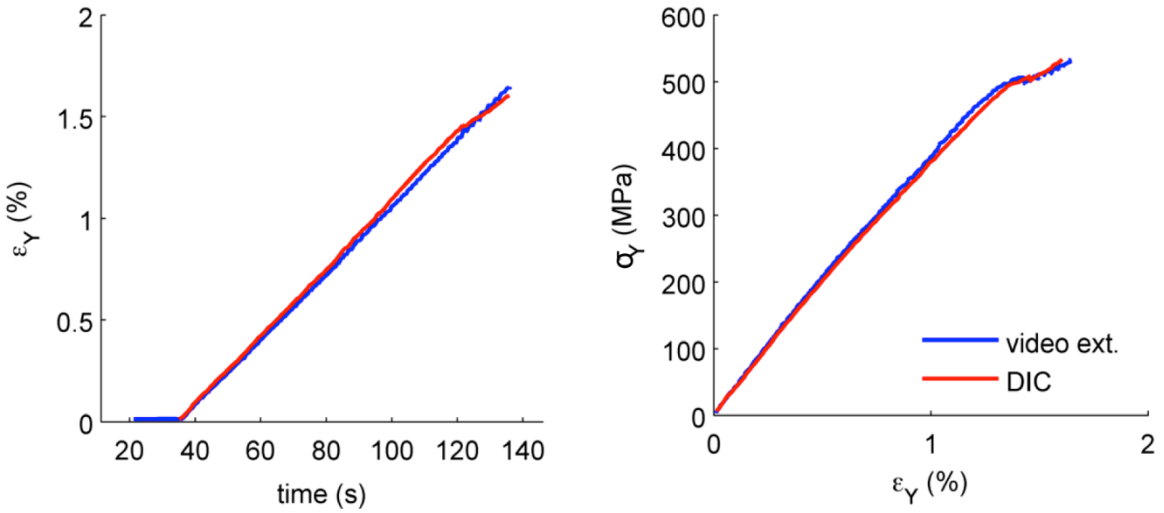

Figure 3.34 Comparison between the laminate strain measurements made with the video extensometer and the DIC system (random virtual extensometer technique). The coupon shown in this figure was tested in strain control, using the video extensometer measurement as feedback to the testing machine (coupon no. 13 Series 6).

3.6 Analysis of the experimental results

The following two sections contain analyses of the experimental results presented in Section 3.5. The analyses investigate whether the non-standard measuring techniques lead to higher material utilization or not.

3.6.1 Characterization of NCFs with a DIC system

The DIC system measures deformations, but so do clip-on extensometers, bonded strain gauges, and video extensometers. While the amount of data captured by the DIC system is far larger than the one captured by any of these three strain measuring techniques, one may wonder if it is actually necessary for the characterization of NCFs.

For the characterization of NCFs, the DIC system has two main advantages over bonded strain gauges, physical extensometers, and video extensometers:

No-contact–The DIC system is never in contact with the specimen. Bonded strain gauges are cumbersome to glue on the specimen, and their measurements require corrections [72,73]. Clip-on extensometers are easy to fix on the specimen, but they are usually removed before its fracture to avoid damage [59]. Video extensometers may require pins to be glued on the surface of the specimen. In the 2nd round of Series 6, the pins moved or flew-off before the fracture of the specimen, presumably due to small fractures at the surface caused by glue-induced strain concentrations.

Repeatability–Bonded strain gauges, clip-on extensometers, and video extensometers render a single measurement associated with their location, which is determined before the mechanical test takes place. With a DIC system, strain measurements take place after the mechanical test through a recording of the specimen surface deformation. The recording allows for multiple strain measurements at different locations on exactly the same specimen.

Both advantages, no contact and repeatability, can interact and lead to higher mean values and lower scatter for laminate stiffness and strength values. This claim is supported by the following two analyses.

3.6.1.1 Better understanding of the laminate response

The characterization of unidirectional laminates (Series 1) is a clear example of how the no-contact and repeatability of the DIC system measurements are advantageous. Figure 3.18 shows how through randomly located virtual extensometers the laminate strain can be measured all the way until till complete fracture. As stated previously, physical extensometers need to be removed before the complete fracture to avoid damage, and the pins of virtual extensometers may fly-off. Additionally, bonded strain gauges and markings for video extensometers are likely to be damaged by the progressive fibre fracture at the edges.

In Section 3.5.1, it was pointed out that the reduction of cross-section area is analogous to necking in steel coupons, and that if this is accounted for, the ultimate stresses are considerably higher than the ones normally reported (see red curve in Figure 3.24). Furthermore, the stress-strain curve would be concave, so according to the definition of the corrected ultimate strain, the ultimate strain and the elastic modulus would define the ultimate stress (see Figure 3.21). Table 3.1 compares the ultimate stress, ultimate strain, and corrected ultimate strain for the coupon presented in Figure 3.24, considering its stress-strain curve as either concave or convex.

Table 3.1 Design values for coupon no. 7 Series 1 whether the stress-strain curve is concave or convex.

	Concave	Convex
ε_u (%)	1.83	1.83
ε_u^c (%)	1.83	1.74
σ_u(MPa)	E $*$ ε_u= 1959	1863

The material utilization gains shown in Table 3.1 are only possible through DIC system based measurements. The repeatability and no contact allow for the location of random virtual extensometers in parts of the specimen that persist until the final fracture. This would be impossible with any of the other three strain measuring techniques. Nevertheless, these gains in material utilization are only relevant for Series 1. They are possible because the progressive fracture at the edges obscures the material response intended to be measured.

3.6.1.2 Appended Paper IV: Loss of accuracy on the characterization of NCFs due to strain measuring techniques

The appended paper IV shows that for NCF laminates, local strain measurements (e.g. bonded strain gages and clip-on extensometers) acting as proxies of global laminate strain contain a random strain measurement error. Furthermore, it demonstrates that this strain measurement error can significantly reduce the accuracy of characterization methodologies for NCF laminates. The strain measurement error pollutes the mechanical property measurements on laminate test specimens, leading to inaccurate statistical inferences.

Figure 3.35 presents boxplots summarizing the scatter of fifty design values for a laminate property. Each one of the fifty design value instances is obtained from a set of mechanical properties determined through single local strain measurements on a set of specimens. For all the design value instances, the specimens are the same. The only thing that changes is the location of the strain measurement in each specimen, and therefore, the strain measurement error in each specimen. The strain measurement error in each specimen causes the scatter of the design values in Figure 3.35. It pollutes the measurement of the mechanical property on each specimen, rendering different value combinations each time the design value is determined (for a more thorough explanation see the appended paper IV). The size of the strain measurement error is inversely proportional to the gauge size of the strain measurement, so the larger the gauge size is (width and length), the smaller the error, and consequently, the smaller the scatter of design values. The thick dashed horizontal line in Figure 3.35 represents the “best estimate” of the design value obtained when the strain measurement error is averaged out with multiple strain measurement replications in each test specimen. For the design value shown in Figure 3.35, the larger the gauge size is, the lower are the chances that the design value determined without strain measurement replications will be smaller than the “best estimate” one.

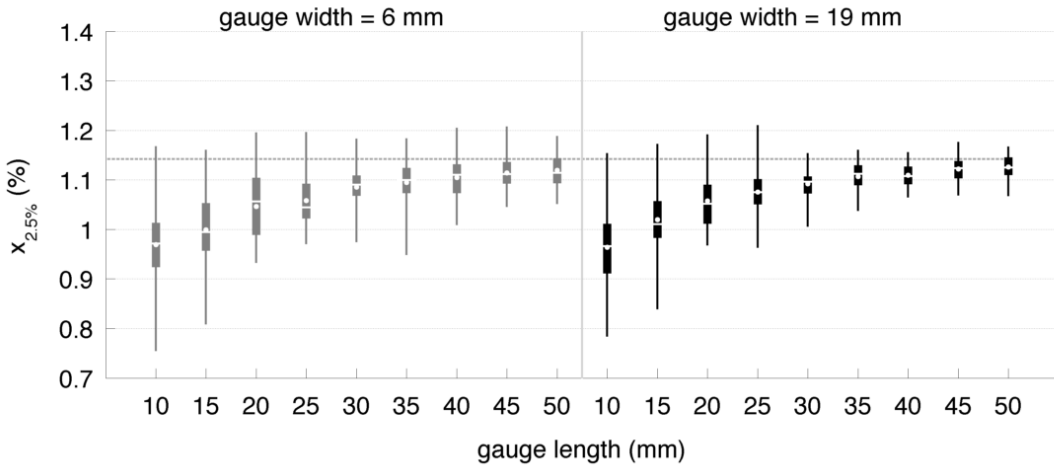

Figure 3.35 Relation between the scatter in the characteristic value of the corrected ultimate strain and the gauge size of a strain measurement. The design value is the 2.5-percentile of the corrected ultimate laminate strain of the Series 6 laminates. The boxplots summarize the scatter as whiskers: 1% to 99%, box: 25% to 75%, circle: average, white line: median.

The main conclusion of this paper is that since the strain measurement error decreases with increasing strain gauge size, strain measurements should be performed with the largest possible gauge size. An additional recommendation is to perform strain measurement replications on the specimens to average out the strain measurement error and obtain the "best estimate" design values. This recommendation is met by the random virtual extensometer strain measuring technique described in Section 3.4.7.4 if large numbers of them are used (e.g. 100). Using this strain measuring technique, improves material utilization by reducing the chance that the design values are unnecessarily low, or as reported in the appended paper IV, that the reported coefficients of variation for the mechanical properties are fictitiously high.

3.6.2 Matrix cracking identification

Experimental identification of matrix cracking is of great value. It allows for the experimental determination of load thresholds and quantitative descriptions (e.g. crack density curves) against which prediction methods can be evaluated. Furthermore, it can motivate less conservative limits for matrix cracking initiation and development (i.e. predictions vs. experiments), improving material utilization.

Some references state that the initiation of matrix cracking in a laminate can be determined through the stress-strain curve [1,47]. The argument is that since matrix cracks reduce the laminate stiffness, a transition-point formed by a bilinear curve fitted to the experimental stress-strain curve can indicate the strain at which matrix cracking initiates. Figure 3.36 presents such an analysis for one coupon in Series 6 (quasi-isotropic laminates). In the figure, the transition-point is marked with a circle at a strain 0.55%. This transition-point was determined by fitting a bilinear curve to the first 80% of the stress-strain curve. The last 20% was disregarded because, since the curve in Figure 3.36 has two inflexions, including it led to a bad fit of the bilinear curve. In the figure, the facet strain plots at the right show that before and at the transition-point (i.e. $\varepsilon_Y = 0.47$ and $\varepsilon_Y = 0.55$) there are bands of highly strained facets (possibly cracks).

The first problem with this definition for the matrix cracking initiation point is that it relies on the loss of laminate stiffness. Figure 3.27 shows a typical stress-stress curve for any of the cross-ply laminates in Series 3; the curve exhibits no loss of stiffness. Matrix cracks did develop on these types of laminate; however, the loss of laminate stiffness due to matrix cracking was so low that it was obscured by the stiffening of the carbon fibres. This method for determining matrix cracking initiation is in the best case under-conservative and in the worst case misleading. To some extent, the limitations of this method are addressed in DNV's CC where it is stated that: "Some matrix cracking tend to develop before the level [the transition-point in the fitted bilinear curve], but significant cracking can be defined this way."

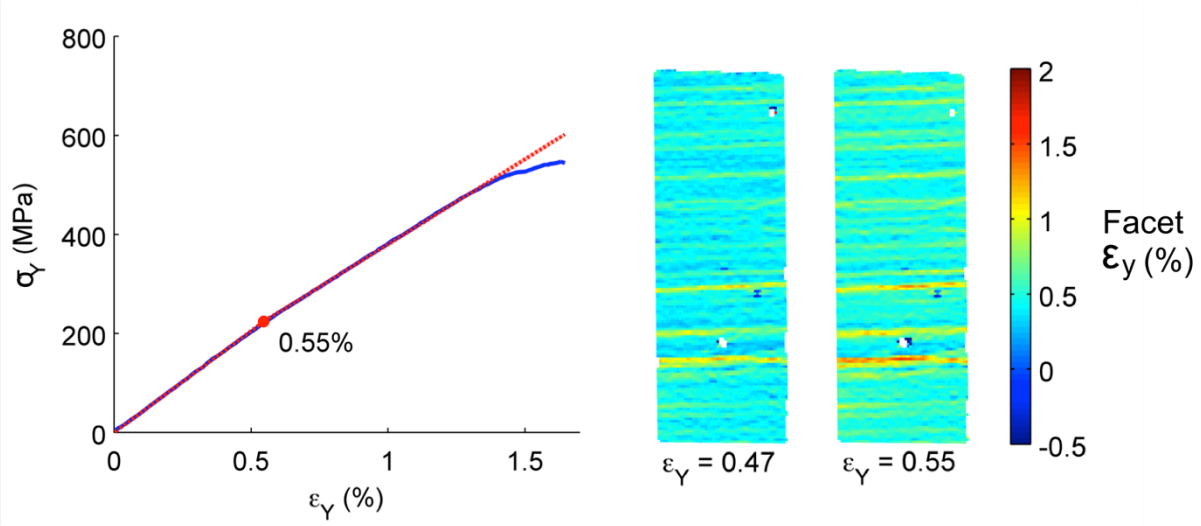

Figure 3.36 Example of a matrix cracking initiation point according to DNV's CC (coupon no. 4 Series 6).

In most investigations dealing with matrix cracking initiation and development, the presence, amount, and characteristics of matrix cracks are determined by stopping the test, removing the specimen, and inspecting it [74,75], while in others, the inspection relies on tomography and X-rays [71,76]. Both types of inspections render the specimens unsuitable for continuing their testing, so multiple specimens inspected at different loads are necessary to determine the full crack development vs. load curve for a given laminate. Clearly, this procedure is costly and cumbersome. If matrix cracks can be identified in DIC system measurements, the DIC system would be an easier and less expensive alternative to these aforementioned methodologies for matrix cracking inspection. However, one clear disadvantage of the DIC system is that matrix cracks can only be detected on the surface of the laminate seen by the system.

Technically, the DIC and AE systems provide enough information for identifying the initiation and development of matrix cracking. The following two sections analyse the results of each technique with respect to identification of matrix cracking.

3.6.2.1 AE system for matrix cracking identification

The AE measurements were intended for identifying the initiation and development of matrix cracking, progressive fibre fracture, and delamination on the specimens. Composite damage mode identification through AE measurements is a widely researched topic. The work by Sause et al. [63] is particularly promising. Sause et al.

champions a machine learning algorithm for clustering the AE events into damage modes through a set of frequency-related parameters. All the parameters are frequency-related because event amplitude and energy are not reliable parameters for characterization. The argument for dismissing them is that their values are inversely proportional to the distance between the event location and the AE system microphones, so the distance would act as a confounding factor in the damage mode identification. Unfortunately, the method proposed by Sause et al. was found after the tests were performed, and it could not be used because the AE measurements were made with narrow band sensors (R15alpha with a resonant frequency of 150 Hz). With narrow band sensors, the AE system cannot provide the partial frequencies required by the Sause et al. method.

An alternative was to use the AE measurements to relate the locations of the AE events to high strain areas observed in the DIC system measurements. This matching would ideally indicate if the high strains were because of fractures or because of high elastic strains. Unfortunately, this alternative use of the AE measurements was also not feasible because all of the AE measurements, except the ones for the unidirectional laminates (Series 1), were unsuccessful.

Figure 3.24 presents AE measurements corresponding to a unidirectional laminate. In the figure, one can appreciate that as the load increases, the number of AE events increases as well (dark grey dots throughout the plot), especially after the first significant drop in cross-section area. Similarly, the maximum absolute energy of the individual events also increases with increasing load, and as one would expect, the event with the largest absolute energy is registered at the final fracture of the specimen. This characteristics indicate that the AE events for this unidirectional laminates were successfully captured. For all other series, the AE measurements were unsuccessful. In Figures 3.27 and 3.32, corresponding to the cross-ply and quasi-isotropic laminates respectively (Series 3 and 6), most of the AE events cluster at a narrow band of absolute energy (it is worth noting that the y-axis limits on Figure 3.24 and Figures 3.27 and 3.32 are different). One could argue that these clustered events are background noise which should have been filtered out, but near to the final fracture of the coupons, the clustering of the events fades out. If it was indeed background noise the fading-out should not occur and the clustered events should be always a lower bound for the events (which are indeed in Figure 3.27, but not in Figure 3.32). Furthermore, a plot of the AE event location showed that all the events were exactly at the location of the microphones and nowhere in between. In the case of Series 5, the AE measurements stopped abruptly shortly after the coupons started being loaded. The reason for the clustering of the AE events at the microphone location and the abrupt halt on the recording could not be determined.

Experimenters interested in the identification of composite damage modes with AE systems are encouraged to consider the Sause et al. method, and correspondingly, use wide-band microphones on their measurements.

3.6.2.2 DIC system for matrix cracking identification

Figure 3.37 presents the ε_y facet strains in one of the specimens of Series 6 (quasi-isotropic laminate with fibres in the transverse direction at the surface) at five different laminate strains. The contour plots at the top and the bottom only differ with respect

to the limits of the colour bars indicating the value for each facet. If the value of the facet exceeds the limit, the colour of the facet is of the limit it exceeds. In the figure, one can appreciate that as the laminate strain increases bands of high strains develop. The facet strains in these bands are significantly larger than the ones of the laminate itself, and in some areas, high strain facets are next to facets with negative strains. Presumably, the negative values are caused by the relaxation of the surface after the formation of a crack. The measurements look promising for the identification of matrix cracks, but a hurdle is defining a matrix crack as a facet strain value (or mix of strain values). The question is: at what strain is the transition from highly strained facet to fractured facet? In the top contours, some facets have strains above 10%. These facets are clearly damaged, but the really sought for value is at which facet strain did the matrix crack form. While matrix cracks are observable on the images taken by the DIC system (see pictures in Figure 3.26) it is possible that the matrix cracks are only visible well after their formation. AE measurements could assist in the identification of the matrix crack formation strain, but as mentioned in Section 3.6.2.1, the AE measurements were unsuccessful.

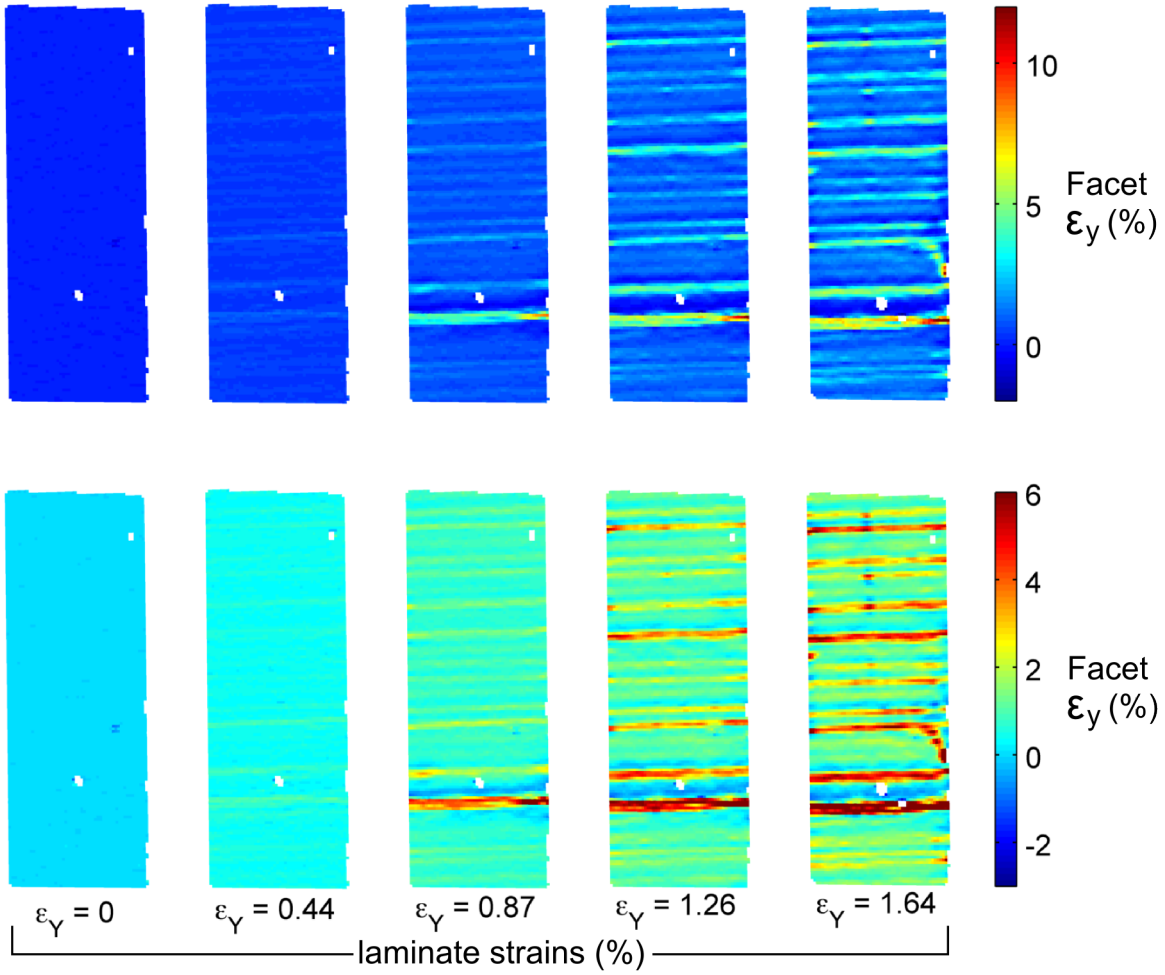

Figure 3.37 Facet strains at five laminate strain values with two different colour coding. Selecting a facet strain that indicates the formation of a matrix crack is not a straightforward choice. (Laminate strain was calculated with the random virtual extensometer technique (coupon no. 4 Series 6.)

An alternative to using facet strains to identify matrix cracks is to use facet locations. When a matrix crack forms on the surface of the laminate, it eventually causes a bump on the surface. Figure 3.38 presents a comparison between the facet strains and out-of-plane facet locations (3-axis in the local coordinate system) of one of the specimens in Series 6 at five different laminate strains. In the figure, one can observe a clear relation between both types of information. To some extent, the out-of-plane location plots assist in the identification of matrix cracks: high strains and an out-of-plane displacement is clearly a crack. But, as with the DIC system images, the problem is that matrix cracks may only lead to out-of-plane displacements well after their formation.

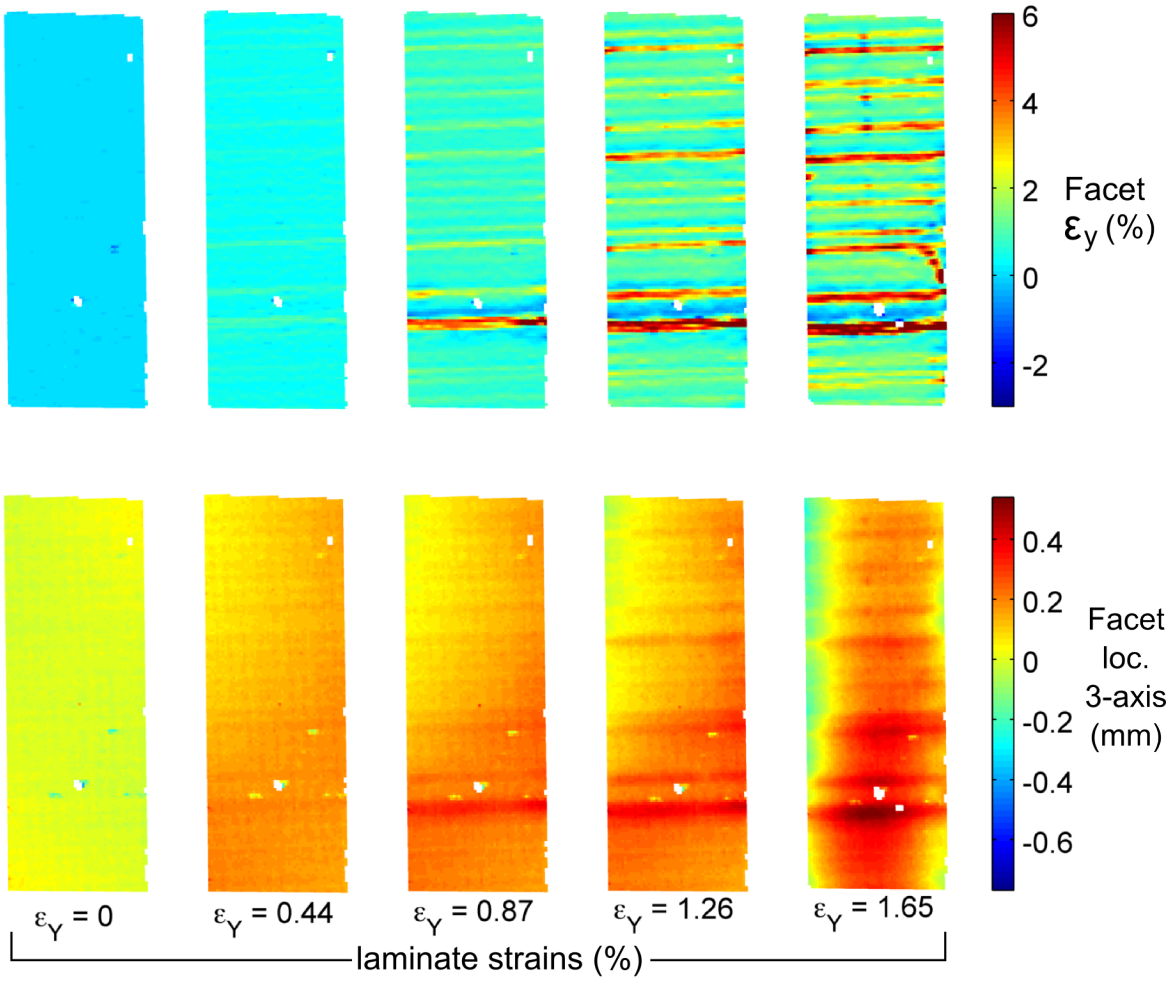

Figure 3.38 Facet strains and locations at five laminate strain values. Laminate strain was calculated with the random virtual extensometer technique (coupon no. 4 Series 6).

A final possible method for estimating the initiation of matrix cracks from DIC measurements is shown in Figure 3.39. The method is relatively simple. The ε_y facet strains of each stage are treated as a sample, and for each of these samples, the average value, 5th percentile, and 95th percentile are calculated. In Figure 3.39, one can observe that at a certain loading (close to 300 MPa) the difference between the average values and the percentiles increases dramatically. This sharp increase is caused by relatively

sudden increase of the spread of the facet values. Presumably, the increase of the spread is caused by the formation of surface cracks. A similar method is presented in [48], were individual facet values are compared against a scatter considered as probable (improbable facet values are somewhat equivalent to the 5th and 95th percentiles in Figure 3.39. The method presented in [48] also shows a sudden increase on the value of the facets, and more importantly, the increase matches and increase in AE events. As explained in Section 3.6.2.1, the AE measurements in this experimental work were not successful, and therefore a similar comparison cannot be made.

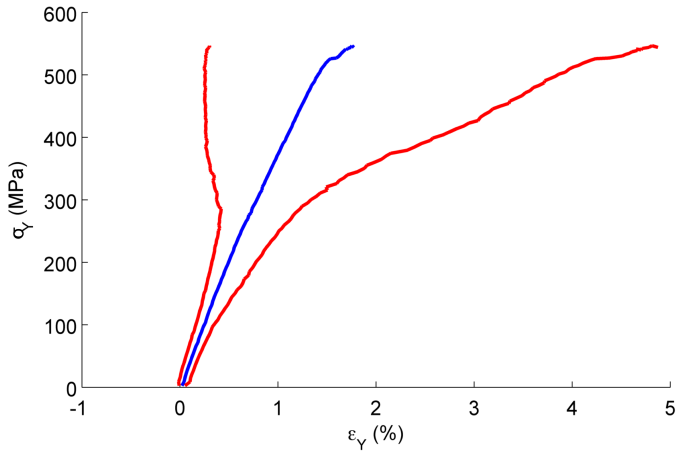

Figure 3.39 Average (blue), 5th and 95th percentiles (red) of the ε_y facet strains at each stage. Steep increase in spread may indicate matrix cracking initiation and the surface of the specimen (coupon no. 4 Series 6).

Overall, these three methods are examples of how DIC measurements can be used along a AE system to identify the initiation and development of matrix cracking. A comparison or deep analysis of the suitability of each of the presented methods was not possible, because the AE measurements were unsuccessful.

3.7 Concluding remarks

The work presented in this chapter aimed at exploring the possibility of improving material utilization by using non-standard measuring techniques in material characterization. A series of mechanical test related to the characterization of an ideal NCF ply and a quasi-isotropic NCF laminate were carried out using two non-standard measuring techniques: DIC and AE systems. Both measuring techniques held promise of allowing the identification of matrix cracking initiation and development, as well as a more accurate measurement of stiffness and strength properties.

The most significant contribution of this experimental work is documented in the appended paper IV. The analysis in this appended paper was neither foreseen nor planned. This paper is the result of a large number of insights while struggling with how to measure laminate strains with the DIC system. The main takeaway of this paper is simple: to characterize a NCF laminate, or any other textile composite, use a strain measuring device with a gauge size as large as possible. Doing so, will potentially lead to more consistent measurement results, improving design values and perhaps leading to consistent conclusions regarding the characteristics of NCFs [56].

The struggle with the DIC system as tool in characterization led to the second major contribution of this experimental work: how to characterize a NCF (or any textile composite) with a DIC system. Considering the contents of the appended paper IV, and the descriptions in this chapter about the different strain measuring techniques, the random virtual extensometer technique is the best one for characterization.

Can non-standard measuring techniques in material characterization lead to higher utilization? Yes. The repeatability and non-contact of the DIC system are valuable advantages compared to standard strain measuring techniques. Furthermore, the identification and imitation of matrix cracking with a DIC system is likely possible if assisted with successful AE measurements.

Explore

Travel through the unknown to learn about it.

4 Structural Design Exploration

As an action, structural design is the process of planning the characteristics of a structure so that it fulfils a purpose. Structural design exploration is the act evaluating different design variations to determine how or if the design can be improved.

In a complex structure, the result of varying a design variable is not trivial. For example, the relation between a design variable and the response of a structure may not necessarily be proportional or even linear. Structural design exploration plays an important role in the design of complex structures because it facilitates understanding the importance of different structural elements in a complex structure, potentially enabling its improvement. Weight is one of the many characteristics of a structure which may be studied through design exploration, and therefore, it can potentially be reduced through it.

The work in this chapter is included in this thesis because, among other things, it tentatively answers a question that naturally arises from the work in Chapters 2 and 3: What is the potential in weight reduction of these approaches? This work is planned to be developed into a journal paper. Section 4.1 presents a brief background of design approaches to structural weight reduction. Section 4.2 presents the objective of the work in this chapter, and Section 4.3 the methodology for reaching it. The results are presented in Section 4.4, and concluding remarks are given in Section 4.5.

4.1 Background

A constrained optimisation problem can be stated as,

$$\text{find } \mathbf{X} = \begin{bmatrix} x_1 \\ x_2 \\ \vdots \\ x_n \end{bmatrix} \text{ that minimizes } f(\mathbf{X}) \tag{4.1}$$

constrained by,

$$g_j(\mathbf{X}) \leq 0 \quad j = 1, 2, \dots, m \tag{4.2}$$

$$l_j(\mathbf{X}) = 0 \quad j = 1, 2, \dots, p \tag{4.3}$$

where $\mathbf{X}$ is the design vector representing n design variables, $f(\mathbf{X})$ is the objective function, and $g_j(\mathbf{X})$ and $l_j(\mathbf{X})$ are inequality and equality constraints respectively. The design space is a n-dimensional Cartesian space where each coordinate represents the value of one of the design variables, and consequently, each point in the design space is a design point. Whether a design point is acceptable or not depends on the design constraints. If the design point meets the constraints, the design point is an acceptable design. In an optimisation problem, there are generally multiple acceptable designs, each of which may have different objective values (the output of the objective function when evaluated with the design point in question). In the entire design space, the acceptable design that renders the lowest objective value is the optimum design. Finding it is the purpose of optimisation methods, which depending on the characteristics of the objective function and the constraints of the problem, may find it or not. The best design is the acceptable design with the lowest objective value *found* through an optimisation method; it may or may not be equal to the optimum design.

Following this mathematical description of a constrained optimisation problem, an engineer has essentially two approaches for reducing the weight of a structure design:

1. Search the design space for a lighter design.
2. Modify the constraints of the design.

An engineer may search the design space with different methods depending on the characteristics of the problem, the available resources, and the benefits associated with the objective value. Some optimisation problems can be solved analytically; the "search" for the optimum design consists of the analytical manipulation of the objective function and constraints. For example, finding the minimum diameter for a weight-critical steel rod that should not yield under a given tensile load is one such problem. Within a minute, a structural engineer can formulate an equation for the minimum diameter of the rod as a function of the yield stress of the steel. As long as

the objective function and constraints of an optimisation problem can be explicitly stated as a function of the design variables, and are both, continuous and differentiable, the optimum design can be found analytically. For all other optimisation problems that do not meet these requirements, approximations to the optimum designs can be found with numerical methods.

All numerical methods consist of an algorithm for searching the best design through the evaluation of design points [77]. An arguably common numerical method for optimising a structure is the iteration of a design following one's understanding of the problem. For example, a structural engineer designing a stiffened shell structure may iterate the thickness of the shell-plate, as well as the spacing and cross-section of the stiffeners to reduce the weight of the overall structure, while complying with deflection constraints. The structural engineer knows that decreasing the thickness of the plate decreases its weight, but it also increases the deflection of the shell-plate when subjected to an out-of-plane pressure. Similarly, he or she would also know that decreasing the spacing between the stiffeners decreases the deflection of the plate, but it also increases the number of stiffeners, which in turn increases the weight of the overall structure. The design iteration may continue until the structural engineer is satisfied with the result, but there is no guarantee that the best design found through this method is near the optimum design of the problem. Nowadays, there are many alternatives to this iteration method that can render better designs. Through mathematical programming techniques and heuristic optimisation algorithms, such as particle swarm optimisation and genetic algorithms, one could technically solve all optimisation problems that cannot be solved analytically [77]. Nevertheless, an important aspect of numerical methods is that their implementation and solution can require a considerable amount of man-hours and computational time and resources. One must first build a parametric model of the structure design that can be evaluated automatically, and then couple it to an algorithm that depending on the number of design variables, may require hundreds, if not thousands, of design point evaluations. From the economical perspective, one may wonder if it is worth it.

Modifying the design constraints is an alternative to searching the design space. In some cases, this approach enables designs with objective values that would be unattainable otherwise. For example, using high-strength steel instead of mild steel on the previous weight-critical steel rod example is a change in the design constraint of the problem. The minimum diameter is constrained by the yield stress of the material, and both materials have roughly the same stiffness and density, but significantly different yield stress. Using high-strength steels allows for a smaller cross-section, resulting in a lighter rod. In this example, the optimum design can be explicitly stated as a function of the design variables, and it is clear that by searching the design space one cannot find a mild steel design as light, or lighter, than the lightest high-strength steel one. Changing the stress constraint of the problem enables otherwise unattainable lighter designs.

In the steel rod example, the design constraint was determined by the material. If the example had been formulated with the material as one of its design variables, using high-strength steel instead of mild steel would not be a modification of the design constraints; it would just be another coordinate in the design space.

Chapters 2 and 3 presented work aimed at modifying design constraints of FRP composite structures; namely, the ones related to the ULS in tension. The motivation for doing so is similar to the one for using high-strength steel instead of mild steel in the previous example. Higher operational limits for the material enables the use of lighter components. In contrast with the steel rod example, the work in Chapters 2 and 3 were not about changing the material, but about changing the considerations about the material. Usually, composite marine structures consist of multiple structural elements and are subjected to more than one load case. While the ULS in tension is a common material constraint for many structural elements, there are more constraints which, depending on the purpose of the structure, its design, and design rules followed, may play a larger role on the attainable objective values. For a complex structure subjected to multiple load cases, such as a hull, the benefits of modifying a design constraint cannot be straightforwardly determined as in the steel rod example.

To recap, a structural engineer may design lighter structures by searching the design space or modifying the constraints of the design problem. As the complexity of the design problem increases (e.g. number of design variables and constraints), searching the design space becomes more costly, and the benefits become less clear. Additionally, identifying the design constraints that limit the most the attainable objective values becomes more difficult, and so does determining the benefits of modifying them.

4.2 Objective

The objective of the work presented in this chapter is to assess the potential of searching the design space (e.g. structural design optimisation) and modifying the design constraints (e.g. improved operational limits and material characterization), as two approaches for weight saving in composite marine structures.

4.3 Methodology

This section is divided in three sections. Section 4.3.1 presents a design exploration methodology for assessing the potential benefits of the two approaches on an optimisation problem. Section 4.3.2 presents the study case on which the methodology is applied, and Section 4.3.3 summarizes all the limitations of the analysis.

4.3.1 Design exploration methodology

We developed a design exploration methodology to assess the potential benefits of modifying design constraints and searching the design space in an optimisation problem that cannot be explicitly stated as a function of the design variables. In its simplest form, our methodology is the following:

1. Sample the design space within the non-modifiable constraints.
2. Evaluate the objective function.
3. Implement the modifiable design constraints.
4. Plot a histogram of the objective values of the acceptable design points.
5. Change the value of the modifiable design constraints.
6. Repeat step 4.

7. Analyse the histograms to determine the potential benefits of the two approaches.

The potential benefits of the two approaches is determined from the objective value histograms of the acceptable design points. Figure 4.1 shows the characteristics of an objective value histogram which are relevant for our method. The range of objective values approximately describes the potential reduction that can be achieved by searching the design space. Whether or not modifying a design constraint is beneficial is determined by comparing the objective value histograms of design points subjected to different sets of design constraints. If the modification of the design constraint renders in a new range with significantly lower bounds, then modifying the design constraint is beneficial. The following two examples illustrate and clarify this methodology.

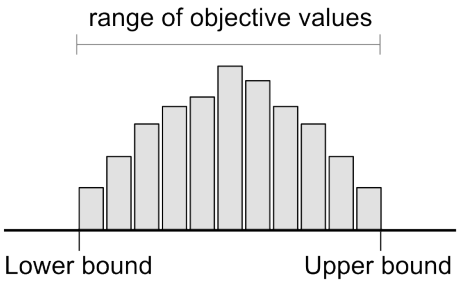

Figure 4.1 Characteristics of the objective value histograms used in the design exploration methodology.

First example

Consider an unitless objective function $f(x_1, x_2)$ that cannot be explicitly stated as a function of the design variables, but it can be evaluated. The two design variables have the upper and lower limits,

$$-10 \leq x_1 \leq 10$$
$$-10 \leq x_2 \leq 5$$

where the upper limit of the x_2 is the only modifiable constraint. We would like to know the potential benefit of increasing its value, as well as the benefit of searching the design space.

Step 1. Sample the design space

The evaluation time of the objective function limits the number of samples that can be generated to study the problem. We would like the feasible number of samples to cover the design space as much as possible, since the better they cover it, the more representative will the analysis be. Latin hypercube sampling is good at filling n-dimensional design spaces, and it is therefore used as the sampling method [78]. Figure 4.2 shows 100 samples in the 2-dimensional design space of this problem. Note that the sampling extends beyond the upper limit of the x_2 constraint. This is necessary for determining the benefits of increasing its value.

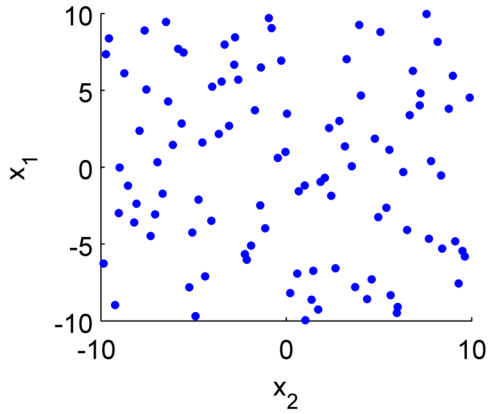

Figure 4.2 Latin hypercube samples on the 2-dimensional design space.

Step 2. Evaluate the objective function

For this example, evaluating the objective function is a straightforward step. Figure 4.3 presents the objective values for each one of the sampled design points.

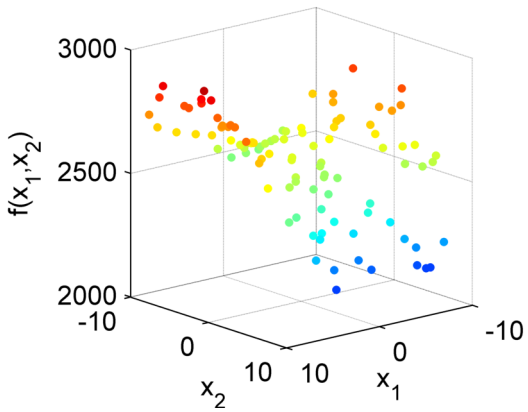

Figure 4.3 Objective values of the sampled design points.

Step 3. Implement the modifiable design constraints

The modifiable design constraints are implemented by removing the design points that do not comply with them. Figure 4.4a shows a scatter plot with the acceptable design points according to the original constraints.

Step 4. Plot a histogram of the objective values of the acceptable design points

Figure 4.4b shows the histogram of the objective values of the acceptable design points in Figure 4.4a. One can read in the plot the lower and upper bound of the objective value histogram of the acceptable design points.

Step 5. Change the modifiable design constraints

Figures 4.4c and 4.4e show the acceptable design points according to two modified sets of constraints with 7.5 and 10 for the upper limit of x_2.

Step 6. Repeat step 4

Figure 4.4d and 4.4f show the histograms corresponding to the objective values of the acceptable design points in Figures 4.4c and 4.4e respectively.

Step 7. Analyse the histograms to determine the potential benefits of the two approaches

The histograms in Figure 4.4 illustrate the potential benefit of increasing the upper limit of the x_2 constraint. As the upper limit is increased, design points with objective values smaller than the ones of the previously accepted design points become acceptable. The lower limit of the range of objective values decreases. This means that modifying the constraint enables design points with desirable objective values that would not be available otherwise.

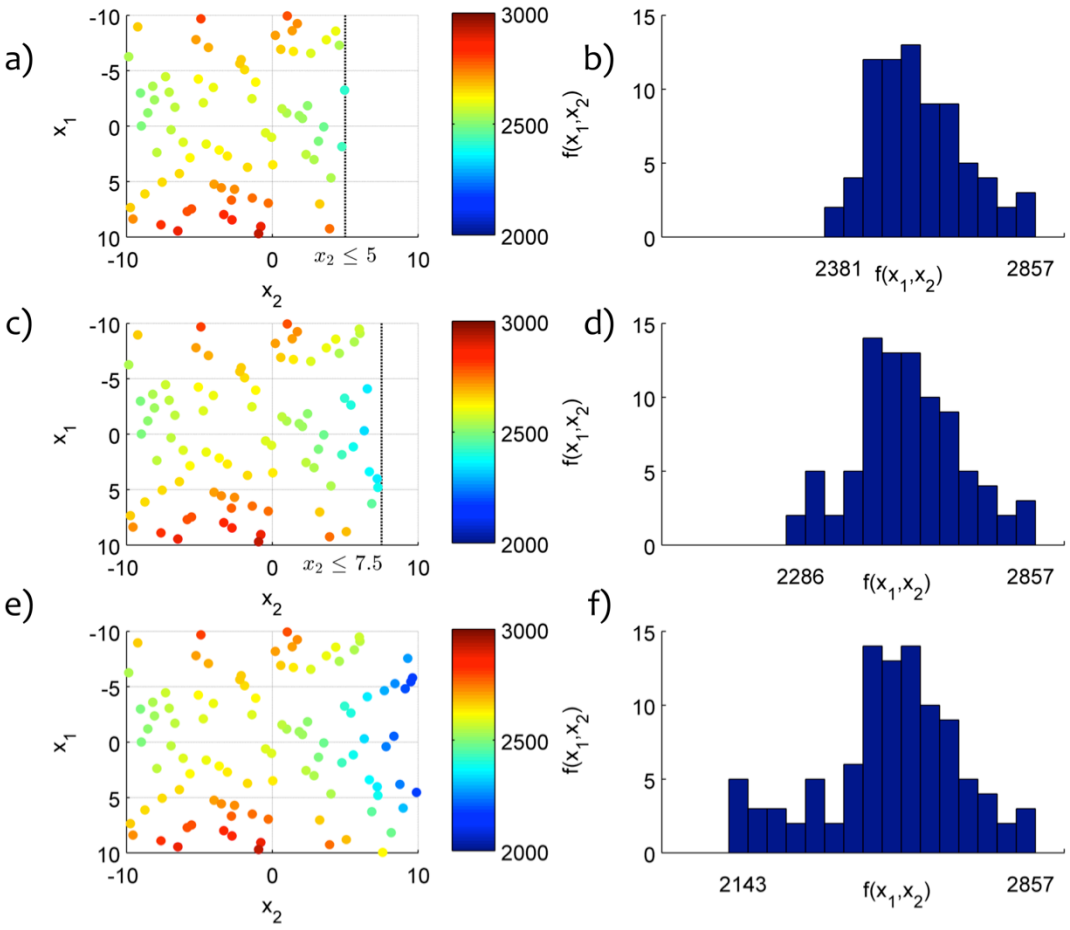

Figure 4.4 Scatter plots showing the acceptable design points for different sets of design constraints (a, c, e) and histograms of their objective values (b, d, f).

Second example

As in the previous example, consider an objective function $f(x_1, x_2)$ that cannot be explicitly stated as a function of the design variables, but it can be evaluated. The two design variables have the upper and lower limits,

$$-500 \leq x_1 \leq 500$$
$$-500 \leq x_2 \leq 200$$

As before, the upper limit of the x_2 is the only modifiable constraint, and we would like to know the potential benefit of increasing its value, as well as the benefit of searching the design space. For brevity, we deal immediately with the last step: analysing the histograms. Figure 4.5 contains the same type of plots as Figure 4.4 for this second example.

From the histograms, one can realize that increasing the x_2 constraint does not enable design points with better objective values. The range of objective values remains the same despite the increase. In other words, there is no benefit on modifying the constraint, as the smaller objective values are available within the original constraints.

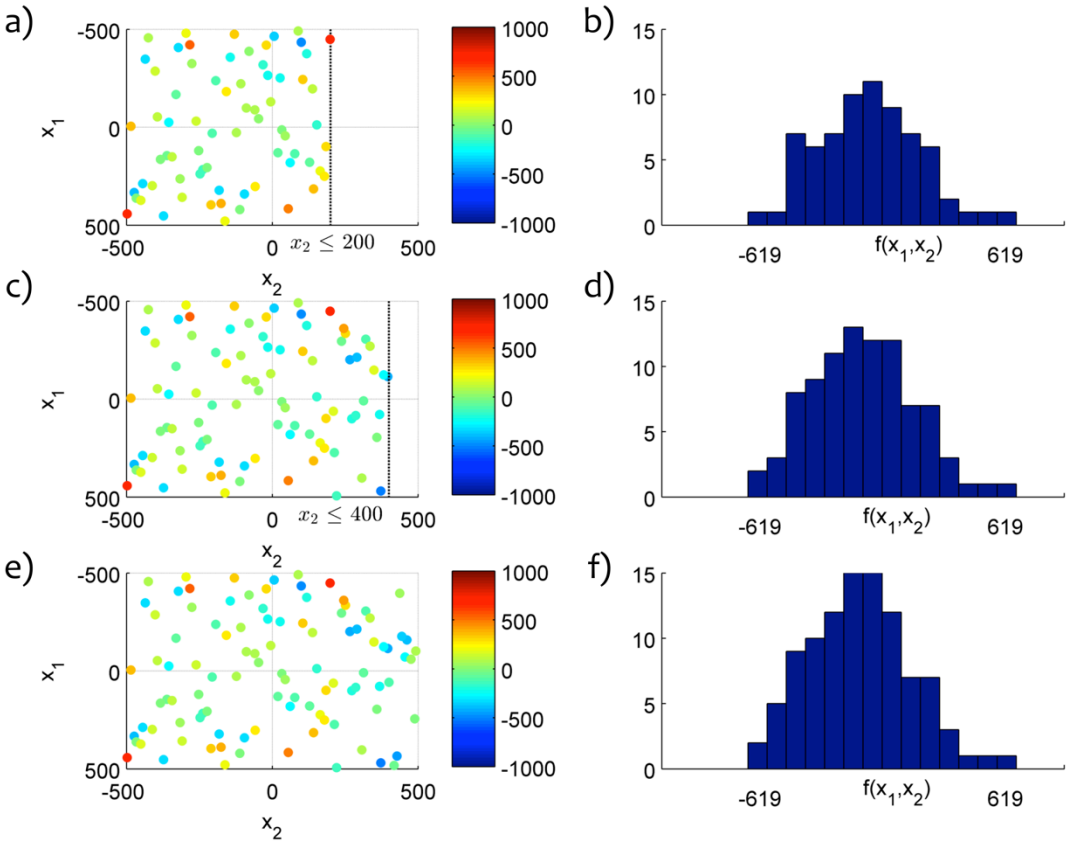

Figure 4.5 Scatter plots showing the acceptable design points for different sets of design constraints (a, c, e) and histograms of the objective values of the acceptable design points (b, d, f).

The two examples show how our design exploration methodology enables the assessment of the potential benefits of searching the design space and modifying the constrains of an optimisation problem. There is, however, one important limitation that must be kept in mind. The potential benefits of both approaches are determined from a random sample of design points, and there is no guarantee that the sample contains the design points with the maximum and minimum objective values within a constrained design space. Therefore, the range and bounds of the objective value histograms are just an approximation. The quality of the approximation depends on the shape of the objective function, the number of samples, and how well these fill the design space. Plotting the histograms of the objective values (rather than just the range) is helpful because it hints how good the ranges are for the different sets of

constraints. In Figure 4.4b, a large fraction of the acceptable design points have an objective value close to the lower bound. To some extent, this characteristic means that the lower bound is well explored, giving some extra credibility to it. However, it may very well be that an acceptable design point with a smaller design point exists.

The analyses of the objective value histograms can be confirmed for the two examples by plotting the objective functions. Figure 4.6 shows a comparison of the shape of the objective functions of both examples and the location of the sampled design points. For the first example (left plot in Figure 4.6), the objective function has a steep negative gradient that begins approximately when $x_2 = 5$. Clearly, increasing the x_2 constraint enables lower objective values. The second example is quite different from the first; its objective function (right plot Figure 4.6) has multiple local minima and maxima throughout the design space. Increasing the x_2 constraint does not enable design points with lower objective values as dramatically as in the first example. The global minimum may be within the newly allowable design space, but in general there is no clear benefit.

Since there are doubts concerning the trustworthiness of the acceptable design bounds, one may ask: why not use optimisation algorithms to find the upper and lower bounds of the acceptable design points? While doing so would render more trustworthy bounds, it would require running the optimisation algorithm with all its hundreds or thousands of evaluations for each set of design constraints. Optimisation algorithms need the design constraints to know where to look. Running an optimisation algorithm for every modification of the design constraints is technically feasible, but time wise prohibitive. For assessing the potential benefits of searching the design space and modifying the constraints, the bounds obtained from random samples were deemed as acceptable.

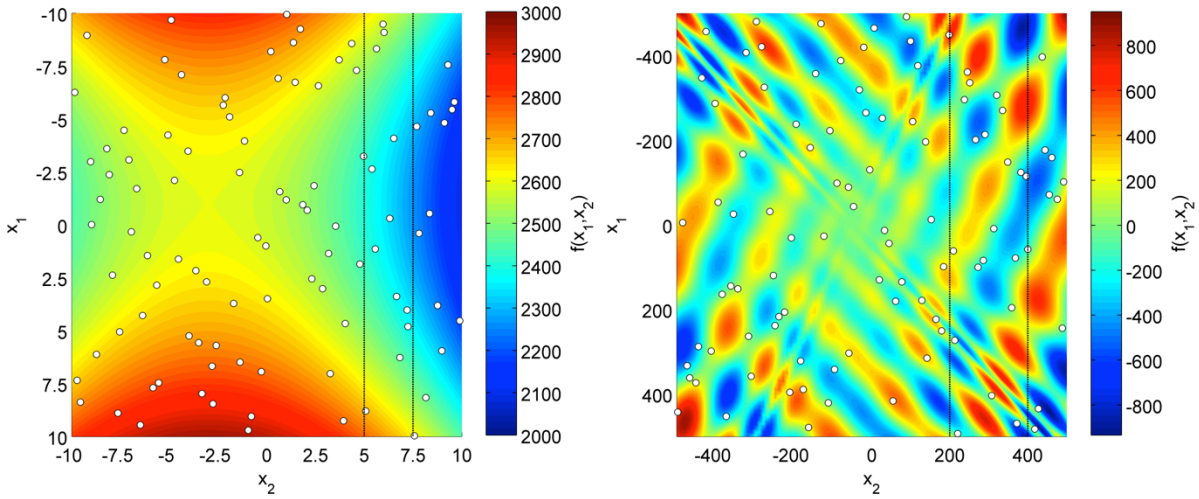

Figure 4.6 Comparison of the shape of the objective function and the location of the sampled design points (left: first example, right: second example). The dotted horizontal lines indicate the original and modified design constraints. The colours are determined by interpolating the areas between the investigated points.

4.3.2 Study case

The study case is the weight optimisation of a catamaran ferry hull girder built with sandwich construction. This type of structure has been built for some time now [79], and the interest for it is increasing [80]. Considering that the findings of our design exploration methodology will, to a large extent, be coupled to the analysed structure, it is reasonable to choose one which is of interest today and of relevance for the future. The hull girder of a catamaran has the additional benefit of being a complex structure subjected to multiple and challenging load cases; therefore, the different behavioural constraints of the material are likely to limit the design. Having all the behavioural constraints active is desirable because it allows for a general comparison of their relative importance, as well as a comprehensive assessment of the potential of the two approaches.

The particulars of the study case catamaran are presented in Table 4.1. With the exception of the characteristics in italics, all of them were determined through a method developed by Molland et al. for estimating dimensions, powering, and seakeeping characteristics of fast ferries [81]. The characteristics in italics are the input required by Molland et al. method, which relies on linear regression, a large database of existing vessels, and experimental measurements for estimating the other characteristics. The input characteristics in Table 4.1 were chosen, based on published characteristics of existing fast ferries [79], so as to render a fairly generic catamaran ferry. Using a generic design is important for this study since, as mentioned previously, it is desirable that the conclusions are as broadly applicable as possible.

The procedure for performing the initial four steps of our design methodology are shown in Figure 4.7. The first step requires the definition of the design variables and the fixed constraints of the problem. For this study case, the fixed constraints are the ones related to the construction of the catamaran hull girder (i.e. side constraints), while the modifiable constraints are the ones related to the acceptance of the structure design based on its performance (i.e. behavioural constraints). Once the design variables and fixed constraints are explicitly defined, step one concludes with the generation of design points through latin-hypercube sampling. The second step, the evaluation of the objective function, is the most technically challenging one. The evaluation requires not only the calculation of the weight of the structure designs (i.e. the objective value), but also the calculation of input for the modifiable constraints (i.e. stresses and strains). In step three, the modifiable constraints are applied to determine whether or not each individual design is acceptable. If the design meets the modifiable constraints, it is labelled as “OK” and used in step four: plotting a histogram of the objective values of the acceptable design points.

The following sections explain in detail the elements of the procedure shown in Figure 4.6.

Table 4.1 Characteristics of the study case fast ferry

Number of passengers (Np)	*275*
Number of crew members (Nc)	*6*
Speed (V)	*30 knots*
Range (Ra)	*200 nautical miles*
Seating area per passenger (As/Np)	*0.65 m^2*
Passenger area to seating area ratio	*1.2*
Length overall to waterline length ratio (Lo/L)	*1.13*
Number of passenger decks	*1*
Number of engines	*2*
Type of engines	*Diesel 1800 rpm*
Engine's specific fuel consumption	*0.2 kg/kWh*
Propulsion system	*Waterjets*
Length overall (Lo)	38.8 m
Waterline length (L)	34.3 m
Breadth of the pontoons (b)	2.83 m
Draught (T)	1.14 m
Depth overall (Do)	8.26 m
Block coefficient (Cb)	0.55
Separation between pontoon centrelines (S)	6.86 m
Installed power (Pi)	2955 kW
Displacement (▽)	126.20 tonnes
Mass of the structure	54.46 tonnes
Mass of the engine	5.76 tonnes
Mass of the gearbox	0.82 tonnes
Mass of the waterjets	0.98 tonnes
Mass of the remaining machinery	8.34 tonnes
Mass of the passengers	28.87 tonnes
Mass of the crew	0.81 tonnes
Mass of the fuel	3.93 tonnes
Mass of the fresh water	2.29 tonnes
Mass of the outfittings	10.16 tonnes

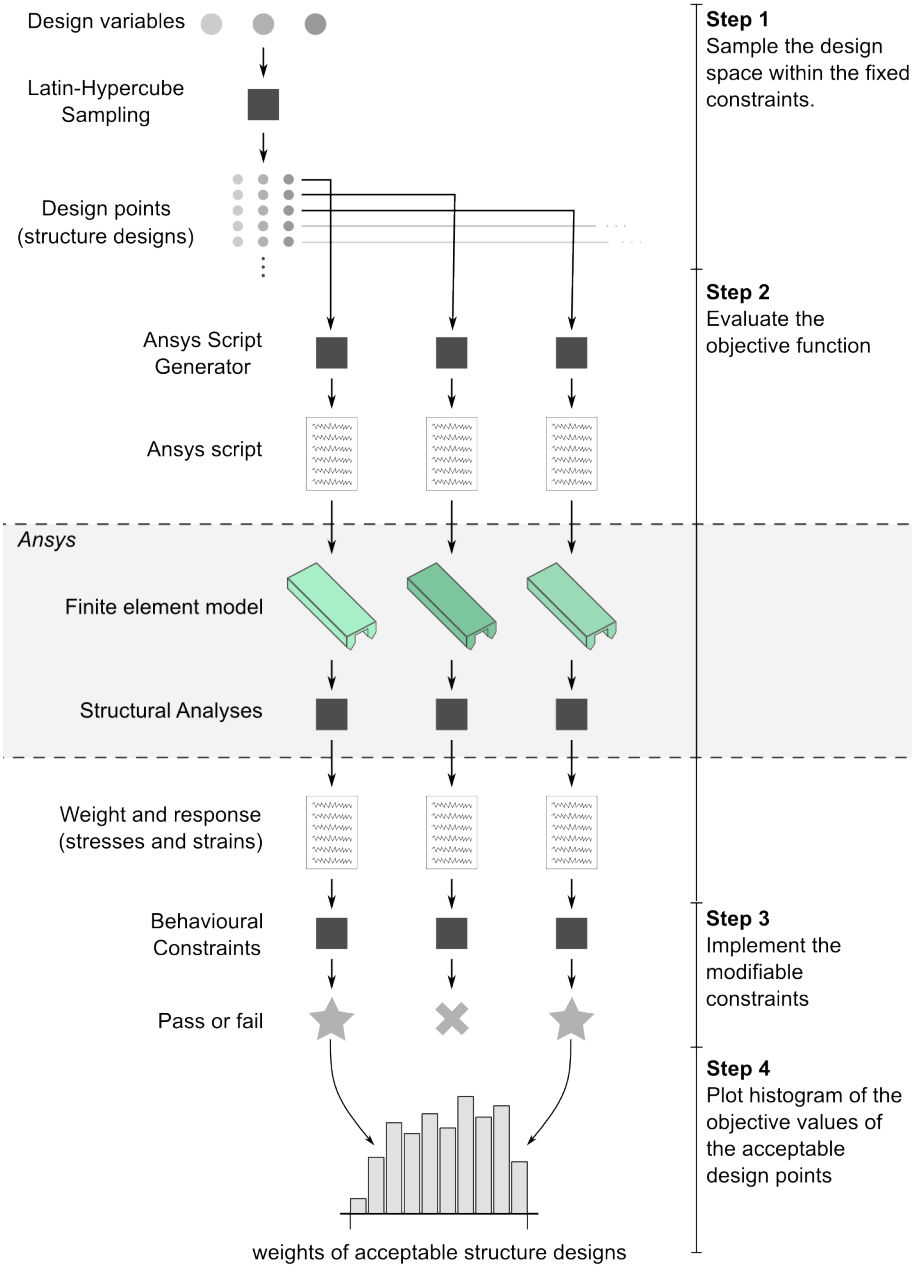

Figure 4.7 Procedure for performing the first four steps of the design exploration methodology for the study case.

4.3.2.1 Design variables

The design variables determine to some extent the shape of the hull girder, and to a full extent, its scantlings. The ranges of values for the design variables are limited by the side constraints problem: manufacturing limitations, material availability, and dimensional requirements and limitations. According to the Molland et al. method [81], the pontoons of our catamaran are to be shaped as Series 64 hulls; however, for this first study case, the shape of the pontoons is simplified dramatically. Figure 4.8 shows the shape of the catamaran hull girder. The separation between the pontoon centrelines (S), the depth of the pontoon (Dp), and the height of the connecting structure (Hc), are the design variables that modify the shape of the catamaran hull

girder. The length of the catamaran (L), breadth of the pontoons (b), and the rake angle (Ra), have the same value for all structure designs.

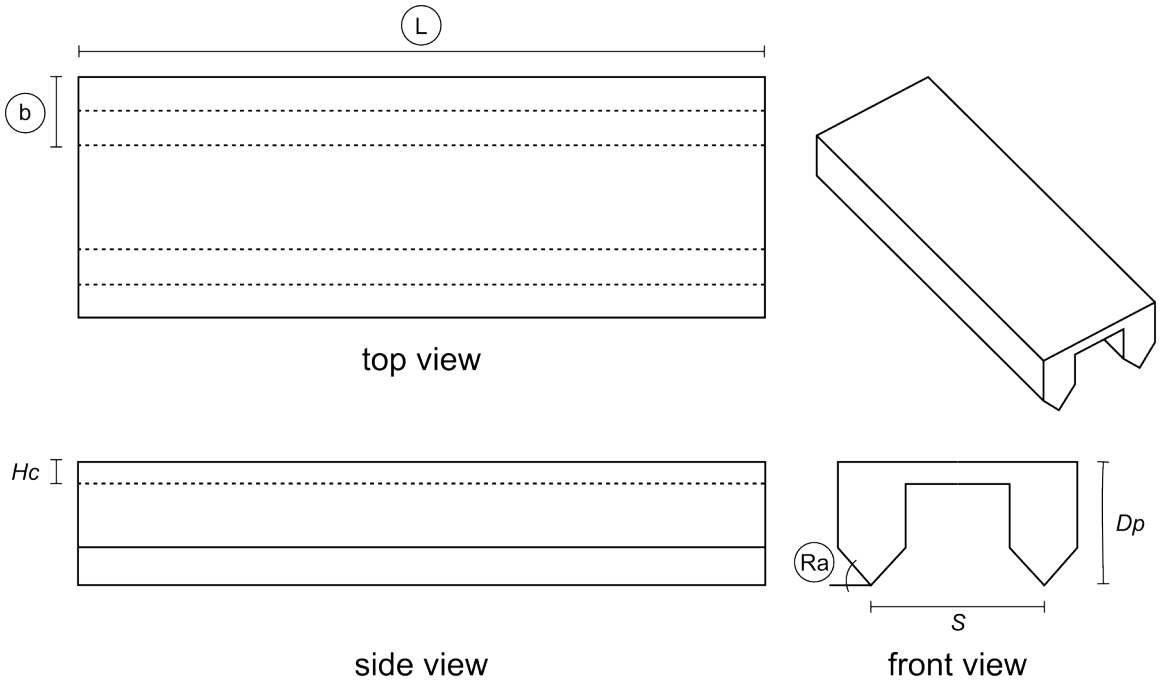

Figure 4.8 Shape of the catamaran hull girder and the parameters (circled labels) and design variables governing its dimensions.

An example of the catamaran hull girder scantlings is shown in Figure 4.9. All the structural elements can be classed as either plates or stiffeners. The shell, bulkheads, and decks are plates, while web frames and girders are stiffeners. Figure 4.9 shows the general construction of the plates and stiffeners. Both plates and stiffeners are built with sandwich construction consisting of carbon/vinylester quasi-isotropic laminate skins and a Divinycell core. The stiffeners have an additional element: a unidirectional laminate at the top acting as a flange. For all structural elements (both plates and stiffeners), the skin and core thicknesses, as well as the type of Divinycell core, are design variables. Additionally, for the stiffeners, the thickness of the unidirectional laminate acting as a flange is also a design variable. Table 4.2 presents the mechanical properties of the laminates and cores.

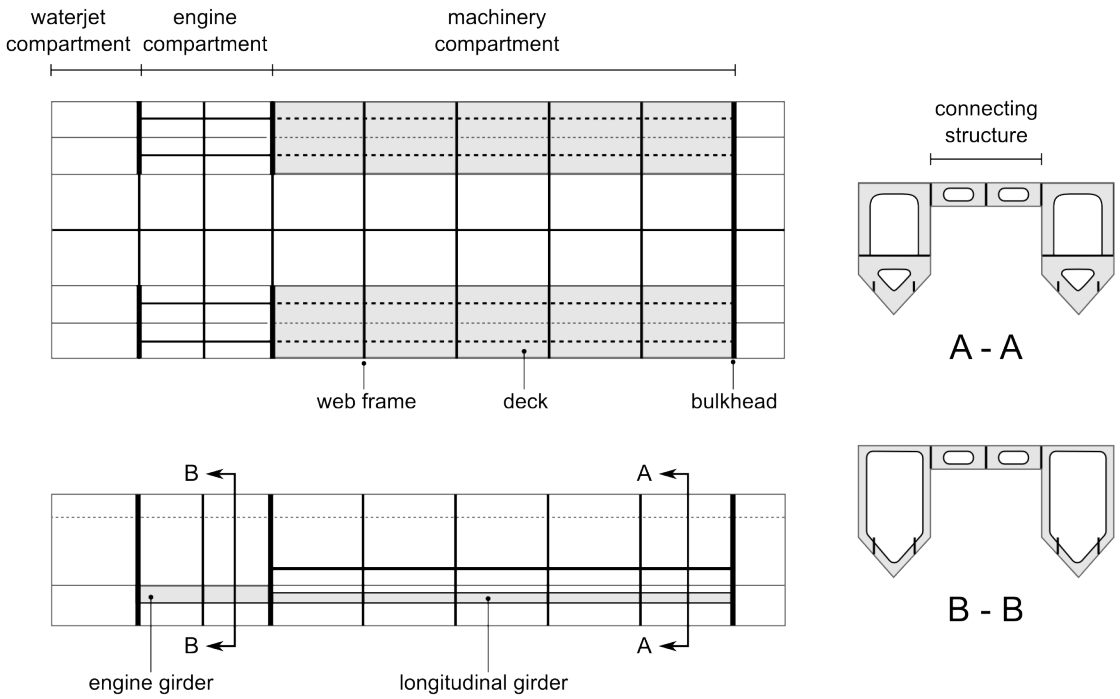

Figure 4.9 Example of the catamaran hull girder scantlings.

The location of all the structural elements, with the exception of the web frames, are design variables. The range of acceptable values is determined by algorithms that guarantee the viability of the scantlings arrangement. The location of each of the two bulkheads defining the waterjet and engine compartments may vary, but only to an extent that guarantees that there is enough space for the waterjet, the engine, and the gearbox plus a margin. Similarly, the location of the collision bulkhead at the fore may vary, but only within the range stated by DNV's HSLC. The lateral location of the engine and longitudinal girders may vary within a range determined by two more design variables: the web height of the longitudinal girders and the location in z-axis of the machinery compartment deck. This dynamic range guarantees that the longitudinal girders do not penetrate the deck. Furthermore, an additional design variable is the existence of the longitudinal girders; in some designs they exist, in some they do not. Finally, the location of the machinery compartment deck relative to the keel and the web heights of the longitudinal and engine girders may vary according to ranges deemed to be reasonable.

Table 4.2 Material properties.

Quasi-isotropic laminate	
Layup	$[0/+45/90/-45]_{iS}$ where $i = 1, 2, \ldots, 8$
Fibre	carbon, Toray T700S
Resin	vinylester, DION 9102-501
Fibre volume fraction	0.5
Elastic modulus, E	42 GPa
Poisson's ratio, v	0.34
Ultimate in-plane tensile strain, ε_{ut}	1.3%
Ultimate in-plane compressive strain, ε_{uc}	0.6 ε_{ut}
Density, ρ	1420 kg/m3
Available thicknesses*	3.78i mm
Unidirectional laminate	
Layup	$[0]_T$
Fibre	carbon, Toray T700S
Resin	vinylester, DION 9102-501
Fibre volume fraction	0.5
Longitudinal modulus, E_1	108 GPa
Transverse modulus, E_2	129 GPa
In-plane shear modulus, E_{12}	3.83 GPa
Out-of-plane shear modulus, E_{23}	4.86 GPa
In-plane Poissons' ratio, v_{12}	0.25
Out-of-plane Poisson's ratio, v_{23}	0.32
Ultimate long. tensile strain, ε_{u1t}	1.7%
Ultimate long. compressive strain, ε_{u1c}	0.6 ε_{ut}
Density	1420 kg/m^3
Available thicknesses	1, 2, 3, …,10 mm

Divinycell core*		**H60**	**H80**	**H100**	**H130**	**H160**	**H200**	**H250**
Elastic modulus, E_c	(MPa)	56	80	105	140	170	230	300
Shear modulus, G_c	(MPa)	16	23	28	40	50	65	81
Shear strength,** τ_u	(MPa)	0.63	0.95	1.4	1.9	2.2	3.2	3.9
Density, ρ	(kg/m^3)	60	80	100	130	160	200	250
Poisson's ratio		0.3	0.3	0.3	0.3	0.3	0.3	0.3
Available thicknesses* (mm)		7, 10, 20, 30, 40, 50						

*The hull bottom panels are restricted to quasi-isotropic laminate thicknesses between 11.34–30.23mm, core thicknesses of 30, 40, and 50 mm, and core types H160, H200, and H250. ** This material property is referred to as the "minimum ultimate shear stress" in DNV's HSLC.

The web frames are divided into three main groups: engine compartment, machinery compartment, and connecting structure web frames. However, in Figure 4.9, one can appreciate that there are two types of web frames in the machinery compartment. An open type above the deck, and a closed type below it. So, the machinery compartment web frames are further divided into two groups: top and bottom. The number of web frames in the engine and machinery compartments respectively are design variables. For the engine compartment web frames, it varies from 1 to 4, and for the machinery

compartment ones, from 3 to 10. The web frames in both groups are evenly distributed along their respective compartment, so the location of each web frame depends on the location of the bulkheads and the number of web frames in the main group. The location of the web frames of the connecting structure match the location of the engine and machinery compartment web frames, and the location of the two engine compartment bulkheads. The web heights of the four groups of web frames are also design variables. For the engine compartment, connecting structure, and top machinery compartment web frames, the web height may vary within a range deemed to be reasonable. On the other hand, the bottom machinery compartment web frames have a dynamic range that adjusts to the position of the deck on the z-axis, so that there is always a manhole. The fillet radii of all the web frames is determined by an custom algorithm to prevent incongruences with the changing web heights.

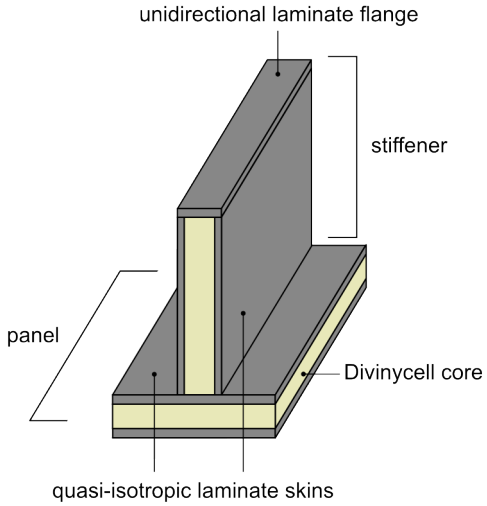

Figure 4.10 General construction of the structural elements.

4.3.2.2 Finite element model and structural analyses

In the study case, the only behavioural constraints considered are the ones related to the structural integrity of the catamaran hull girder. In other words, the structure must withstand the static and dynamic loads which can act on the catamaran under operating conditions. DNV's Classification Note 30.8 states the load cases that a catamaran hull girder must withstand [82]. Whether or not the structure withstands these load cases is determined through criteria based on stresses and strains. The purpose of the finite element model and the structural analyses is to calculate the stresses and strains in the structure under the load cases stated in these classification rules.

The finite element software used for the structural analysis is Ansys [83]. Each finite element model corresponding to a structural design is automatically built by the software following instructions written in Ansys' parametric design language. Figure 4.11 shows how sandwich panels and stiffener webs are modelled with 3-layered shell elements, while stiffener flanges are modelled with beam elements. The quasi-isotropic laminates and the core materials are modelled as isotropic linear elastic materials,

while the unidirectional laminate, is modelled as a transversely isotropic material. An example of a complete catamaran hull girder surface model is shown in Figure 4.12.

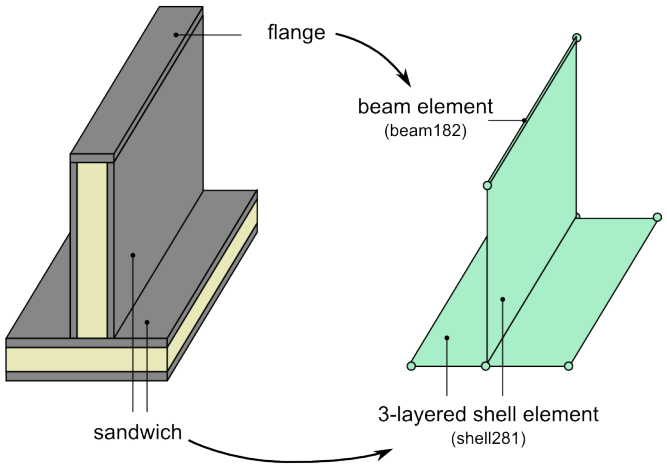

Figure 4.11 Finite element modelling of the structural elements.

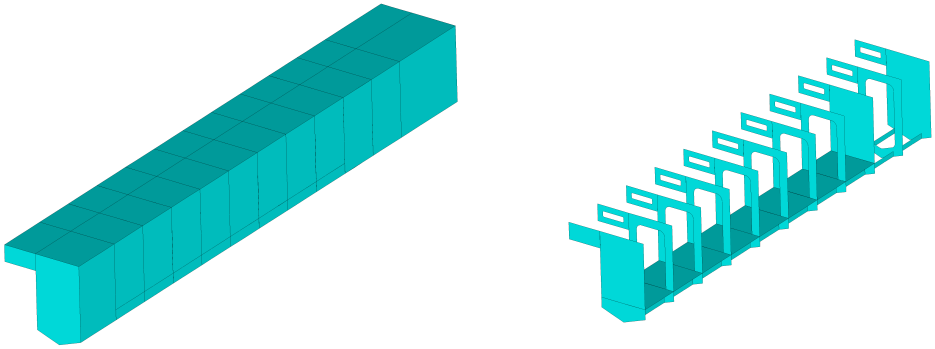

Figure 4.12 Surface model of the catamaran hull girder.

The loads to which the catamaran hull girder is subjected to can be divided into two groups: local and sea loads. The local loads are the ones corresponding to all the elements contributing to the displacement of the catamaran with the exception of the weight of the structure. In Table 4.1, these elements are: passengers and crew, outfittings, remaining machinery, engines and gearboxes, waterjets, and fuel and fresh water tanks. The masses of all these elements are used to calculate the local loads carried by the structure under the different load cases. Figure 4.13 shows the location and manner in which the local loads are applied. The magnitudes of these loads depend on the vertical acceleration to which the catamaran is subjected to. Since the vertical acceleration is not the same for all the load cases, the magnitudes of the internal loads vary between the load cases; however, their location and manner of application remain the same.

An important detail is that for every structure design, the longitudinal centre of gravity of the hull girder is different. The variation is due to differences in the location and construction of the structural elements between the different designs. Zero-trim is achieved in each structure design by adjusting the location of the remaining machinery and outfittings loads. Figure 4.13 pictures a case where zero-trim can be achieved by only adjusting the location of the remaining machinery load. For this case, the outfittings load is applied along with the passengers and crew load. If zero-trim cannot be achieved by setting the remaining machinery load as forward as possible (fore-end next to the collision bulkhead), the longitudinal distribution of the outfittings load is narrowed and adjusted forward. For some structure designs, zero-trim cannot be achieved with neither of these two approaches. These structure designs are removed from the design exploration analysis.

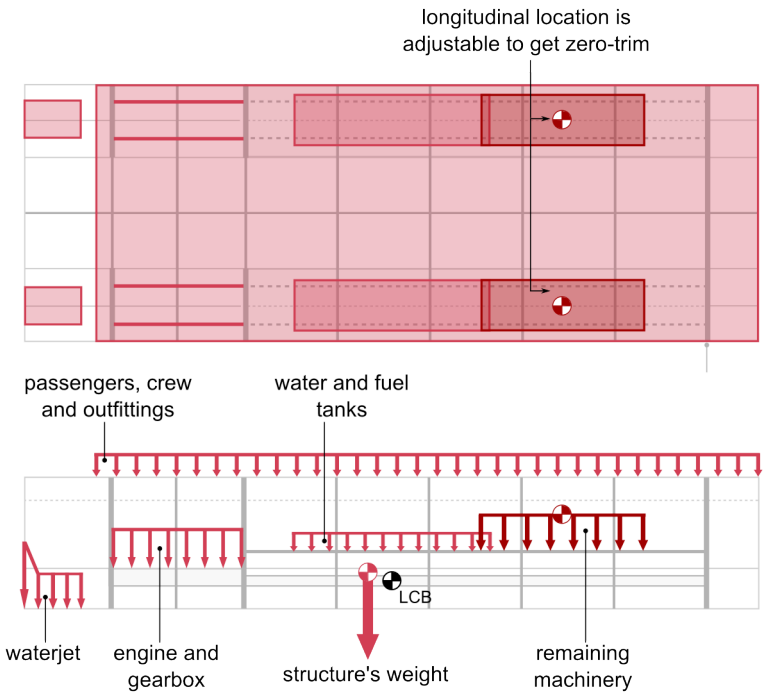

Figure 4.13 Local loads on the catamaran hull girder.

The load cases considered are shown in Figure 4.14. Note that the sea loads are the only loads pictured. The magnitude and location of a sea load follows the requirements of DNV's classification Note 30.8 and DNV's HSLC. For brevity, the reader is referred to both documents for the sea load details.

A non-linear static analysis is run for every structure design and loading condition. Since all the structure designs and load cases are symmetric, only half of hull girder is modelled. To prevent rigid body motion, the movement of the finite element model is constrained by spring elements, each of which is rigidly fixed to a point in space. The reaction forces on the springs are recorded to guarantee that the structural analyses are performed correctly. If the reaction forces exceed 1000 N in any of the structural analyses, the structure design is flagged. The mesh size in the finite element models is between 160 and 200 mm. A mesh convergence analysis for one of the structure designs showed that with these mesh sizes the maximum stresses and strains of the hull

shell and machinery compartment deck converge. For the web frames, girders, and bulkheads, the maximum stresses and strains did not fully converge with these mesh sizes; however, the maximum stresses and strains for these structural elements occur at the joints were the stresses and strains are unrealistically high (see Section 4.4). Therefore, for the purpose of these analyses, the mesh sizes were deemed as adequate, considering that the high stresses and strains at the joints lead to conservative results.

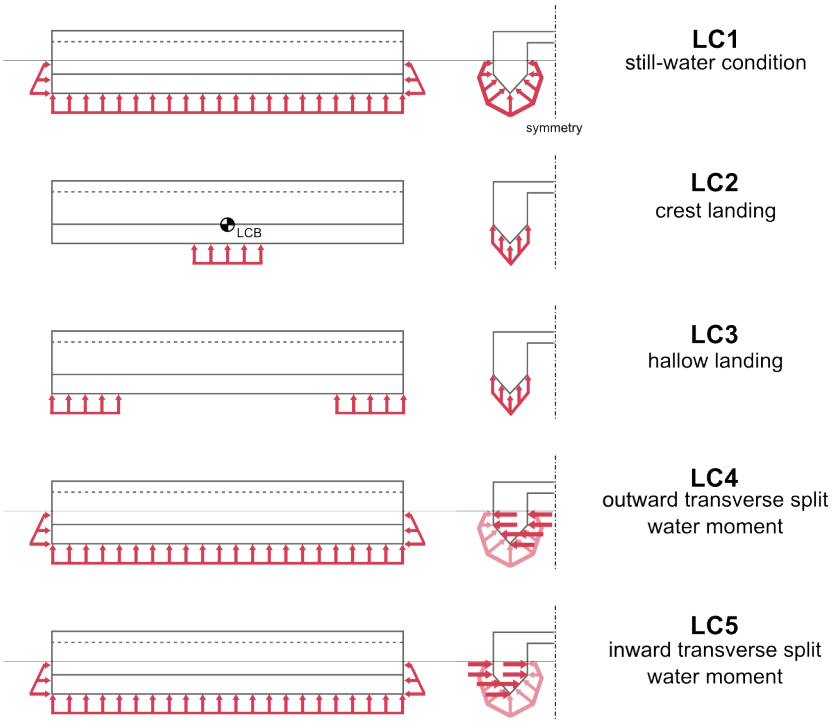

Figure 4.14 Load Cases (LC) for the structural analyses. Only the sea loads are pictured. For the local loads, see Figure 4.13.

4.3.2.3 Behavioural constraints

In this study case, the only behavioural constraint considered are the ones related to structural integrity. Namely, material strength and buckling. The constraints follow DNV's HSLC, and are expressed as inequalities. The values which should not be exceeded are determined from equations found in DNV's HSLC and the material properties in Table 4.2.

Laminate strength

$$\varepsilon_t \leq \varepsilon_{t,max} = 0.3\varepsilon_{tu} \tag{4.4}$$

$$\varepsilon_c \leq \varepsilon_{c,max} = 0.3\varepsilon_{cu} \tag{4.5}$$

where ε_t and ε_c are the maximum tensile and compressive strains in a laminate, and $\varepsilon_{t,max}$ and $\varepsilon_{c,max}$ are the maximum allowable tensile and compressive strains of said

laminate[2]. The study case has two types of laminates: quasi-isotropic and unidirectional. Laminate strength in tension and compression for these two laminate types are treated as independent behavioural constraints.

Core shear strength

$$\tau_c \leq \tau_{c,max} = 0.4\tau_u \tag{4.6}$$

where τ_c is the maximum core shear stress, and $\tau_{c,max}$ is the maximum allowable core shear stress. None of the bottom hull panels are considered to be subjected to slamming loads, so the "minimum ultimate dynamic shear stress" of the core material stated in DNV's HSLC is not used in this study case.

Local skin buckling (aka. wrinkling)

$$\sigma_c \leq \sigma_{cr} = 0.5(\mathrm{E} \cdot \mathrm{E_c} \cdot \mathrm{G_c})^{1/3} \tag{4.7}$$

where σ_c is the maximum laminate stress in compression and σ_{cr} is the critical buckling load for sandwich skin laminates under compression.

Henceforward, the individual Behavioural Constraints (BC) are referred to with the following reference numbers:

BC1. Tensile strength of the quasi-isotropic laminate
BC2. Compressive strength of the quasi-isotropic laminate
BC3. Tensile strength of the unidirectional laminate
BC4. Compressive strength of the unidirectional laminate
BC5. Core shear strength
BC6. Local skin buckling

All these behavioural constraints can be expressed as inequalities of the form,

$$x \leq x_{max} = \frac{mp}{sf} \tag{4.8}$$

where x_{max} is the maximum allowable stress or strain, sf is the safety factor, and mp is a material property or a number derived from material properties (as in the local buckling constraint). Step 5 in our design exploration methodology (see Section 4.3.1) is changing the modifiable constraints. Potentially, the maximum allowable value could be more permissible if the mp had a higher value, sf had a smaller value, or both. In terms of the original values, the constraints can be also expressed as,

[2] This constraint is stated in Pt.3 Ch.4 Sec.5 B502 of DNV's HSLC in terms of stresses, and not in strains as done here. Since the material is linear elastic and the material properties are adjusted for congruency, both expressions are equivalent. An alternative definition is also stated in Pt.3 Ch.4 Sec.1 C502, where the maximum allowable strain is expressed as in Equation 1.1 with the safety factors of Table 2.1. This expression is also equivalent.

$$v \leq F \cdot v_{max} = \frac{F_{mp} \cdot mp}{F_{sf} \cdot sf} \tag{4.8}$$

where F_{mp} and F_{sf} are factors representing a potential increase on the values of the material property and a reduction of the safety factor respectively, while F represents the quotient of the division of these two factors. For this study case, we will consider possible a maximum beneficial change of 10% for both F_{mp} and F_{sf}. Table 4.3 shows the values for F that different combinations of F_{mp} and F_{sf} values render. Different combinations of values for F_{mp} and F_{sf} result in similar values of F. For modifying the histograms we will use F = 1.00, 1.05, 1.10, 1.15, and 1.20. These values can be compared to the ones in Table 4.3 to interpret the corresponding possible changes in mp and sf.

Table 4.3 Modification factors for the behavioural constraints.

	0%	5%			10%			5% and 10%	
F_{mp}	1.00	1.05	1.00	1.05	1.10	1.00	1.10	1.05	1.10
F_{sf}	1.00	1.00	0.95	0.95	1.00	0.90	0.90	0.90	0.95
F	1.00	1.05	1.05	1.10	1.10	1.11	1.22	1.16	1.16

4.3.3 Limitations

The following are the most important limitations of this study case:

- *Hull shape of the pontoons*–The shape is simplified because the algorithms that draw the scantlings in the finite element model are not robust when dealing with curved surfaces. Future version of these algorithms will address this limitation.
- *Joints between panels and stiffeners*–This type of structural joint includes adhesives, interfacing core materials, and over-laminates. None of these elements are modelled, so the joints in the finite element model are less rigid than they should be and their weight is not accounted for.
- *Superstructure*–Considering the large masses attributed to the passengers, crew, and outfittings, as well as its possible small contribution to the total weight of the structure [84], the superstructure is not included in the structural analyses and weight calculations. The superstructure will be modelled in future study cases.
- *Modal response*–Requirements with respect to the natural frequencies and vibrations of hull girder structure are important behavioural constraints which composite structures can easily violate. In this study case, the modal response is not calculated due to calculation time constraints. Future study cases will include it.
- *Modelling of the quasi-isotropic laminate*–The quasi-isotropic laminate is modelled as an isotropic linear elastic material; therefore, the flexural and out-of-plane stiffness of the laminate are to some extent inaccurate. This inaccuracy is likely to have a negligible effect on the calculation, as the quasi-isotropic laminates working as sandwich skins are subjected to mostly in-plane loadings.
- *Load cases*–Two of the load cases stated in DNV's Classification Note 30.8 for catamarans are not considered: "Torsion moment/pitch connecting moment" and "combination of longitudinal bending and torsion". Both load cases were

not considered in the analyses because the algorithms used in the finite element model were restricted to symmetric load cases. Future study cases will include these load cases.

- *Shear failure of the stiffener webs skins*–This behavioural constraint is described in DNV's HSLC; however, it is not implemented in this study. The simple way in which joints are modelled leads to high shear stress concentration zones in the stiffeners (see Section 4.4), which cannot be satisfactorily removed *for this behavioural constraint* with the current version of our algorithms. Future study cases will include this constraint.

4.4 Results

For this study case, 1200 different structure designs were generated with latin-hypercube sampling. Out of these 1200, only 758 structure designs are used in the design exploration analysis. The other structure designs were scrapped for one of three following reasons:

1. A configuration of the local loads resulting in zero-trim could not be found for the structure design.
2. The non-linear structural analysis did not converge.
3. Ansys could not mesh appropriately the structure design.

Figure 4.15 shows the histogram of the weights of the acceptable structure designs within the 758 ones sampled. Whether the designs were acceptable or not was determined by,

- considering only load cases 1 to 3, and
- setting $F = 1.00$ for all the behavioural constraints.

The x-axis range of the histogram plot, (approximately 16 to 80 tonnes) is the range of weights of all the sampled structure designs, both acceptable and unacceptable. Figure 4.15 also shows pie charts indicating the fraction of the evaluated samples deemed as acceptable and unacceptable, as well as an analysis of the unacceptable ones. The analyses of the unacceptable structure designs informs which behavioural constraint is the foremost limiting one (by calculating the fraction between $v/v_{\max}$), as well as in which loading condition and structural element. For example, in the figure, one can observe that less than half of the evaluated samples were deemed as acceptable and that most of the unacceptable ones failed due to BC2 and BC6. BC2 was violated mostly in LC2 and on the web frame webs (WFWB), while BC6 was violated mostly in LC3 and in the hull shell (SHELL).

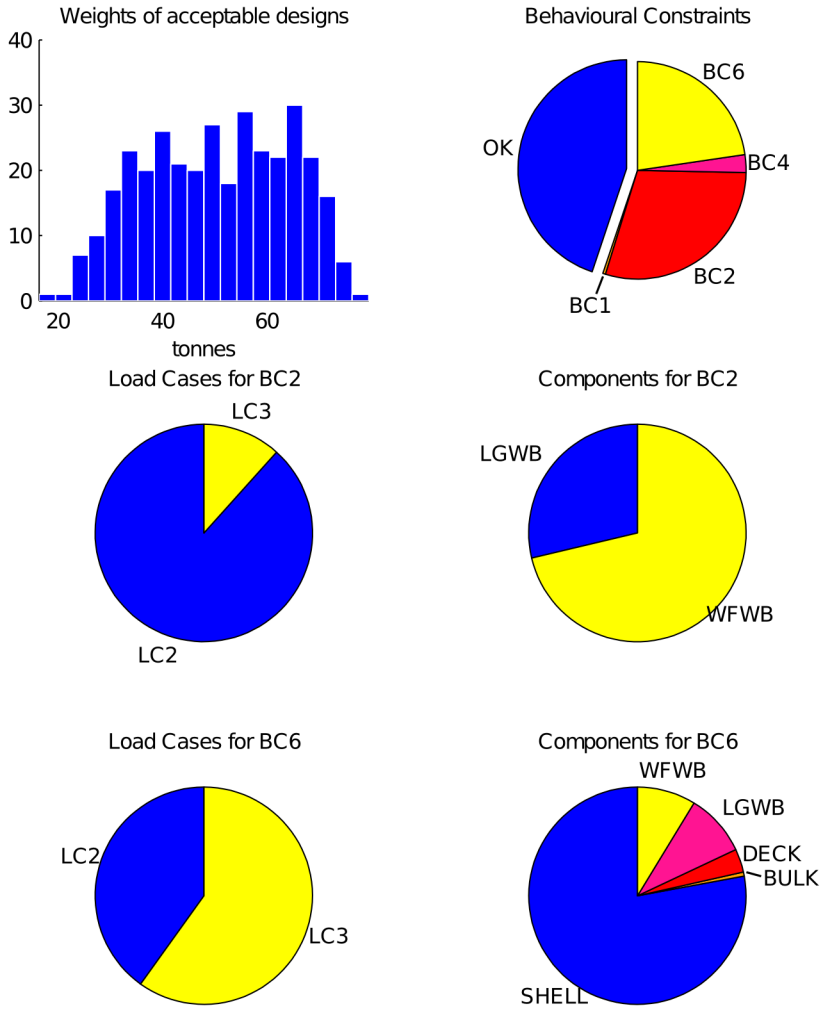

Figure 4.15 Analysis of the structure designs considering only the load cases 1 to 3 and $F = 1.00$ for all behavioural constraints. (OK: acceptable design, SHELL: hull shell; DECK: deck in the machinery compartment; BULK: all bulkheads; WFWB: all web frame webs; LGWB: all longitudinal girder webs). For the identity of the Behavioural Constraints (BC), see Section 4.3.2.3.

Since the range of the histogram matches the weight range of all the samples structure designs, one can infer that an increase on the F-factor for any of the behavioural constraints will not lower the lower bound of the histogram. In other words, modifying the constraints (reducing the safety factor or improving the material properties) will not enable otherwise unattainable lighter structure designs. Figure 4.16 corroborates this inference. This figure shows the histograms for different values of the F-factor corresponding to BC2, while keeping the F-factors of all the other constraints set to 1.00. In the figure, one can observe that the range of the histogram does not change; however, increasing the F-factor for the BC2 increases the number of structure designs deemed as acceptable (i.e. the histogram grows upwards).

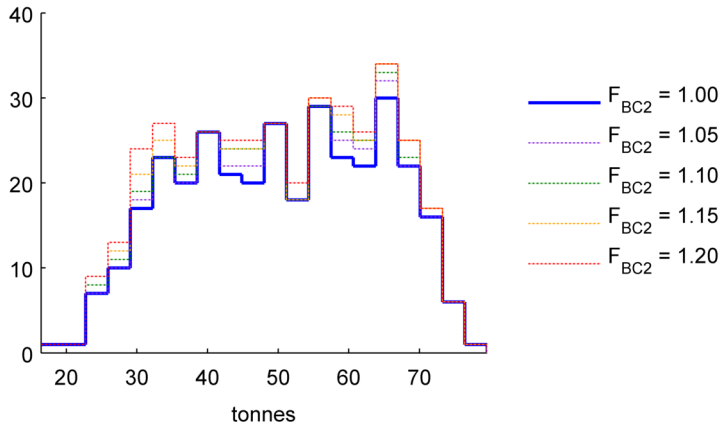

Figure 4.16 Changes in the weight histogram considering load cases 1 to 3 with different F-factors for BC2 (the F-factors of all other behavioural constraints are set to 1.00.)

The results in the Figures 4.15 and 4.16 considered only the load cases 1 to 3 in the evaluation of the structure designs. Figures 4.17 and 4.18 show the results for the case where,

- all load cases are considered, and
- setting $F = 1.00$ for all the behavioural constraints.

In stark contrast with the previous results, the histograms are missing in Figures 4.17 and 4.18 because none of the structure designs met the original or modified behavioural constraints (i.e. all the designs were deemed as unacceptable). The pie charts in Figure 4.17 show that, as before, BC2 and BC6 are the most important behavioural constraints and that they are violated mostly in load cases 4 and 5. The structure designs cannot meet the behavioural constraints in load cases 4 and 5 because of the simplifications made on the finite element model joints. The stresses and strains are unfair at the joint between the connecting structure and the pontoon, and at the joints between the longitudinal girders and the other structural elements (see Figure 4.19). In these zones, a real structure would have some extra core material, adhesive, and overlamination spreading out the loads.

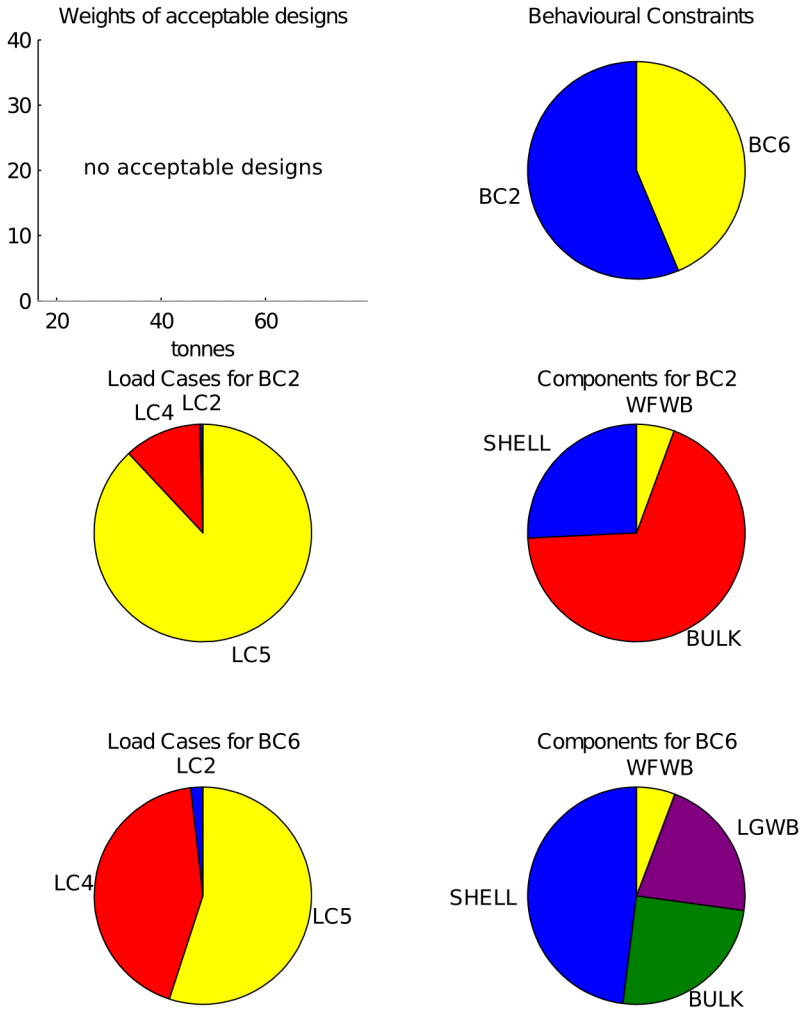

Figure 4.17 Analysis of the structure designs considering all the load cases (1 to 5) and $F = 1.00$ for all behavioural constraints. None of the structure designs is deemed as acceptable.

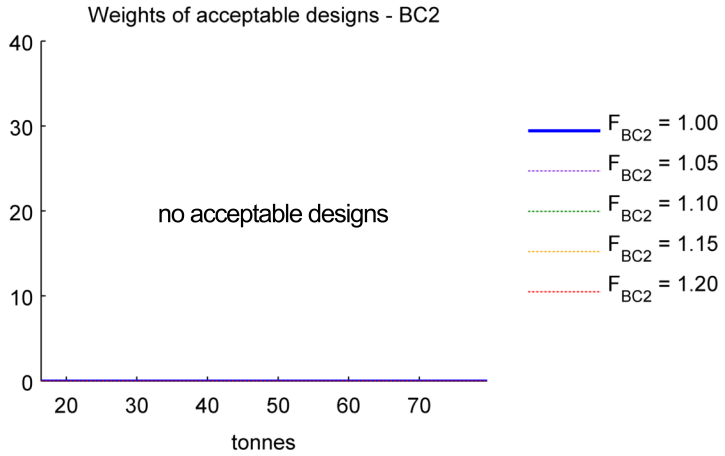

Figure 4.18 Changes in the weight histogram considering all the load cases (1 to 5) with different F-factors for BC2 (for all other behavioural constraint $F = 1.00$). Despite the changes, none of the structure designs is deemed as acceptable.

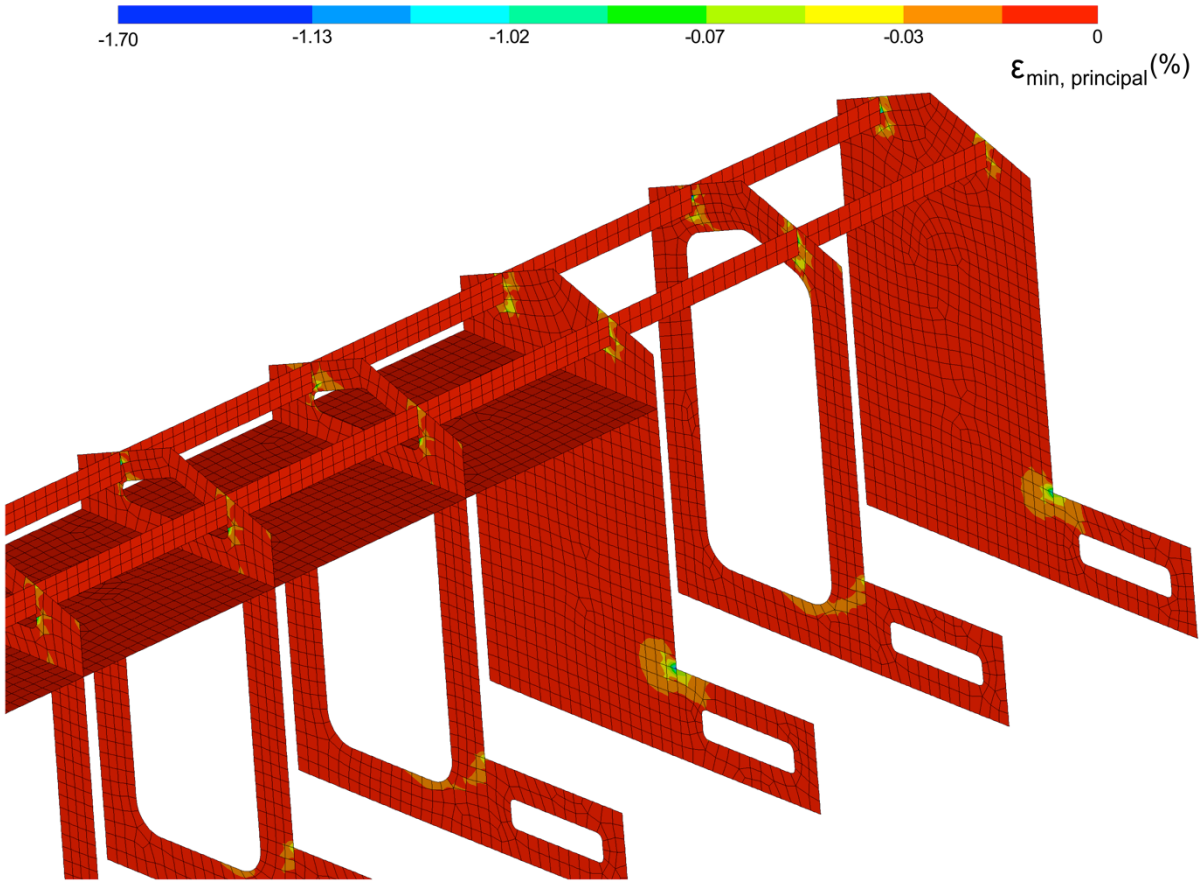

Figure 4.19 Strain concentration zones in the finite element model (view from below): joint of the connecting structure with the pontoon, and the joints between the longitudinal girders and other structural elements (pictured: minimum principal strain (%) in the skin laminates of the scantlings).

Figures 4.20 and 4.21 show the results for the case where,

- all load cases are considered,
- setting $F = 1.00$ for all behavioural constraints, and
- sensitive joint zones are removed from LC4 and LC5.

Figure 4.22 shows which are the sensitive joint zones. The violation of behavioural constraints within these zones are ignored, and the most limiting constraint occurs always outside them. In Figure 4.20 one can see that most of the structure designs are rejected when $F = 1.00$ for all the behavioural constraints. Again, BC2 and BC6 are the most limiting constraints and are mostly violated in LC5. Figure 4.21 shows that changing BC2 results in a small change on the range of weights of the acceptable designs. Going from $F_{BC2} = 1.00$ to $F_{BC2} = 1.20$ does decrease the lower bound of histogram, but the small number of acceptable designs close to the bound indicates that the bound may not be so trustworthy. As in Figure 4.16, increasing the F-factor for the BC2 increases the number of structure designs that are acceptable.

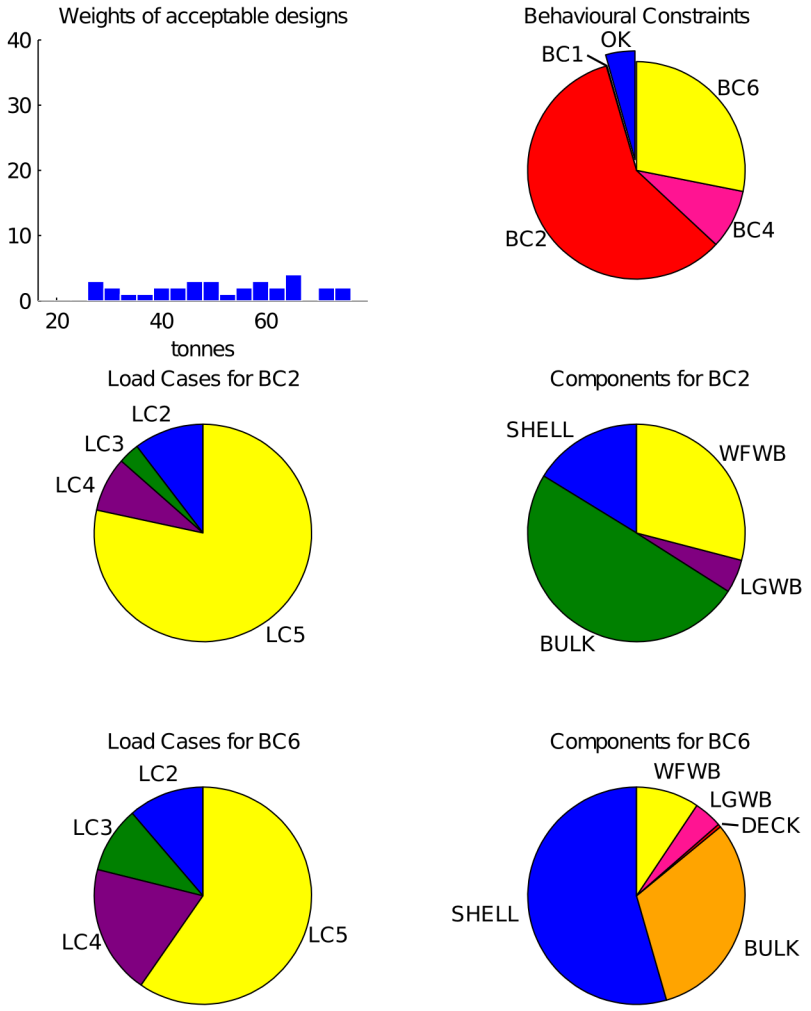

Figure 4.20 Analysis of the structure designs considering all the load cases (1 to 5) and with $F = 1.00$ for all behavioural constraints, but removing the zones in Figure 4.22 during the evaluation of the behavioural constraints for LC4 and LC5.

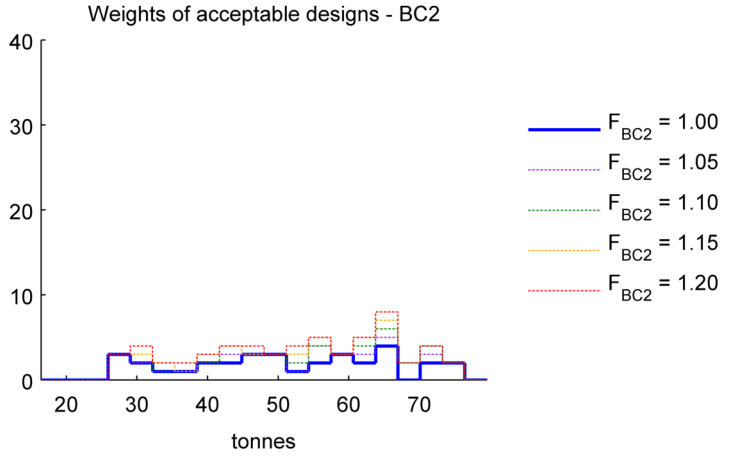

Figure 4.21 Changes in the weight histogram considering all the load cases (1 to 5) with different F-factors for behavioural constraint 2 (the F-factors of all other behavioural constraint are set to 1.00), but removing the zones in Figure 4.22 during the evaluation of the behavioural constraints for loading cases 4 and 5.

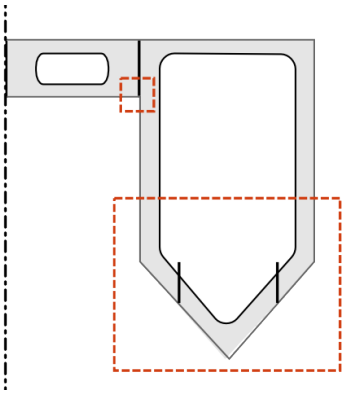

Figure 4.22 Zones excluded from the evaluation of the behavioural conditions for loading cases 4 and 5.

Finally, Figure 4.23 shows the results for the case where,

- all load cases are considered,
- the sensitive joint zones in Figure 4.22 are removed from LC4 and LC5, and
- setting $F = 1.20$ for BC2, BC4, and BC6 (the 3 most limiting behavioural constraints in Figure 4.20), and $F = 1.00$ for all others.

This is an example of an ideal case were the most limiting behavioural constraints are modified through higher material strength and lower safety factors. The histogram of the weights of the acceptable structure designs has the same range as the one in Figure 4.20, so further modifying BC2, BC4, and BC6 did not enable lighter designs (at least for the current sample). However, one can see that the change on the constraints considerably increased the number of designs deemed as acceptable.

The results in Figure 4.20, 4.21, and 4.23 are the final ones of our design exploration methodology. The three figures show that modifying the design constraints did not enable significantly lighter structure designs than the ones obtainable by searching the design space (the study case is more like example 2 than example 1 in Section 4.3.1).

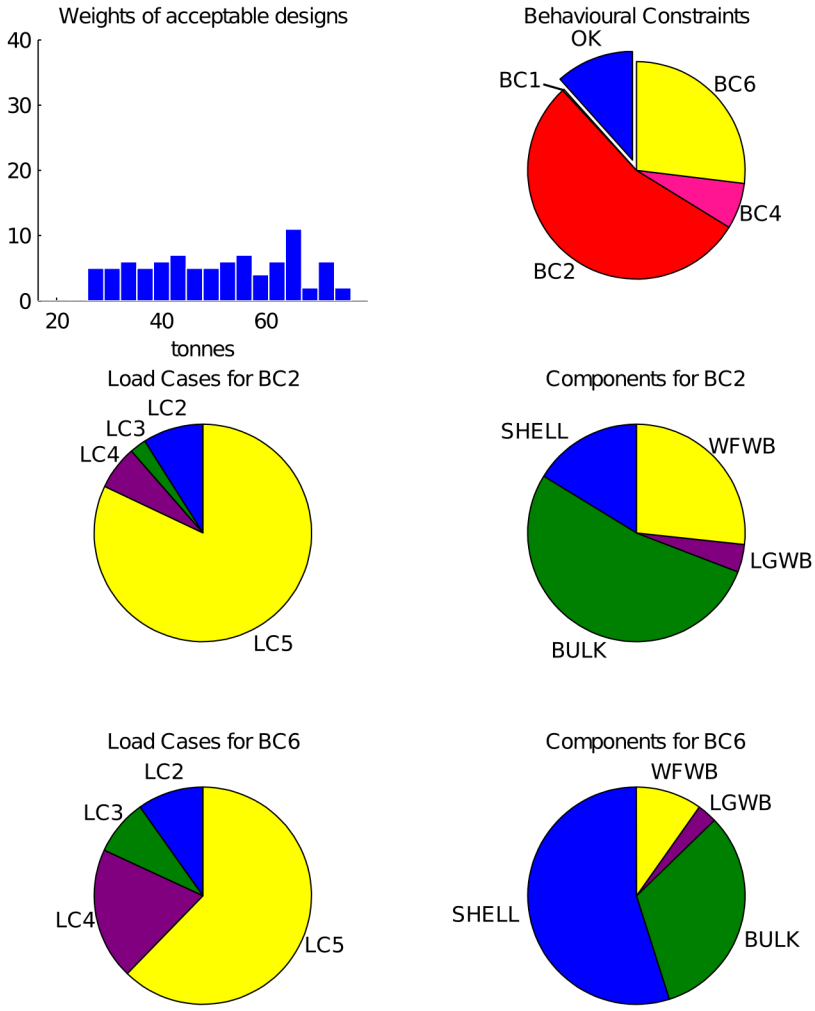

Figure 4.23 Analysis of the structure designs considering all the load cases (1 to 5), removing the zones in Figure 4.22 during the evaluation of the behavioural constraints for LC4 and LC5, setting $F = 1.20$ for BC2, BC4 and BC6 and $F = 1.00$ for all the other constraints.

4.5 Concluding remarks

The objective of the work presented in this chapter was to assess the potential of searching the design space and modifying the design constraints, as approaches for reducing the weight of composite marine structures. Our design exploration methodology indicates that searching the design space has the largest potential, as modifying the design constraints did not enable previously unattainable lighter structure designs. This result does not mean that modifying the design constraints is not beneficial. Weight reduction can definitely be achieved by modifying the design constraints; however, the results indicate that for a large hull built with sandwich-construction, any weight reduction achieved by modifying the constraints is also achievable by searching the design space.

The applicability of this conclusion regarding the relative potential of both approaches to other composite marine structures is uncertain. To the author's knowledge, this study is original and no other study comparing searching the design space and

modifying the design constraints of marine structures has been published. Without any other similar investigation, the only evidence supporting this conclusion is the one presented here, and it consists of a study case with some notable limitations. Considering the complexity of the structure, and the author's first guess on how the results would turn out, it seems futile to try predict how will a less simplified hull or more load cases will affect the conclusion. An improved study case and additional study cases are necessary strengthen this conclusion and broaden its applicability.

Opportunity

Set of circumstances that makes it possible to do something.

5 Conclusions

The objective of this PhD work was to reduce the weight of composite marine structures, so as to make them more economically attractive. Three approaches for reaching this objective were presented, investigated, and discussed:

1. Motivating higher material strength operational limits through reliability analyses (reducing R in Equation 1.1).
2. Obtaining more accurate mechanical properties through advanced measuring techniques (increasing ε_{uf} in Equation 1.1).
3. Searching for better structure designs (reducing ε_i in Equation 1.1).

From a broad point of view, none of these three approaches is novel. Reliability of composites has been investigated for decades; DIC and AE systems are commonly used in modern experimental investigations; and searching for better structure designs through optimisation algorithms is an approach currently researched and available to industry.

The novelty of this PhD work lies in the details of the presented approaches.

Mechanical and probabilistic models for reliability analyses of composite materials were the central theme of the studies presented in Chapter 2, and appended papers I, II and III. We thoroughly explored the effects of using different models on the reliability estimations, and benchmarked the reliability estimates obtained with common mechanical models, against the ones obtained with a mechanical model proven to accurately predict the initiation, development, and loss of stiffness caused by matrix cracking. The use of a mechanical model accounting for the progressive

degradation of the composite material is an important step forward in the composite reliability field according to a recent survey [85]. The results show that strength reliability analyses of FRP laminates in tension are frail and uncertain, because uncertain details of the probabilistic and mechanical models, as well as definitions of laminate failure, highly influence the reliability estimates. Considering that in a structure very low probabilities of failure are sought, with the current knowledge, engineers should be conservative. For example, the Weibull distribution should be use for the probabilistic modelling of strength properties. Despite that our studies deal mostly with cross-ply laminates (a type of laminate uncommon in marine composite structures), several of the conclusions are widely applicable. Probabilistic modelling of ply properties and the definition of laminate failure due to matrix cracking are aspects common to all laminate types that will affect reliability estimates. Our studies on the estimation of operational limits do not provide a mature and straightforward approach for reducing the weight of composite structures, but they do elucidate the aspects which hold the largest opportunities for weight reduction (aspects such as choice of probability distributions and definition of laminate failure). These aspects indicate research areas of interest.

Measuring laminate strain in NCF laminates was one central theme of the work presented in Chapter 3, and the theme of appended paper IV. The details of this seemingly straightforward action were shown to have large consequences on the accuracy of a characterization method. First, the work in appended paper IV extended, strengthened, and clarified conclusions made in [86-88], regarding the effects of the strain measurement error induced by inhomogenous surface displacement fields. Second, the work in Chapter 3 showed in detail how a DIC system can be used for the characterization of NCF laminates, and that the repeatability and non-conact of the DIC system are valuable advantages compared to standard strain measuring techniques. Combined, the works presented in Chapter 3 and appended paper IV provide a mature and straightforward approach for reducing the weight of composite structures: for the characterization of NCF laminates (or other textile laminates), use a strain measuring technique with a large strain gauge, or even better, a DIC system with a script for taking multiple virtual extensometer strain measurements per coupon. Doing so, will reduce or nearly eliminate the strain measurement error, and therefore, improve the accuracy of the characterization method. The second central theme of the work in Chapter 3 was the identification and measurement of matrix cracking through the DIC and AE systems. Our contributions to this problem are modest. A researcher, interested in the topic, may find our insights and approaches useful or worthy of continuation.

In design rules, mechanical properties and safety factors determine the operational limits of the materials in a composites structure (e.g. maximum allowable stresses or strains). The work in the appended papers, and Chapters 2 and 3, strives to modify both properties and factors so as to increase the operational limits. What is the gain of doing so? What is the weight reduction that a 10% increase would lead to? Chapter 4 answers these questions, while simultaneously comparing the potential of such an increase against searching the design space. To the author's knowledge, this study is the first of its kind. Weigh reduction can definitely be achieved by modifying the design constraints; however, the results indicate that for a large hull built with sandwich construction, any weight reduction achieved through lower safety factors or

more accurate mechanical properties could alternatively be achieved by searching the design space. This conclusion may or may not be bound to the study case or the simplifications made in the structural analyses; further investigations are necessary to strengthen it. The work in Chapter 4 does not provide a new approach for reducing the weight of marine composite structures; it indicates where the largest opportunities lie.

"Bang for the buck."

Each of the approaches presented in this PhD work is an opportunity for weight reduction. Each of these opportunities has two characteristics of great importance: cost and worth. Cost should be interpreted as the effort, time, and money, necessary to exploit the opportunity, while worth should be interpreted as the possible weight reduction achievable through it. Obtaining more accurate mechanical properties through better laminate strain measuring techniques is a long hanging fruit. This opportunity is arguably the one worth the least, but the cost of taking it is minimal. On the other hand, the cost of searching for better structure designs is high, but this opportunity is arguably the one worth the most. The high cost comes from building robust parametric structure designs. Finally, motivating higher material operational limits through reliability analysis is the opportunity with the lowest worth to cost ratio. Its cost is high because the mechanical and probabilistic models required by this opportunity are not mature enough, and therefore, need to be further researched.

6 Future Work

The work presented in Chapter 4 will be further developed to strengthen the conclusions drawn from it and to be used in other types of studies. The further development of the work will consist of addressing the limitations stated in Section 4.3.3 (e.g. implement a more realistic hull shape and the joints) and performing a sensitivity analysis with respect to the design variables. The sensitivity analysis will answer whether or not there are combinations of design variables that result in rejected structure designs (only 758 out of 1200 structure designs met the zero-trim constraint and had viable meshes), as well as which design variables can be omitted. Once fully developed, the work in Chapter 4 will be published as a journal paper.

An ambition for a future study is to compare the results of optimisation algorithms coupled to analytical structural calculations of marine composite structures (such as [89]), against the ones of an identical algorithm coupled to our finite element analyses. Such a study would show if there is a large benefit of using finite element analyses for the structural optimisation of marine composite structures.

References

[1] DNV. (2013). Offshore Standard DNV-OS-C501: Composite Components. Høvik, Norway: Det Norske Veritas.

[2] DNV. (2013). Rules for Classification of High Speed, Light Craft and Naval Surface Craft. Høvik, Norway: Det Norske Veritas.

[3] IMO. (2012). EEDI-rational, safe and effective. Available online at: http://www.imo.org/MediaCentre/HotTopics/GHG/Pages/EEDI.aspx [Last accessed 23 April 2015].

[4] DNV. (2012). Shipping 2020. Høvik, Norway: Det Norske Veritas.

[5] Faber, J., Nelissen, D., Hon, G., Wang, H., Tsimplis, M. (2012) Regulated slow steaming in maritime transport. Delft, The Netherlands: CE Delft.

[6] Hertzberg, T. (2009). LASS, Lightweight Construction Applications at Sea. Borås, Sweden: SP Technical Research Institute of Sweden.

[7] Evegren, F., Hertzberg, T., Rahm, M. (2011) LASS-C: Lightweight construction of a cruise vessel. Borås, Sweden: SP technical Research Institute of Sweden.

[8] Hertzberg, T. (2015). Lightweight composite approved for ship. Available online at: http://www.bwz.se/sp/b.aspx?l=be8ff09f-a077-40b2-9178-c34a07df6cd6&r=39907&rcrc=65C1A0EF [Last accessed 23 April 2015].

[9] BESST Breakthrough in European Ship and Shipbuilding Technologies. (2013). Innovative lightweight materials and their application. Available online at: http://www.besst.it/BESST/workpackage.xhtml?wp=6 [Last accessed 23 April 2015].

[10] ABS. (2013). Ship Energy Efficiency Measures. Houston, USA: American Bureau of Shipping.

[11] BESST Breakthrough in European Ship and Shipbuilding Technologies. (2013). Available online at: http://www.besst.it [Last accessed 23 April 2015].

[12] Shenoi, R. A., Dodkins, A. R., (2000). Design of ships and marine structures made from FRP composite materials. In: "Comprehensive Composite Materials", Vol. 6, edited by Kelly, A., Zweben, C. Amsterdam, The Netherlands: Elsevier, pp. 1–21.

[13] Garnich, M. R., Akula, V. M. K. (2009) Review of degradation models for progressive failure analysis of fiber reinforced polymer composites. *Applied Mechanics Reviews* **62**(1): 010803.

[14] Soden, P. D., Kaddour, A. S., Hinton, M. J. (2004) Recommendations for designers and researchers resulting from the world-wide failure exercise. *Composites Science and Technology* **64**: 598-604.

[15] Kaddour, A. S., Hinton, M. J. (2013) Maturity of 3D failure criteria for fibre-reinforced composites: Comparison between theories and experiments: Part B of WWFE-II. *Journal of Composite Materials* **47**(6-7):925–966.

[16] Kaddour, A. S., Hinton, M. J., Li, S., Smith, P. A. (2011) Damage prediction in polymeric composites: Up-date of Part(A) of the third World-Wide Failure Exercise (WWFE-III). In: *18th International Conference on Composite Materials (ICCM18) in Jeju, South Korea, August 21-26, 2011*.

[17] GL. (2003) Rules for Classification and Construction I-Ship Technology. Hamburg, Germany: Germanisher Lloyd.

[18] ISO. (2008) ISO 12215-5:2008 Small craft–Hull construction and scantlings–Part:5 Design pressures for monohulls, design stresses, scantlings determination. Geneva, Switzerland: International Organization for Standarization.

[19] Gayton, N., Mohamed, A., Sorensen, J., Pendola, M., Lemaire, M. (2004). Calibration methods for reliability-based design codes. *Structural Safety* **26**: 91-121.

[20] Vallbo, S. (2005). Material selection considerations for polymer composite structures in naval ship applications. *Journal of Sandwich Structures and Materials* **7**: 413–429.

[21] JCSS. (2001). Probabilistic model code. Copenhagen, Denmark: Joint Committee on Structural Safety.

[22] Beetz, C. P. (1982) Strain-induced stiffening of carbon fibres. *Fibre Science and Technology* **16**: 219–229.

[23] Masters, J. E., Reifsnider, K. L. (1982) An investigation of cumulative damage development in quasi-isotropic graphite/epoxy laminates. In:. "Damage in Composite Materials", vol. 772, edited by Reifsnider, K. L. Baltimore, USA: ASTM International, pp. 40–62.

[24] Flaggs, D. L., Kural M. H. (1982). Experimental determination of the in situ transverse lamina strength in graphite/epoxy laminates. *Journal of Composite Materials* **16**(2): 103–116.

[25] Jen, K. C., Sun, C. T. (1992). Matrix cracking and delamination prediction in graphite/epoxy laminates. *Journal of Reinforced Plastics and Composites* **11**(10): 1163–1175.

[26] Parvizi, A., Garrett, K. W., Bailey, J. E. (1978). Constrained cracking in glass fibre-reinforced epoxy cross-ply laminates. *Journal of Materials Science* **13**: 195–201.

[27] Wang, A. S. D., Kishore, N. N., Li, C. A. (1985). Crack development in graphite epoxy cross-ply laminates under uniaxial Tension. *Composites Science and Technology* **24**(1): 1–31.

[28] Sun, C. T., Jen, K. C. (1987). On the effect of matrix cracks on laminate strength. *Journal of Reinforced Plastics and Composites* **6**(3): 208–222.

[29] Varna, J., Joffe, R., Akshantala, N. V., Talreja, R. (1999). Damage in composite laminates with off-axis plies. *Composites Science and Technology* **59**(14): 2139–2147.

[30] Talreja, R. (1985). Transverse cracking and stiffness reduction in composite laminates. *Journal of Composite Materials* **19**(4): 355–375.

[31] Nairn, J. A. (2000). Matrix microcracking in composites. In: "Comprehensive Composite Materials", Vol. 2, edited by Kelly, A., Zweben, C. Amsterdam, The Netherlands: Elsevier, pp. 403–432.

[32] O'brien, T. K. (1982). Characterization of delamintation onset and growth in a composite laminate. In: "Damage in Composite Materials", vol. 772, edited by Reifsnider, K. L. Baltimore, USA: ASTM International, pp. 140–167.

[33] Crossman, F.W., Wang, A. (1982). The dependence of transverse cracking and delamination on ply thickness in graphite/epoxy laminates. In: "Damage in Composite Materials", vol. 772, edited by Reifsnider, K. L.

Baltimore, USA: ASTM International, pp. 118–139.
[34] Wang, A. (1984). Fracture mechanics of sublaminate cracks in composite materials. *Composites Technology Review* **6**(2): 45–62.
[35] Nairn, J. A., Hu, S. (1992). The initiation and growth of delaminations induced by matrix microcracks in laminated composites. *International Journal of Fracture* **57**(1): 1–24.
[36] Pagano, N. J., Schoeppner, G. A. (2000). Delamination of polymer matrix composites: problems and assessment. In: "Comprehensive Composite Materials", Vol. 2, edited by Kelly, A., Zweben, C. Amsterdam, The Netherlands: Elsevier, pp. 1–96.
[37] Berthelot, J. M. (2003). Transverse cracking and delamination in cross-ply glass-fiber and carbon-fiber reinforced plastic laminates: static and fatigue loading. *Applied Mechanics Reviews* **56**(1): 111–147.
[38] Hallet, S. R., Jiang, W. G., Khan, B., Wisnom, M. R. (2008). Modelling the interaction between matrix cracks and delamination damage in scaled quasi-isotropic specimens. *Composites Science and Technology* **68**(1): 80–89.
[39] Singh, C. V., Talreja, R. (2010). Evolution of ply cracks in multidirectional composite laminates. *International Journal of Solids and Structures* **47**(10): 1338–1349.
[40] Barbero, E. J., Sgambitterra, G., Adumitroaie, A., Martinez, X. (2011). A discrete constitutive model for transverse and shear damage of symmetric laminates with arbitrary stacking sequence. *Composite Structures* **93**(2): 1021–1030.
[41] Tsai, S. W., Wu, E. M. (1971). A general theory of strength for anisotropic materials. *Journal of Composite Materials* **5**(1): 58–80.
[42] Puck, A. (1998). Failure analysis of FRP laminates by means of physically based phenomenological models. *Composites Science and Technology* 48: 1045-1067.
[43] Barbero, E. J. (2011). Introduction to Composite Materials Design. Boca Raton, USA: CRC Press.
[44] Cui, W., Wisnom, M. R. (1993). A combined stress-based and fracture-mechanics-based model for predicting delamination in composites. *Composites* **24**(6): 467-474.
[45] Farrokhabadi, A., Hosseini-Toudeshky, H., Mohammadi, B. (2011). A generalized micromechanical approach for the analysis of transverse crack and induced delamination in composite laminates. *Composite Structures* **93**(2): 443–455.
[46] US DoD. (2002). Composite Materials Handbook-MIL 17: Polymer Matrix Composites: Materials Usage, Design, and Analysis, Vol. 3. Philadelphia, USA: US Department of Defense.
[47] Mallick, P. K. (2007). Fiber-Reinforced Composites: Materials, Manufacturing, and Design. Boca Raton, USA: CRC Press.
[48] Ivanov, D.S. (2009). Damage Analysis of Textile Composites. Leuven, Belgium: Katholieke Universiteit Leuven.
[49] Vallons, K. (2011). The Behaviour of Carbon Fibre-Epoxy NCF Composites Under Various Mechanical Loading Conditions. Leuven, Belgium: Katholieke Universiteit Leuven.
[50] ASTM. (2014). ASTM D3039 Standard Test Method for Tensile Properties

of Polymer Matrix Composite Materials. West Conshohocken, USA: ASTM International.

[51] ASTM. (2013). ASTM D3518/D3518M Standard Test Method for In-Plane Shear Response of Polymer Matrix Composite Materials by Tensile Test of a +-45° Laminate. West Conshohocken, USA: ASTM International.

[52] Seartex. (2014). Learjet 85 aircraft takes off for the first time – with SAERTEX non-crimp fabrics on board. Available online at: http://www.saertex.com/en/current/news/jungfernflug-des-learjet-85-mit-multiaxialgelegen-ncf-von-saertex-an-bord [Last accessed 23 April 2015].

[53] Satyanarayana, A., Bogert, P. B., Aitharaju, V., Aashat, S., Kia, H. Damage simulation in non-crimp fabric composite plates subjected to imact loads. In: *29th American Society for Composites Technical Conference in La Jolla, USA, September 8-10, 2014.*

[54] Dry Composites. (2013). BMW i3: first mass produced composite car in production. Available online at: http://www.drycomposites.com/bmw-i3-first-mass-produced-composite-car-in-production/ [Last accessed 23 April 2015].

[55] Bibo, G. A., Hogg, P. J., Kemp, M. (1997). Mechanical characterization of glass- and carbon-fibre-reinforced composites made with non-crimp fabrics. *Composite Science and Technology* **57**: 1221–1241.

[56] Mouritz, A. P., Cox, B. N. (2000). A mechanistic approach to the properties of stitched laminates. *Composites Part A* **31**(1): 1–27.

[57] Lomov, S. V., Belov, E. B., Bischoff, T., Ghosh, S. B., Truong, T. C., Verpoest, I. (2002) Carbon composites based on multiaxial multiply stitched preforms. Part 1. Geometry of the preform. Composites Part A **33**(9): 1171–1183.

[58] Roberts, J. (2010). Performance of non-crimp fabric composites in shear. *Key Engineering Materials* **425**: 45–59.

[59] Hodgkinson, J. M., editor. (2000). Mechanical Testing of Advanced Fibre Composites. Boca Raton, USA: CRC Press.

[60] ASTM. (2010). ASTM E83–10a Standard Practice for Verification and Classification of Extensometer Systems. West Conshohocken, USA: ASTM International.

[61] Hart-Smith, L. (2000). Backing-out composite lamina strengths from cross-ply testing. In: "Comprehensive Composite Materials", Vol. 5, edited by Kelly, A., Zweben, C. Amsterdam, The Netherlands: Elsevier, pp. 1–13.

[62] GL. (2006). Rules for Classification and Construction II– Materials and Welding. Hamburg, Germany: Germanischer Lloyd.

[63] Sause, M. G. R., Gribov, A., Unwin, A. R., Horn, S. (2012). Pattern recognition approach to identify natural clusters of acoustic emission signals. *Pattern Recognition Letters* **33**(1): 17–23.

[64] ASTM. (2014). ASTM D6641/D6641M-14 Standard Test Method for Compressive Properties of Polymer Matrix Composite Materials Using a Combined Loading Compression (CLC) Test Fixture. West Conshohocken, USA: ASTM International.

[65] Adrien Leygue. (2014). Plane fit. Available online at: http://www.mathworks.com/matlabcentral/fileexchange/43305-plane-fit/content/affine_fit.m [Last accessed 23 April 2015].

[66] Ivanov, D., Ivanov, S., Lomov, S. V., Verpoest, I. (2009). Strain mapping

analysis of textile composites. *Optics and Lasers in Engineering* **47**: 360–370.

[67] Gliesche, K., Hübner, T., Holger, O. (2005). Investigations of in-plane shear properties of ±45°-carbon/epoxy composites using tensile testing and optical deformation analysis. *Composites Science and Technology* **65**: 163–171.

[68] El-Chiti, F., Lopez-Anido, R. A., Dagher, H. J., Thompson, L. D., Muszynski, L., Hess, P. E. (2005). Experimental approach for characterizing VARTM composites using a 3-D digital image correlation system. In: *2005 SEM Annual Conference & Exposition on Experimental and Applied Mechanics*.

[69] Kashfuddoja, M., Prasath, R. G. R., Ramji, M. (2014). Study on experimental characterization of carbon fiber reinforced polymer panel using digital image correlation: a sensitivity analysis. *Optics and Lasers in Engineering* **62**: 17–30.

[70] Soden, P., Hinton, M., Kaddour, A. (1998). Lamina properties, lay-up configurations and loading conditions for a range of fibre-reinforced composite laminates. *Composites Science and Technology* **58**(7): 1011–1022.

[71] Truong, T. C., Vettori, M., Lomov, S. V., Verpoest, I. (2005). Carbon composites based on multi-axial multi-ply stitched preforms. Part 4. Mechanical properties of composites and damage observation. *Composites Part A* **36**: 1207–1221.

[72] Perry, C. C. (1989). Strain-Gage Reinforcement Effects on Orthotropic Materials. In: "Manual on Experimental Methods for Mechanical Testing of Composites" edited by Pendleton, R. L., Tuttle, M. E. Bethel, USA: Society of Experimental Mechanics, pp. 39-44.

[73] Slaminko, S. (1989). Strain gages on composites temperature compensation. In: "Manual on Experimental Methods for Mechanical Testing of Composites" edited by Pendleton, R. L., Tuttle, M. E. Bethel, USA: Society of Experimental Mechanics, pp. 27-29.

[74] Nairn J. A., Hu, S., Bark, J. S. (1993).A critical-evaluation of theories for predicting microcracking in composite laminates. Journal of Materials Science **28**(18): 5099–5111.

[75] Edgren, F., Mattsson, D., Asp, L., Varna, J. (2004). Formation of damage and its effects on non-crimp fabric reinforced composites loaded in tension. *Composites Science and Technology* **64**(5): 675–692.

[76] Scott, A. E., Mavrogordato, M., Wright, P., Sinclair, I., Spearing, S. M. (2011). In situ fibre fracture measurement in carbon–epoxy laminates using high resolution computed tomography. *Composites Science and Technology* **71**(12): 1471–1477.

[77] Rao, S.S. (2009). Engineering Optimization. Hoboken, USA: John Wiley & Sons, Inc.

[78] Viana, F. A. C. (2013). Things you wanted to know about the Latin hypercube design and were afraid to ask. In: *10th World Congress on Structural and Multidisciplinary Optimization in Orlando, USA, May 19-24, 2013*. 11 p.

[79] Phillips, S. J. (2008). Jane's High-Speed Marine Transportation 2008-2009. Coulsdon, UK: Jane's Information Group.

[80] Mosgaard, M. A., Riisgaard, H., Kerndrup, S. (2014). Making carbon-fibre

composite ferries a competitive alternative: the institutional challenges. I*nternational Journal of Innovation and Sustainable Development* **8**(3): 290–310.

[81] Molland, A. F., Karayannis, T., Taunton, D. J., Sarac-Williams, Y. (2003). In: *Proceedings of the 8th International Marine Design Conference in Athens, Greece, 5-8 May.* pp. 47-60.

[82] DNV. (1996). Classification Notes No. 30.8 Strength Analysis of Hull Structures in High Speed and Light Craft. Høvik, Norway: Det Norske Veritas.

[83] ANSYS Inc. ANSYS Academic research, Release 15.0.

[84] Ahuja, G. (2007). Application of a Sandwich Construction on a Superstructure of a High Speed Ferry. Gothenburg, Sweden: Chalmers University of Technology.

[85] Chiachio, M., Chiachio, J., Rus, G. (2012). Reliability in composites – A selective review and survey of current development. *Composites Part B* **43**(3): 902–913.

[86] Ifju, P. G., Masters, J. E., Jackson, W. C. (1995). The use of moiré interferometry as an aid to standard test-method development for textile composite materials. *Composites Science and Technology* **53**: 155–163.

[87] Masters J. E., Ifju, P. G. (1997). Strain gage selection criteria for textile composite materials. *Journal of Composites Technology & Research* **19**(3): 152–167.

[88] Lang, E. J., Chou, T. W. (1998). The effect of strain gage size on measurement errors in textile composite materials. *Composites Science and Technology* **58**: 539–548.

[89] Stenius, I., Rosén, A., Kuttenkeuler J. (2011). On structural design of energy efficient small high-speed craft. *Marine Structures* **24**(1): 43–59.